Studies on methods for specific detection of abnormal isoform of prion protein and its application

異常型プリオンタンパク質の特異的検出法とその応用に関する研究

Akio Suzuki

CONTENTS

ABBREVIATIONS

aa	amino acid
Ab	antibody
Ag	antigen
Bo	bovine
BH	brain homogenate
BSE	bovine spongiform encephalopathy
Bv	bank vole
C-BSE	classical bovine spongiform encephalopathy
CH	constant regions of heavy chain
CJD	Creutzfeldt-Jakob disease
CL	constant regions of light chain
CNS	central nervous system
ctrl	control
CWD	chronic wasting disease
DAPI	4', 6'-diamino-2-phenylindole, dilactate
EGFP	enhanced green fluorescent protein
ELISA	enzyme-linked immunosorbent assay
F2A	2A fragment from foot-and-mouth virus
FBS	fetal bovine serum
Fc	fragment crystallization
Fd	antigen-binding fragment and constant regions of heavy chain
Gdn	guanidinium
GSS	Gerstmann-Sträussler-Scheinker
Ha	hamster
HCl	hydrochloride
Hu	human
IFA	immunofluorescence assay
IgG	immunoglobulin G
IRES	internal ribosome entry site
k_a	association rate constant
k_d	dissociation rate constant
K_D	dissociation constant
mAb	monoclonal antibody

MoPrP	mouse prion protein
NBH	normal brain homogenate
NC	negative control
PBS	phosphate-buffered saline
PBST	phosphate-buffered saline containing 0.1% Tween 20
PFA	paraformaldehyde
PK	proteinase K
PMCA	protein misfolding cyclic amplification
PrP^{C}	cellular isoform of prion protein
PrP^{Sc}	abnormal isoform of prion protein
PrP^{Sc}-res	proteinase K-resistant abnormal isoform of prion protein
PrP^{Sc}-sen	proteinase K-sensitive abnormal isoform of prion protein
rAb	recombinant antibody
RACE	rapid amplification of cDNA end
Rb	rabbit
rCerPrP	recombinant cervid prion protein
rFab	recombinant antigen-binding fragment
RT-QuIC	real-time quaking-induced conversion
RU	response unit
SCN	thiocyanate
ScN2a-3-22L	N2a-3 cells persistently infected with 22L prion strain
Sh	sheep
SPR	surface plasmon resonance
ThT	thioflavin T
tris	tris(hydroxymethyl)aminomethane
UTR	untranslated region
VH	variable regions of heavy chain
VL	variable region of light chain

PREFACE

Prion diseases, also known as transmissible spongiform encephalopathies, are fatal neurodegenerative diseases, including Creutzfeldt-Jakob disease (CJD), Gerstmann-Sträussler-Scheinker syndrome (GSS), and fatal familial insomnia in humans, scrapie in sheep and goats, chronic wasting disease (CWD) in cervids, and bovine spongiform encephalopathy (BSE) (Prusiner, 1998). Prion disease in humans can be classified as sporadic, hereditary, and, to a lesser extent, acquired forms such as iatrogenic CJD, variant CJD, and kuru (Prusiner, 1998; Will, 2003). Animal prion diseases usually occur by ingestion of prion-contaminated substances. CWD and scrapie occur by horizontal transmission under natural circumstances through the tissues (Andreoletti *et al*., 2002; Pattison *et al*., 1972), body fluid (Mathiason *et al*., 2006) and excretions (Tamguney *et al*., 2009) contaminated with prions, and the prion-contaminated environment (Georgsson *et al*., 2006; Miller *et al*., 2004; Pritzkow *et al*., 2015), whereas classical BSE (C-BSE) cases have occurred in the artificial ingestion of prion-contaminated feedstuff (Wilesmith *et al*., 1988).

The causative agents of prion disease, prions, are mainly composed of an abnormal isoform of prion protein (PrP^{Sc}) (Prusiner, 1998). The term “prion”, derived from proteinaceous infectious particle, is named based on prion hypothesis: the infectious agent of proteins but lacks nucleic acid as a genome. PrP^{Sc} is generated from host-encoded cellular isoform of PrP (PrP^{C}) via binding of PrP^{C} to PrP^{Sc} and subsequent conformational conversion from α-helix-rich PrP^{C} to β-structure-rich PrP^{Sc}. After prion infection, PrP^{Sc} is produced and accumulated in the central nervous system (CNS) during a long latency period. During disease progression, microglial activation, astrogliosis, synaptic loss, vacuolation of neuropil and neurons, and neuronal cell death are observed in the CNS. However, a mechanistic relationship between accumulation and propagation of PrP^{Sc} and neuronal cell death is still not fully understood.

Prions spread horizontally via the prion-contaminated animal tissues and prion-

contaminated environment. Additionally, prions may appear naturally in aged animals as sporadic diseases (Houston and Andreoletti, 2019). If PrP^{Sc} was shed into the environment via carcasses, body fluids, and excretions of prion-infected animals, it could persist for a long time on pasture and soil (Haley and Hoover, 2015; Pritzkow *et al*., 2015), and environment contaminated with prions can be a source of horizontal transmission. Additionally, the transmission of C-BSE to humans as variant CJD (Will *et al*., 1996) has been caused via consumption of BSE-contaminated products. Furthermore, low level of prion infectivities or amyloid seeding activities have been detected in the edible portion of atypical BSE-infected cattle (Balkema-Buschmann *et al*., 2011; Sawada *et al*., 2019; Suardi *et al*., 2012). Therefore, continuous monitoring of prions among animals in ranch or wildlife is necessary for an early response for the appearance of disease cases and ensuring the safety and security of animal products. Taken together, methods for specific detection of PrP^{Sc} are required not only to elucidate the mechanisms for prion propagation and pathogenesis but also to disclose a potential presence of prion diseases in animals.

Although PrP^{Sc} and PrP^{C} have the same primary structure, PrP^{Sc} can be distinguished from PrP^{C} by biochemical and biophysical properties such as a high β-structure content, resistance to protease digestion, and insolubility to nonionic detergent (Meyer *et al*., 1986). For detecting PrP^{Sc} in the tissues by immunocytochemistry, hydrated autoclaving is commonly used to detect PrP^{Sc} from formalin-fixed paraffin-embedded tissue sections (Kitamoto *et al*., 1991). Removal of PrP^{C} by proteinase K (PK) also enables us to detect only PrP^{Sc} in prion-infected cells (Holscher *et al*., 1998). However, these methods involve harsh treatments that affect tissue or cell architecture. Furthermore, it has been reported that PrP^{Sc} comprises PK-resistant PrP^{Sc} (PrP^{Sc}-res) and PK-sensitive PrP^{Sc} (PrP^{Sc}-sen) (Pastrana *et al*., 2006; Tzaban *et al*., 2002) and that a part of PrP^{Sc}-sen particles exhibits higher infectivity and higher conversion-inducing activity than PrP^{Sc}-res (Silveira *et al*., 2005). Thus, the proper methods that can detect both

PrP^{Sc}-res and PrP^{Sc}-sen, and that can distinguish PrP^{Sc}-sen from PrP^{C} without severe damage in tissue or cell structures are required for detailed analyses of the mechanism of prion propagation and pathogenesis.

Anti-PrP antibodies (Abs) have been produced using various PrPs as immunogens, such as recombinant PrP (Korth *et al*., 1997; Somerville *et al*., 1997), purified PrP^{Sc} (Bendhein *et al*., 1984; Shinagawa *et al*., 1986), and PrP synthetic peptides (Piccardo *et al*., 1998; Shinagawa *et al*., 1986), and DNA encoding PrP (Krasemann *et al*., 1999). Anti-PrP Abs have also been produced by molecular genetic methods such as phage display after immunization of *Prnp* deficient mice (Williamson *et al*., 1998). Indeed, various anti-PrP Abs have been produced so far (Bolton *et al*., 1991; Kascsak *et al*., 1987; Kim *et al*., 2004b; Polymenidou *et al*., 2008; Williamson *et al*., 1996). However, since PrP^{C} and PrP^{Sc} share the primary structure, most of anti-PrP Abs can bind to both isoforms (Kascsak *et al*., 1987; Khalili-Shirazi *et al*., 2005; Peretz *et al*., 1997), which are referred to as pan-PrP Abs. Several PrP^{Sc}-specific monoclonal Abs (mAbs) have also been produced (Horiuchi *et al*., 2009; Korth *et al*., 1997; Masujin *et al*., 2013; Moroncini *et al*., 2004; Paramithiotis *et al*., 2003; Ushiki-Kaku *et al*., 2010). Although these mAbs appeared to immunoprecipitate PrP^{Sc} specifically, the PrP^{Sc}-specific reactivity in other experimental condition, such as immunocytochemistry remains unclear.

Despite such technical restriction, PrP^{Sc}-specific staining using pan-PrP Abs in immunofluorescence assay (IFA) after treatment of fixed cells with a chaotropic agent, such as guanidinium (Gdn) salt (Taraboulos *et al*., 1990), has greatly contributed for analyses of PrP^{Sc} in prion-infected cells (Marijanovic *et al*., 2009; Pimpinelli *et al*., 2005; Veith *et al*., 2009). However, since most pan-PrP Abs cannot distinguish PrP^{Sc} from PrP^{C}, manipulation such as detector gain or exposure time is required to set a threshold level just above the signals from immunoreacted PrP^{C}. Recently, it has been reported that mAb 132 recognizing mouse PrP (MoPrP) amino acids (aas) 119−127, which is classified as a group of pan-PrP Abs because of

the reaction to both PrP^{C} and PrP^{Sc} in immunoblot analysis, enables the PrP^{Sc}-specific staining in cells or frozen tissue sections in IFA (Sakai *et al*., 2013; Tanaka *et al*., 2016; Yamasaki *et al*., 2014a; Yamasaki *et al*., 2012) and flow cytometry (Yamasaki *et al*., 2018). These studies indicate mAb 132 as indispensable tools for analyzing prion propagation and neuropathogenesis. Despite these benefits of mAb 132 in PrP^{Sc}-specific staining, the mechanism of how mAb 132 specifically detects PrP^{Sc} remains unclear.

PrP^{Sc} is produced by binding host PrP^{C} to pre-existing PrP^{Sc} and subsequent conformational conversion of PrP^{C} into PrP^{Sc} (Prusiner, 1998). During this process, PrP^{Sc} acts as a seed. Thus, detection of PrP^{Sc} is generally used for diagnosis of prion diseases and/or detection of prions. Immunohistochemistry, immunoblotting, and enzyme-linked immunosorbent assay (ELISA) have been used as a gold standard for PrP^{Sc} detection and indeed applied for diagnosis of prion diseases and disclosure of prion-infected animals. However, the sensitivity of these immunobiochemical and immunohistochemical methods was not enough to detect low levels of prions (Balkema-Buschmann *et al*., 2011; Dassanayake *et al*., 2016; McNulty *et al*., 2019). Bioassays using appropriate gene-modified mice could be sensitive enough to detect low levels of prions (Buschmann and Groschup, 2005; Fischer *et al*., 1996; Kong *et al*., 2008; Scott *et al*., 1989). However, bioassays require extremely long experimental periods, e.g., more than two years, to detect low levels of prions.

In the past two decades, novel *in vitro* prion amplification methods such as protein misfolding cyclic amplification (PMCA) (Saborio *et al*., 2001), quaking-induced conversion (Orru *et al*., 2009), and real-time quaking-induced conversion (RT-QuIC) (Atarashi *et al*., 2011) have been developed to detect prions. PMCA, in which brain homogenates containing PrP^{C} and materials containing PrP^{Sc} are treated with cycles of sonication, boosts the conversion of PrP^{C} into PrP^{Sc} with remarkable of sensitivity. Thus, PMCA has been used for the detection of low levels of prions in tissues and body fluids (Haley and Richt, 2017; Orru *et al*., 2009; Saborio *et*

al., 2001). PMCA has also been used for *de novo* generation of infectious prions (Castilla *et al*., 2005; Deleault *et al*., 2007; Wang *et al*., 2010), which proves the protein only hypothesis of the causative agent, prions; infectious prions were generated only from purified PrP^{C} and poly(A) RNA (Deleault *et al*., 2007) or from recombinant PrP (rPrP), phospholipid, and RNA (Wang *et al*., 2010) by PMCA.

RT-QuIC reaction, in which rPrP and materials containing PrP^{Sc} are treated with cycles of mixing and settling, detects the amyloid seeding activity of PrP^{Sc}. The formation of amyloid fibrils can be detected by the fluorescence of thioflavin T (ThT), an amyloid binding dye, using fluorescence microplate reader in real-time. RT-QuIC is much easier than PMCA but highly sensitive. Therefore, RT-QuIC reaction is also used for the diagnosis of prion diseases, disclosure of prion-infected animals, and detection of low levels of prions. RT-QuIC detects the amyloid seeding activity of PrP^{Sc}. However, this method interferes with the inhibitory factor(s) present in tissue homogenates and body fluids (Hoover *et al*., 2017; Orru *et al*., 2011; Wilham *et al*., 2010). Therefore, effect of inhibitory factor(s) must be reduced to detect low levels of prions from a high concentration of tissue homogenates. The concentration of PrP^{Sc} by immunoprecipitation or iron oxide beads that removes inhibitory factor(s) from samples, or removal of lipids by alcohol extraction, have been reported to reduce the influence of inhibitory factor(s) (Denkers *et al*., 2016; Hoover *et al*., 2017; Orru *et al*., 2012). However, a simpler method is still desirable for the practical application of RT-QuIC. rPrPs from bank vole (Bv) (Orru *et al*., 2015), hamster (Ha) (Henderson *et al*., 2015; Peden *et al*., 2012), and human (Hu) (Atarashi *et al*., 2011) have been widely used as substrates for RT-QuIC reactions. However, RT-QuIC reactions using these substrates tended to be affected by the inhibitory factor(s) in tissue homogenates. In the recent study in my laboratory, the use of cervid rPrP (rCerPrP) in RT-QuIC enables us to detect atypical BSE prions from tissues of cattle affected with atypical BSEs, even in the highest concentration of tissue homogenates from the CNS (Sawada *et al*.,

2019). The reason why RT-QuIC with rCerPrP is less affected by the inhibitory factor(s) in tissue homogenates than the other rPrPs remains to be elucidated; the mechanism will facilitate to improve RT-QuIC reaction.

In my doctoral dissertation, in Chapter I, I describe the mechanisms for PrP^{Sc}-specific reaction of mAb 132, which enables us to detect PrP^{Sc} in cells and tissues in immunocytochemistry and immunohistochemistry. In Chapter II, I describe the utility of rCerPrP in detecting BSE and CWD prions in RT-QuIC reaction, and in Chapter III I describe CWD monitoring in Japan using RT-QuIC with rCerPrP as a substrate.

CHAPTER I

Binding mechanisms of abnormal isoform of prion protein specific detection by anti-prion protein monoclonal antibody 132.

INTRODUCTION

Anti-PrP Abs have been used for the PrP^{Sc} detection. However, a high amino acid (aa) sequence similarity of PrP among animal species (Wopfner *et al*., 1999) and the same primary structure between PrP^{C} and PrP^{Sc} limited the production of Abs against species-specific epitope and PrP^{Sc}-specific Abs. Several PrP^{Sc}-specific mAbs have been produced so far (Horiuchi *et al*., 2009; Korth *et al*., 1997; Masujin *et al*., 2013; Moroncini *et al*., 2004; Paramithiotis *et al*., 2003; Ushiki-Kaku *et al*., 2010). These mAbs appeared to immunoprecipitate PrP^{Sc} specifically. However, efficacy of PrP^{Sc}-specific reaction in other experimental condition, such as immunohistochemistry is largely unclear.

In spite of such technical limitation, the pretreatment of fixed cells with a chaotropic agent such as guanidinium (Gdn) salt (Taraboulos *et al*., 1990) enabled the PrP^{Sc}-specific staining in IFA using pan-PrP Abs that can bind to both isoforms of PrP (Kascsak *et al*., 1987; Khalili-Shirazi *et al*., 2005; Peretz *et al*., 1997). However, the detection required the manipulation of detector gain or exposure time to decrease the signals from immunoreacted PrP^{C}. Recently, we reported mAb 132 recognizing mouse PrP (MoPrP) aa 119−127 is useful for reliable PrP^{Sc}-specific staining in cells or frozen tissue sections by IFA without PK treatment (Sakai *et al*., 2013; Tanaka *et al*., 2016; Yamasaki *et al*., 2014a; Yamasaki *et al*., 2012) and flow cytometry (Yamasaki *et al*., 2018), even though this mAb is classified as a group of pan-PrP Ab. We also reported that mAb 132 detects both PrP^{Sc}-sen and PrP^{Sc}-res if not all (Shan *et al*., 2016). Although brief pretreatment of cells or tissue sections with Gdn salt is still required for PrP^{Sc}-specific staining with mAb 132, this mAb shows little reactivity with native PrP^{C} in cells and tissues so that manipulation of conditions for acquiring fluorescence image can be minimized. Despite the benefit of mAb 132 in PrP^{Sc}-specific staining, the mechanism of the PrP^{Sc}-specific detection remains unclear.

In Chapter I, I extensively analyzed the reactivity and binding kinetics of mAb 132

and its derivatives by enzyme-linked immunosorbent assay (ELISA) and surface plasmon resonance (SPR) to clarify the mechanism of PrP^{Sc}-specific detection by mAb 132 in IFA.

MATERIALS & METHODS

1. Hybridomas culture and RNA extraction

Hybridomas producing mAbs 132 (epitope: MoPrP aa 119−127), 31C6 (epitope: MoPrP aa 143−149), and 44B1 (epitope: discontinuous epitope comprised of MoPrP aa 155−231) were cultured as described elsewhere (Kim *et al*., 2004b). Total RNA was extracted from hybridomas using TRIzol reagent (Life Technologies, USA) according to the manufacturer's instructions.

2. Expression plasmids of recombinant antibodies

2-1. Cloning of heavy and light chain of immunoglobulin genes

Cloning of heavy chain (HC) and light chain (LC) genes of mAb 31C6 (accession numbers: HC-31C6, LC026056; LC-31C6, LC026057), 44B1 (accession numbers: HC-44B1, LC037230; LC-44B1, LC037231) and 132 (accession numbers: HC-132, LC028384; LC-132, LC028385), and construction of expression plasmids for recombinant Ab (rAb) (Figure I-2B) were performed as shown in Figure I-1. Primers for cloning of full-length mAbs are shown in Table I-1. The cDNA encoding a part of variable regions of HC and LC (VH, VL) were amplified by RT-PCR using degenerate primers reported elsewhere (Kettleborough *et al*., 1993) (Figure I-1A). PCR products were cloned into pCRII-TOPO (Invitrogen, USA) and nucleotide sequences were determined using a BigDye terminator v3.1 Cycle Sequencing Kit (Applied Biosystems, USA) and ABI-3100 Avant sequencer (Applied Biosystems). Then, 5' and 3' cDNA fragments of HC and LC of mAbs 31C6 and 132 were amplified by 5' and 3' rapid amplification of cDNA end (RACE) as described previously (Horiuchi *et al*., 1997, 1998). The cDNA fragments encoding 5'-untranslated region (UTR) and VH and VL of mAb 44B1 were separately amplified by nested PCR, and two DNA fragments were assembled by assembly PCR (Stemmer *et al*., 1995). Finally, the full-length cDNA fragments of HC and LC of mAbs

31C6 and 44B1 were assembled as shown in Figure I-1A. Since both mAbs 132 and 31C6 are immunoglobulin G_1 (IgG_1) (Kim *et al*., 2004b) and nucleotide sequence analysis showed that they shared their primary structures of constant regions of HC and LC (CH, CL), the complete HC and LC genes of mAb 132 were assembled by replacing the cDNA fragments of the VH and VL of mAb 31C6 with the corresponding cDNA fragments of mAb 132, respectively (Figure I-1A). For the construction of recombinant antigen-binding fragment (rFab) gene (Figure I-2A), cDNA fragments coding VH-CH1 (Fd) region of mAbs 31C6, 44B1, and 132 were amplified from plasmids containing the corresponding HC genes using specific primers (Figure I-1B). Primers for construction of monovalent mAb genes are shown in Table I-2.

Table I-1. Specific primers for the cloning of Abs.

Constructs	Primer names *	Sequences
mAb 31C6	31C6VHF1 [a3]	5'-CTGTCTATCCACTGGCCCCT-3'
	31C6VHF2 [a3]	5'-ACCCTGGGATGCCTGGTCAA-3'
	31C6VHR1 [a1, a2]	5'-CGTGGTGTGCTGCTGGCCGGGT-3'
	31C6VHR2 [a2]	5'-CTGGCTGGGCCAGGTGCTGG-3'
	31C6VHR3 [a2]	5'-CTGGGAAGGTGTGCACACCG-3'
	31C6VLF1 [a3]	5'-GGAGTCCCATCAAGGTTCAG-3'
	31C6VLR1 [a1, a2]	5'-CGTGGTGCTGCTGGCCGGGT-3'
	31C6VLR2 [a2]	5'-GCCAGTGGATAGACTGATGG-3'
	31C6VLR3 [a2]	5'-TTGACCAGGCATCCCAGAGT-3'
mAb 44B1	ANC3'_SLIC [a2, a5]	5'-AATCTAGACTAAAGAATTCCAGTCAGTCAGTCATAGTC-3'
	44B1VHF1 [a3]	5'-CCCTGTGTGTGGAGGTACAA-3'
	44B1VHR1 [a1]	5'-CGCGGTGTTGCTGGCCGGG-3'
	44B15'VHR1 [a1]	5'-GGAGTTACTTGTACAGTA-3'
	44B15'VHR2 [a2]	5'-GGTGTTCCTGGCATTGTCTC-3'
	44B15'VHR3 [a2]	5'-TGGTGAATCGGCCCTTCACA-3'
	44B1VHR2 [a4]	5'-GGCTGGGCCAGGTGTTCGAG-3'
	44B1VHR3 [a4, a5]	5'-GACTGCAGGAGAGCTGGGAA-3'
	44B1VLF1 [a3]	5'-AGTGGGTCTAGGACAGACTT-3'
	44B15'VLR1 [a1]	5'-CCCCTCCGAATGTATACGGA-3'
	44B15'VLR2 [a2]	5'-GGTGAAGTCTGTCCTACACC-3'
	44B15'VLR3 [a2]	5'-GCCACTGAACCTGGCAGGGA-3'
	31C6VLR2 [a4]	5'-GCCAGTGGATAGACTGATGG-3'
	31C6VLR3 [a4, a5]	5'-TTGACCAGGCATCCCAGAGT-3'
mAb 132	ANC3'_SLIC [a2]	5'-AATCTAGACTAAAGAATTCCAGTCAGTCAGTCATAGTC-3'
	31C6VHF1 [a3]	5'-CTGTCTATCCACTGGCCCCT-3'
	31C6VHF2 [a3]	5'-ACCCTGGGATGCCTGGTCAA-3'
	31C6VHR1 [a1, a2]	5'-CGTGGTGTGCTGCTGGCCGGGT-3'
	31C6VHR2 [a2]	5'-CTGGCTGGGCCAGGTGCTGG-3'
	31C6VLR1 [a1, a2]	5'-CGTGGTGCTGCTGGCCGGGT-3'
	31C6VLR3 [a2]	5'-TTGACCAGGCATCCCAGAGT-3'
	31C6VLF1 [a3]	5'-GGAGTCCCATCAAGGTTCAG-3'
	132VLF [a3]	5'-GCCTGAAGATTTTGGGAGTT-3'

*: Superscript letters in primer name are corresponding to the steps of 5' or 3' rapid amplification of cDNA end (RACE), or assembly PCR shown in Figure I-1A. The detailed description is as follow:

a1: Primers used for the cDNA first strand synthesis for 5' RACE. The primer for 3'-RACE (dTAnc) has been shown elsewhere (Horiuchi *et al*., 1998).

a2: Primers for 5' RACE. The gene fragments encoding the 5'-terminal region of each chain were amplified by nested PCR. The forward primers for mAb 31C6 (ANC1, 3) and mAbs 44B1, 132 (ANC1) have been shown elsewhere (Horiuchi *et al*., 1998). The ANC3'_SLIC is modified primer of ANC3 including *Xba* I site (under lined sequence).

a3: Primers for 3' RACE. The 3'-terminal gene fragment of each heavy and light chain (HC, LC) was amplified by nested PCR. The reverse primers (dTAnc1, 2) have been shown elsewhere (Horiuchi *et al*., 1998).

a4: Gene fragments encoding variable and constant regions of HC (VH, CH), and those of LC (VL, CL) of mAb 44B1 were separately amplified using these primers with forward primers, V_{Kc} or V_{Hd} (Kettleborough *et al*., 1993).

a5: Assembly PCR primers for the 5'-terminal gene fragments of mAb 44B1. After assembling the product of 5' RACE and amplification of variable-constant region, assembled gene fragments only including the 5'-untranslated region (UTR) of mAb 44B1 were amplified.

Table I-2. Specific primers for the cloning of monovalent Abs.

Constructs	Primer names *	Sequences #
rFab-31C6	ANC3'_SLIC [b]	5'-AATCTAGACTAAAGAATTCCAGTCAGTCAGTCATAGTC-3'
	31C6Fd_R [b]	5'-TTTCTAGAACCACAATCCCTGGGCACAATTTTCTT-3'
rFab-44B1	ANC3'_SLIC [b]	5'-AATCTAGACTAAAGAATTCCAGTCAGTCAGTCATAGTC-3'
	44B1Fd_R [b]	5'-AATCTAGACTGTGTTATGGGCACTC-3'
rFab-132	ANC3'_SLIC [b]	5'-AATCTAGACTAAAGAATTCCAGTCAGTCAGTCATAGTC-3'
	132Fd_R [b]	5'-TTTCTAGAACCACAATCCCTGGGCACAATTTTCTT-3'
rFab-132-F2A[$]	132LC_F [c1, c4]	5'-AATCTAGAATGAGTGTGCTCACTCAGGTCCTG-3'
	132LC_2A_R [c1]	5'-CAACTTGAGAAGGTCAAAATTCAAAGTCTGTTTCACACACTCATTCCTGTT-3'
	F2A_R1 [c3]	5'-CAACTTGAGAAGGTCAAAATTCAAAGTCTGTTT-3'
	F2A_R2 [c3]	5'-CTCCACGTCCTCCCGCCAACTTGAGAAGGTCAAA-3'
	F2A_F [c3]	5'-TGGCGGGAGACGTGCACTCCAACCCAGGGCCCA-3'
	132Fd_2A_F [c2]	5'-TCCAACCAGGGCCCATGGGATGGAGCTGTATC-3'
	132Fd_Myc_R [c2, c4]	5'-ACCAGAACCGCCACCGCCTGATACTTCTGGGAC-3'

*: Superscript letters in primer name are corresponding to the steps of PCR shown in Figures I-1B and C. The detailed description is as follow:
b: Primers for the amplification of VH-CH1 (Fd) region of mAbs 31C6, 44B1 and 132 (Figure I-1B).
c1 and c2: Primers used for the amplification of gene fragment including LC with 2A fragment from foot-and-mouth virus (F2A) portion (c1), Fd region with F2A portion (c2) (Figure I-1C).
c3: Primers used for the elongation of F2A portion of the fragment of LC and Fd with F2A (Figure I-1C).
c4: Primers for the assembly PCR to amplify the fusion genes with F2A (Figure I-1C).
#: Under line in the sequences indicates *Xba* I site.
$: Any expression plasmid for rFab-F2A was not obtained because the constructs never cloned without irregular single base addition in the F2A sequence even though the same primers for construction of rF(ab')$_2$-132-enhanced green fluorescent protein (EGFP) (Table I-3) were used.

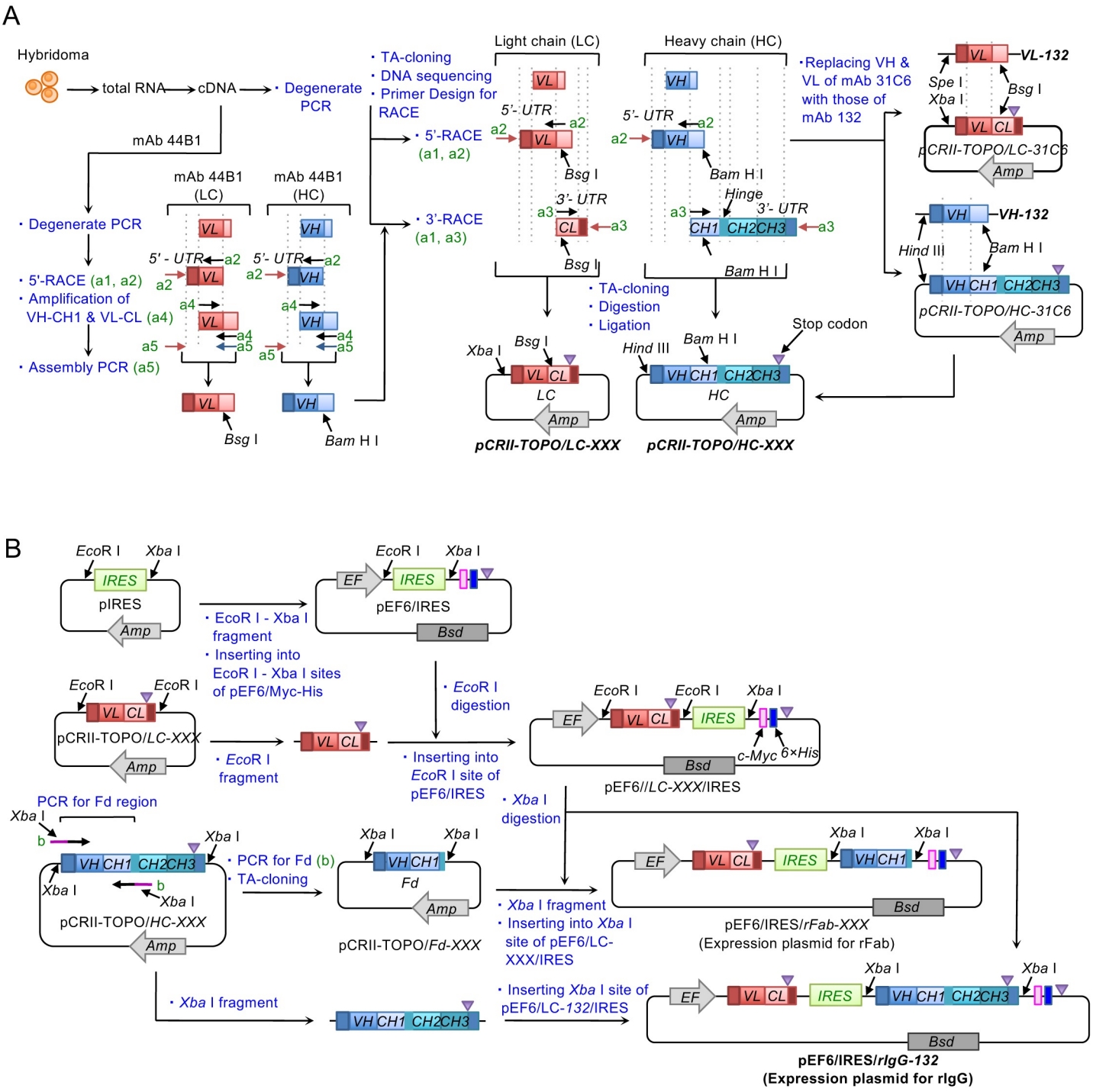

Figure I-1 Strategy for molecular cloning of antibodies and construction of the expression plasmids.
(A) Cloning of monoclonal antibodies (mAbs) 31C6, 44B1 and 132. DNA fragments of light chain (LC) and heavy chain (HC) amplified by degenerate PCR, and 5' or 3' rapid amplification of cDNA end (RACE) are indicated in the same color as shown in Figures I-2A and B. The fragments encoding variable region of HC (VH) and variable region of LC (VL), and constant regions of HC1 (CH1) and constant regions of LC (CL) in the amplified fragments are laid to overlap each other. The restriction enzyme in each step indicates the unique enzymes used for assembling full length genes. The assembling the DNA fragment from 5'-untranslated region (UTR) to CH or CL of mAb 44B1 is indicated in the left part, whereas the replacement the of VH and VL of mAb 31C6 with those of mAb 132 is shown in the right part. Names for completed plasmid are indicated in bold. (B) Construction of the bicistronic plasmid with internal ribosomal entry site (IRES). Restriction enzymes used for digestion are shown in each step. Arrows at the top and bottom on HC-132 indicate the specific primers to amplified the DNA fragment encoding VH-CH1 (Fd)-132 without stop codon of recombinant antigen-binding fragment (rFab) (Table I-2). Primers containing the *Xba* I site are indicated with purple.

C

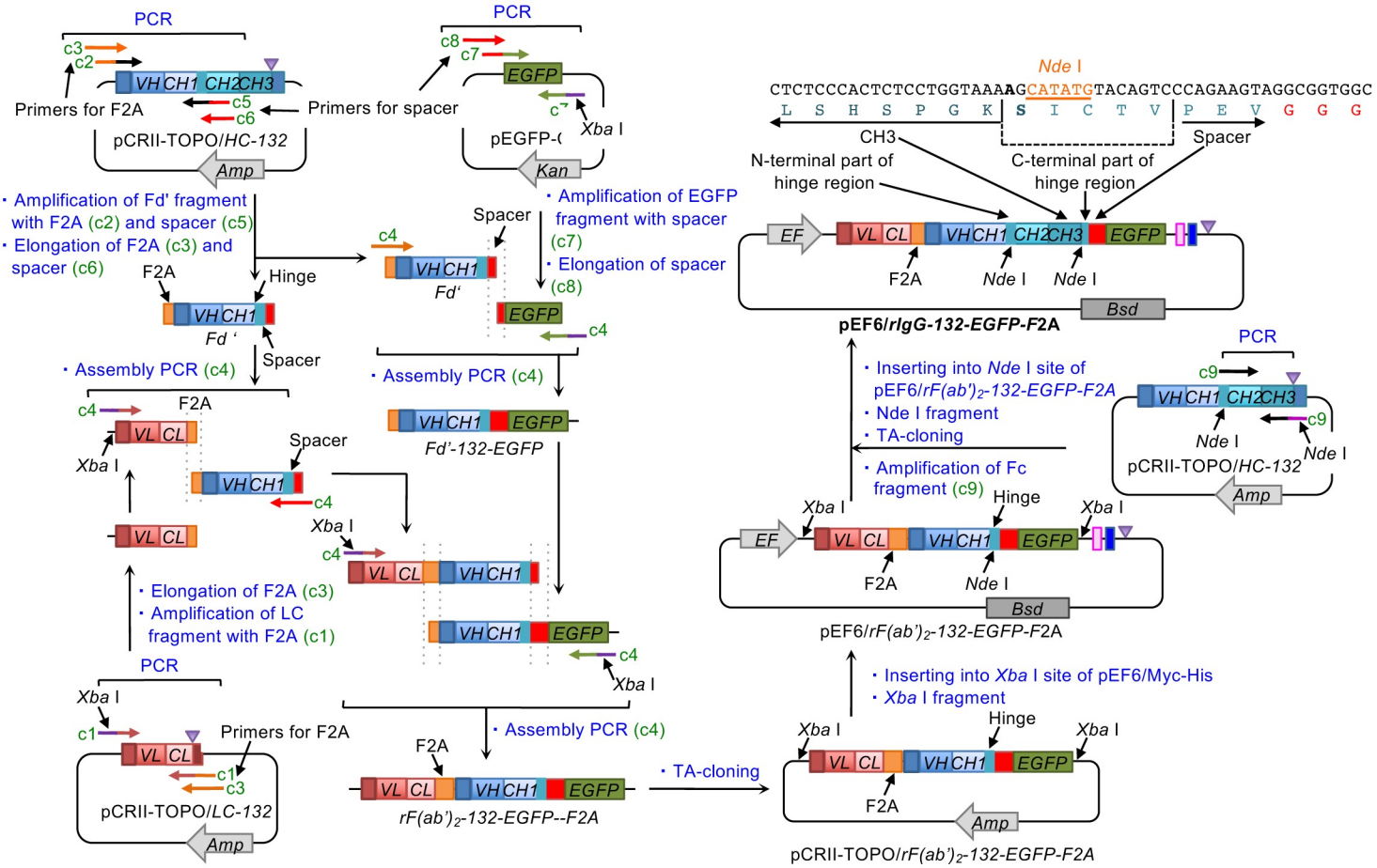

Figure I-1 continued.

(C) Construction of the expression plasmid for rF(ab')$_2$-enhanced green fluorescent protein (EGFP) (Figure I-4A) fused with self-cleavage 2A peptide from foot-and-mouth virus (F2A). The amplified fragments encoding LC, Fd region and EGFP were indicated with the same color as shown in Figures I-2A, B and 4A. Region-specific sequences in primers (Table I-3) were drawn in dark pink (LC), orange (F2A), red (spacer, GGGGSGGGGSGGGGS), dark green (EGFP), and black (Fd, CH2 (not shown) or Fc). The *Xba* I or *Nde* I site in primers was drawn in purple. In assembly PCR, the complementary regions in amplified fragments are laid to overlap each other. The nucleotide and deduced aa sequences at the connected region of rIgG-132-EGFP were shown uppermost. The bold "A" and underlined letter indicates the nucleotide substitution for the mutation Cys to Ser and the *Nde* I site, respectively.

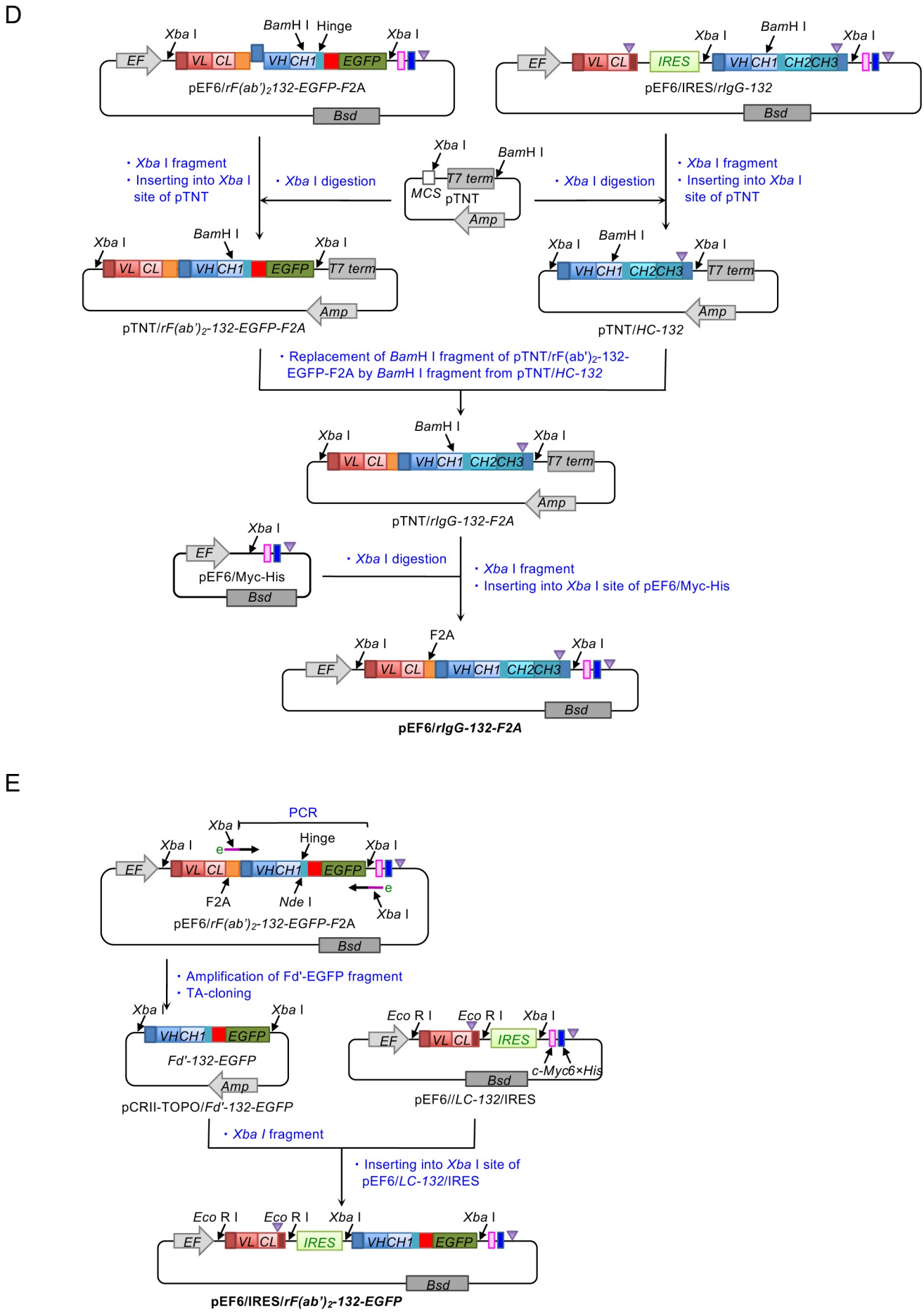

Figure I-1 continued.
(D, E) Methods for exchanging the gene fragments from (D) F2A to IRES, or (E) IRES to F2A.

2-2. Construction of bicistronic expression plasmids

The bicistronic expression plasmids with gene fragment encoding internal ribosome entry site (IRES) (Jostock *et al*., 2004) were constructed as shown in Figure I-1B. The gene fragment encoding IRES amplified from pIRES vector (Clontech, USA) was cloned into the *Eco*R I and *Xba* I sites of pEF6/Myc-His (Invitrogen) to generate pEF6/IRES/Myc-His. The cDNA fragments encoding the LC of mAbs 31C6, 44B1, and 132 were inserted into the *Eco*R I site of pEF6/IRES/Myc-His. Then, the cDNA fragments encoding Fd (VH-CH1) region of mAbs 31C6, 44B1, and 132 or entire HC of the mAb 132 were sequentially inserted into the *Xba* I site (Figures I-1B, I-2A and B).

2-3. Construction of expression plasmids with self-cleavage 2A peptide region from foot-and-mouth virus

The expression plasmid for the production of the Fab fragment and IgG was also constructed using the gene fragment of self-cleavage 2A peptide region from foot-and-mouth virus (F2A) (Donnelly *et al*., 2001). Schematic illustration for construction is shown in Figure I-1C and D. For assembling the fusion gene for expressing rFab-132 with F2A, DNA fragments encoding LC without stop codon and Fd region of mAb132 were amplified from pCRII-TOPO/LC-132 and pCRII-TOPO/HC-132, respectively. The F2A fragment was elongated onto both PCR products by sequentially performed PCR using primers with F2A sequences. Then, assembly PCR was carried out using primers, 132LC_F and 132Fd-Myc_R (Table I-2). The expression plasmid for rIgG-132 with F2A was constructed by replacing the HC fragment with that of rF(ab')$_2$-132-enhanced green fluorescent protein (EGFP) (Figure I-4A) as shown in Figure I-1D. pTNT vector (Promega, USA) was used for the replacing the gene fragment.

2-4. Construction of the expression plasmids for fusion proteins of mAb 132 and EGFP

The fusion genes of mAb 132 and EGFP, which are referred as mAb 132-EGFP (Figure I-4A) were constructed by assembly PCR (Stemmer *et al*., 1995). Primers for construction of mAb 132-EGFP are shown in Table I-3. pEGFP-C1 vector (Clontech) was used for the amplification of the gene fragment coding EGFP. To construct a bicistronic expression plasmid for monovalent rFab-132-EGFP, the assembled Fd-EGFP gene was inserted into the *Xba* I site of pEF6/LC-132/IRES (Figure I-1B). The expression plasmid for rFab-132-EGFP fused with F2A was constructed by the same method as rIgG-132-F2A (Figure I-1D).

On the other hand, the fusion gene expressing bivalent mAb 132-EGFP with F2A was assembled as shown in Figure I-1C. Mainly, each DNA fragment of rF(ab')$_2$-132-EGFP encoding LC without stop codon, VH-CH1-hinge (Fd') region, and EGFP without first methionine was amplified from the corresponding plasmids. The F2A and spacer fragments were elongated onto the PCR products using another set of primers. Then, fusion genes encoding Fab'-F2A and F2A-Fd'-EGFP were assembled by assembly PCR. Finally, the entire fusion gene encoding rF(ab')$_2$-132-EGFP with F2A was assembled by assembly PCR using 132LC_F and EGFP_R. After TA-cloning and sequence determination, excised rF(ab')$_2$-132-EGFP-F2A gene with *Xba* I was inserted into pEF6/Myc-His. Then, the fusion gene expressing CH3 deleted rIgG-132-EGFP (rIgG(ΔCH3)-132-EGFP) and rIgG-132-EGFP (Figure I-4A), with F2A were constructed using rF(ab')$_2$-132-EGFP-F2A gene as follow (Figure I-1C). DNA fragments encoding CH2 and CH2-CH3 (fragment crystallization (Fc)) regions were amplified by PCR using specific primers (Table I-3). After TA-cloning and sequence determination, each fragment excised with *Nde* I was inserted into the *Nde* I site of pEF6/rF(ab')$_2$-132-EGFP-2A.

To construct the bicistronic expression plasmids for rF(ab')$_2$-132-EGFP, rIgG(ΔCH3)-132-EGFP and rIgG-132-EGFP, DNA fragments encoding Fd'-EGFP, Fd'-CH2-EGFP and Fd'-

Fc-EGFP was amplified from corresponding expression plasmid with F2A using Fd-EGFP_F and EGFP_R. After TA-cloning and sequence determination, each *Xba* I digested fragment was inserted into the *Xba* I site of pEF6/LC-132/IRES (Figure I-1E).

Table I-3. Specific primers for construction of fusion proteins.

Constructs	Primer names *	Sequences $
rFab-132-EGFP	ANC3'_SLIC c0	5'-AATCTAGACTAAAGAATTCCAGTCAGTCAGTCATAGTC-3'
	ANC3'_SLIC c0	5'-AATCTAGACTAAAGAATTCCAGTCAGTCAGTCATAGTC-3'
	132EGFP1_R c0	5'-CTTGCTCACACCACAATCCCTGGGCACAAT-3'
	132EGFP1_F c7	5'-CCCAGGGATTGTGGTGTGAGCAAGGGCGAG-3'
	EGFP_R c7	5'-AATCTAGACTTGTACAGCTCGTCCATGCCGAGAGT-3'
rF(ab')$_2$-132-EGFP	132LC_F c1, c4	5'-AATCTAGAATGAGTGTGCTCACTCAGGTCCTG-3'
	132LC_2A_R c1	5'-CAACTTGAGAAGGTCAAAATTCAAAGTCTGTTTCACACACTCATTCCTGTT-3'
	F2A_R1 c3	5'-CAACTTGAGAAGGTCAAAATTCAAAGTCTGTTT-3'
	F2A_R2 c3	5'-CTCCACGTCCTCCCGCCAACTTGAGAAGGTCAAA-3'
	F2A_F c3, c4	5'-TGGCGGGAGACGTGCACTCCAACCCAGGGCCCA-3'
	132Fd_2A_F c2	5'-TCCAACCAGGGCCCATGGGATGGAGCTGTATC-3'
	132Fd_G4S_R c5	5'-ACCAGAACCGCCACCGCCTGATACTTCTGGGAC-3'
	Gly4Ser_R c4, c6	5'-ACCGCCGGAGCCACCGCCACCAGAACCGCCACC-3'
	G4S_EGFP_F1 c7	5'-GGCGGTTCTGTGAGCAAGGGCGAGGAGCTGTTC-3'
	G4S_EGFP_F2 c8	5'-GGTGGCTCCGGCGGTGGCGGTTCTGTGAGCAAG-3'
	EGFP_R c4, c7, e	5'-AATCTAGACTTGTACAGCTCGTCCATGCCGAGAGT-3'
	132Fd_EGFP_F e	5'-AATCTAGAATGGGATGGAGCTGTATCATCCTCTTT-3'
rIgG(ΔCH3)-132-EGFP	132Fc_F c9	5'-AAGCCTTGCATATGTACAGTCCCAGAAGTA-3'
	132CH2_R c9	5'-TTTCATATGCTGCCTTTGGTTTTGGAGATGGT-3'
rIgG-132-EGFP	132Fc_F c9	5'-AAGCCTTGCATATGTACAGTCCCAGAAGTA-3'
	132Fc_R c9	5'-TTTCATATGCTTTTACCAGGAGAGTGGGAGAG-3'

*: Superscript letters in primer name are corresponding to the steps of PCR shown in Figures I-1C and E. The detailed description is as follow:
c0: Primers used for amplification of Fd region of rFab-132-EGFP. After assembling with separately amplified EGFP without spacer, Fd-EGFP gene was inserted into pEF6/*LC-132*/IRES (Figure I-1B).
c1-c4: The same usage of c1-c4 in Table I-2.
c5: Primer for the addition of the spacer sequence at the 3'-terminus of Fd' fragment.
c6 and c8: Primers for the elongation of the spacer sequence onto Fd' fragment (c6) or EGFP (c8).
c7 and c9: Primers for the amplification of EGFP (c7) or Fc fragments (c9).
e: Primers for the amplification of Fd'-132-EGFP gene from pEF6/*rF(ab')$_2$-132-EGFP-2A* (Figure I-1E).
$: Under line in the sequences indicates *Xba* I or *Nde* I site. Bold "T" in 132Fc_R and 132Fc_R indicate the nucleotide substitution for the amino acid substitution from Cys to Ser (Figure I-1C).

3. Expression and purification of recombinant Abs

3-1. Expression of recombinant Abs

HEK293T cells were split in a ratio of 1:10 into 6 cm dishes 36 h before transfection. Plasmids for expression of rAb fragments (4 μg) were transfected using Lipofectamine 2000 reagent (Invitrogen) according to the manufacturer's instructions. Twenty-four hours after transfection, the medium was replaced with DMEM containing 10% fetal bovine serum (FBS) (Gibco, USA) and 1% Penicillin Streptomycin (Gibco) and the cells were incubated for 24 h. Then, the cells were fed with fresh Opti-MEM and incubated for further 48 h and 96 h, for the expression plasmids containing an IRES (Jostock *et al*., 2004) and F2A (Donnelly *et al*., 2001), respectively. On the other hand, transfection of the expression plasmids containing IRES and F2A into 293F cells (Invitrogen) was performed according to the manufacturer's instructions with minor modifications. The 293F cells passaged at least five time were split at 0.7×10^6/ml into 250 ml spinner flasks (Corning, USA) using 80−100 ml FreeStyle 293 Expression Medium (Gibco) containing 0.5% Antibiotics/Antimycotic (Gibco). After incubation for 24 h, plasmids mixed with 293Fection Transfection reagent (Invitrogen) in Opti-Pro MEM (Gibco) were added into the 293F cell suspension at 1.0×10^6/ml with FreeStyle 293 Expression Medium. The cells were cultured for 4 days at 37˚C with 8% CO_2.

3-2. Purification of recombinant Abs

The culture supernatants from 293F cells were dialyzed twice against phosphate-buffered saline (PBS, pH 7.2) using Spectra/Pore 7 (Funakoshi, Japan) at 4˚C. After removal of precipitates by centrifugation at 2,300 ×g for 5 min at 4˚C, the supernatant was loaded onto a Ni^{2+}-immobilized 5 ml HiTrap Chelating HP column (GE Healthcare, UK) by circulating the supernatant for 6 h. After washing the column with 20 ml PBS, 1M imidazole in PBS was applied to elute bound materials and the elutes were manually collected as 1 ml fractions.

Fractions containing rFab-132, rFab-132-EGFP, and rIgG-132-EGFP were further loaded onto a HiLoad 16/600 Superdex 200 pg column (GE Healthcare) and separated using ÄKTAexplore 10S system (GE Healthcare) at a flow rate of 1.5 ml/min. After discarding the first 20% column volume as a void fraction, the isocratic elutes were collected in 1.5 ml fractions. In the case of rIgG-132, Protein G Sepharose 4 Fast Flow (GE Healthcare) was used for purification.

4. Immunostaining

4-1. Immunoblotting

SDS-PAGE and western transfer under non-reducing condition were carried out as described previously (Kim *et al*., 2004b) without using 2-mercaptoethanol or an antioxidant. After blocking of Immobilon-P transfer membrane (Millipore, USA) with 5% skim milk, Fab regions were directly probed with 1:5,000 diluted Anti-Mouse IgG (Fab specific)-Peroxidase antibody produced in goat (Sigma, USA). Antigen (Ag)-antibody complexes were visualized with ECL Western Blotting Detection Reagents (GE Healthcare) using LAS-3000 chemiluminescence image analyzer (Fujifilm, Japan).

4-2. ELISA

ELISA using recombinant MoPrP (rMoPrP) as Ag was carried out as described elsewhere (Kim *et al*., 2004b). rMoPrP pretreated with 6 M Gdn hydrochloride (HCl) (2 ng/μl) was adsorbed to the wells (100 ng/well) of a U96 Maxisorp Nunc-immuno plate (Nunc, Denmark) overnight at room temperature (r.t.). After blocking with 5% FBS in PBS containing 0.1% Tween 20 (PBST), the wells were incubated with primary Abs for 1 h at r.t. After washing with PBST, wells were incubated with 100 μl of 1:5,000 diluted Anti-Mouse IgG (Fab specific)-Peroxidase antibody produced in goat in PBST containing 0.5% FBS. Finally, antigen-antibody complexes were detected by adding 100 μl of 3, 3', 5, 5'-tetramethylbenzodine (Sigma)

colorimetric substrate, and the absorbance at 450 nm was measured with an Ascent micro-plate reader (Labsystems, Finland).

4-3. PrP^{Sc}-specific immunofluorescence staining

PrP^{Sc}-specific immunofluorescence staining was performed as described elsewhere (Yamasaki *et al*., 2014b; Yamasaki *et al*., 2012) with minor modification. Briefly, cells in eight-well chamber were fixed with 4% paraformaldehyde (PFA), and remaining PFA was quenched with 100 mM glycine in PBS. Cells were then permeabilized with 0.1% Triton X-100 in PBS, and treated with 5 M Gdn thiocyanate (SCN) for 15 min at r.t. After blocking with 5% FBS in PBS (FBS-PBS) for 30 min at r.t., cells were incubated with recombinant mAb 132 fragments or Alexa Fluor 647 labeled mAb 132 overnight at 4˚C. Cell nuclei were stained with 4', 6'-diamino-2-phenylindole, dilactate (DAPI).

The immunofluorescence staining for frozen sections was performed as described elsewhere (Sakai *et al*., 2013; Yamasaki *et al*., 2018) with minor modifications. Briefly, the frozen brain sections were fixed and permeabilized as described above. Then, the sections were treated with 2.5 M GdnSCN for 15 min at r.t. The sections were blocked with 5% FBS-PBS for 1 h at r.t. and were incubated with anti-PrP mAbs or anti-panleukopenia virus mAb P2-284 (Horiuchi *et al*., 1997) used as a negative control at 1 μg/ml in 1% FBS-PBS overnight at 4˚C. The bound Abs were probed with 0.4 μg/ml Alexa Fluor 488 $F(ab')_2$ fragment of goat anti-mouse IgG (H+L) (Invitrogen) in 1% FBS-PBS for 1 h at r.t. Cell nuclei were stained with DAPI, and the sections were mounted with ProLong Glass antifade mountant (Invitrogen). The fluorescent images were acquired using LSM700 and analyzed with ZEN software (Zeiss, Germany) as described elsewhere (Yamasaki *et al*., 2014a; Yamasaki *et al*., 2014b).

5. SPR

The affinity of Ab binding was determined from SPR sensorgrams measured in multi- and single-cycle kinetics analysis using Biacore X100 (GE Healthcare). Multi-cycle kinetics analysis was performed as follows: mAbs 31C6 and 132 were directly immobilized on the surface of a CM5 sensorchip (GE Healthcare) as ligands at approximately 1,000 response unit (RU) according to the manufacturer's instructions. The real-time association responses of injected rMoPrP as analyte to Abs were measured for 180 sec. After measuring the association phase, the dissociation responses were measured while the surface of the sensorchip was washed with HBS-EP+ buffer (GE Healthcare) for 600 sec. The sensorchip was regenerated with 10 mM NaOH according to the manufacturer's instructions.

Single-cycle kinetics analysis using rMoPrP as a ligand was performed as follows: 1,706.7 and 140.9 RU of rMoPrP were immobilized on a CM5 sensorchip using 1 μM and 100 nM rMoPrP, respectively. The association responses of Abs to rMoPrP were measured for 120 sec, and then the dissociation responses were measured for 3,600 sec for IgG-31C6 and IgG-132, and 600 sec for rFab-31C6 and rFab-132, respectively. For repeated measurements, the sensorchip was regenerated once (80 sec for rFab-31C6 and IgG-31C6) or twice (80 and 60 sec for rFab-132 and IgG-132, respectively) with 10 mM NaOH.

The binding responses of IgG-132 and IgG-31C6 captured on the sensorchip to rMoPrP were measured as follows. Anti-mouse IgG antibody in the Mouse Antibody Capture Kit (GE Healthcare) was immobilized on a CM5 sensorchip according to the manufacturer's instructions. Then, 10 nM of IgG was applied until the response reached approximately 500 RU. The association and dissociation responses for injected rMoPrP were measured for 120 sec and 600 sec, respectively. Data processing and determination of association rate constant (k_a), dissociation rate constant (k_d), and dissociation constant (K_D) by fitting were performed using BIAevaluation software (GE Healthcare).

RESULTS

1. Production of recombinant mAb 132

It has been reported that mAb 132 hardly reacts with native PrP^{C} molecule on the cell surface (Kim *et al*., 2004a) but reacts with denatured PrP^{C} and PrP^{Sc} in immunoblot analysis and rPrP in ELISA (Kim *et al*., 2004b), suggesting that this mAb is classified as a pan-PrP mAb. To examine the mechanism of the PrP^{Sc}-specific detection by mAb 132 in IFA, I cloned the heavy and light chains genes of this mAb and constructed expression plasmids for mono- and bivalent forms of rAbs (rFab and rIgG) (Figure I-2A) and their derivatives (Figure I-4A).

Two expression systems were used to co-express the two peptide chains of heavy and light chain from a single plasmid (Figure I-2B); one system was bicistronic expression using IRES (Jostock *et al*., 2004) and the other was C-terminal cleavage by ribosomal skipping using a self-cleavage 2A peptide from F2A peptide (Donnelly *et al*., 2001). I could construct all the expression plasmids using IRES for rFabs 132, 31C6 and 44B1 and recombinant mAb 132 (rIgG-132). However, I successfully obtained only the expression plasmids using F2A peptide for rIgG-132 because constructs for rFab of mAbs 132, 31C6 and 44B1 could not be subcloned without an irregular single base insertion in the region coding the F2A peptide. The expression and assembly of rIgG-132 and rFabs in the culture supernatants of HEK293T cells transfected with each expression plasmid were evaluated by immunoblotting (Figure I-2C). Expression plasmid with F2A produced a lesser amount of rIgG-132 than that with IRES. However, bicistronic expression using IRES produced considerable amount of free and dimeric light chains (Figure I-2C, LC and LC_2, respectively), which were not observed in the use of the expression plasmid with F2A. The production of such byproducts was also observed in the supernatants of rFabs (rFab-132, rFab-31C6 and rFab-44B1) using IRES (Figure I-2C). These results suggest that the expression plasmids with F2A peptide are preferable for producing rAbs because of traces of unwanted byproducts such as LC and LC_2.

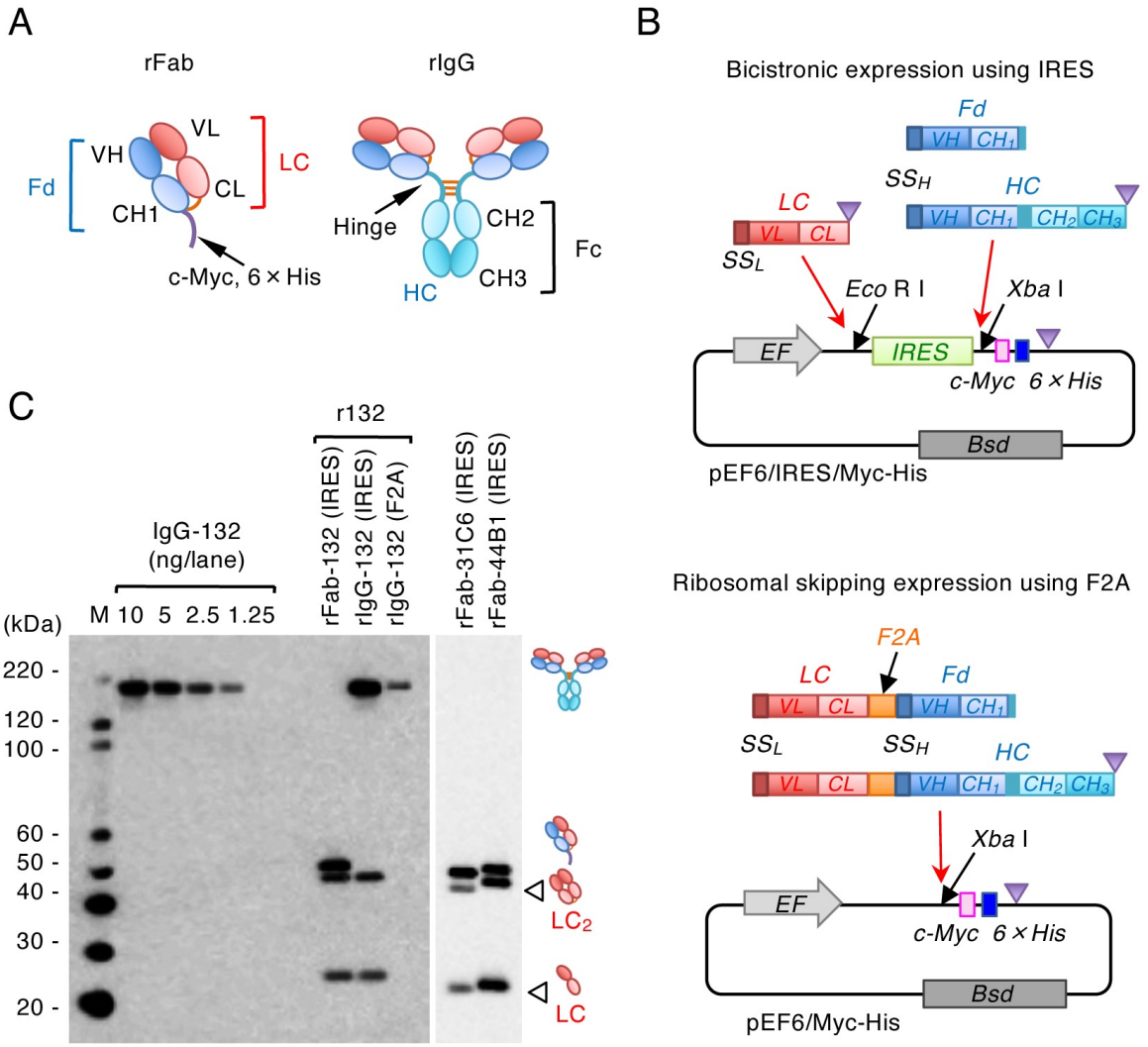

Figure I-2 Production of recombinant antibody fragments.

(A) Molecular design of mono- (rFab) and bivalent (rIgG) forms. The light chain (LC) and heavy chain (HC) or VH-CH1 (Fd) region are depicted with reddish and bluish colors, respectively. Intermolecular disulfide bonds are drawn in orange lines, whereas the C-terminal epitope tail comprised of c-Myc epitope (c-Myc) and a hexa-histidine tag (6 × His) is drawn in purple. Fc, fragment crystallization; CH1−3, constant regions 1−3 of HC; CL, constant region of LC; VH, variable region of HC; VL, variable region of LC. (B) Schematic illustration of two expression systems. DNA fragments for an IRES and self-cleavage 2A peptide from F2A are shown in green and orange, respectively. For producing antibody fragments into culture supernatants, HC and LC genes possess their own signal sequences (SS_H and SS_L). EF, a promoter of the human elongation factor gene; Bsd, blasticidine-resistant gene. (C) Analysis of molecular assembly of antibody (Ab) fragments. Immunoblot analysis was carried out using authentic mAb 132 (IgG-132, 1.25−10 ng/lane) and supernatants of HEK293T cells transfected with expression plasmids containing IRES (rFab, rIgG) or F2A (rIgG) under non-reducing condition. Corresponding pictures on the right indicate the band of IgG, rIgG, or rFab, whereas arrowheads indicate the bands of free and dimeric LC (LC_2). Molecular mass markers on the left are in kDa.

2. Reactivity of mono- and bivalent forms of recombinant mAb 132 fragments to rMoPrP

The reactivity of the mono- and bivalent forms of mAb 132, rFab-132 and rIgG-132 to rMoPrP were assessed using ELISA (Figure I-3). Supernatants of HEK293T cells transfected with each expression plasmid were used for the immunoreaction after estimation of concentrations equivalent to Fab portion by immunoblot analysis. The reactivities of rFab-31C6 and rFab-44B1, rFab fragments of pan-PrP mAbs 31C6 and 44B1, respectively, were comparable to those of the corresponding authentic IgGs. In contrast, the reactivity of rFab-132 was much weaker than that of authentic IgG (IgG-132) and rIgG-132. The rFab-132 reacted very weakly even at the highest concentration used (0.3 nM), whereas rIgG-132 and IgG-132 reacted positively even at the 30-fold lower concentration (0.009 nM) (Figure I-3A). The Ag concentration-dependent reactivity of these Abs was shown in Figure I-3B. rFab-31C6 and rFab-44B1 showed the similar reactivity to each of the authentic IgGs. However, rFab-132 could not bind to rMoPrP efficiently compared to rIgG-132 and IgG-132. It was worth noting that the reactivity of IgG-132 and rIgG-132 was decreased depending on the concentration of rMoPrP compared to those of IgG-31C6 and IgG-44B1, suggesting a larger amount of rMoPrP may be required to obtain efficient binding of mAb 132 than mAbs 31C6 and 44B1 even though the bivalent binding may increase the binding efficacy of mAb 132.

To confirm the reactivity of the mono- and bivalent forms of mAb 132, rFab-132 and rIgG-132 were purified from the supernatants of spinner-cultured HEK293F cells transfected the corresponding expression plasmids using Ni^{2+} and Protein G affinity chromatography, respectively. Immunoblot analysis of the purified Abs were carried out to estimate the concentration equivalent to Fab portion and to evaluate efficient removal of LC products (Figure I-3C). The reactivity of the purified Abs was assessed by ELISA. IgG-132 and rIgG-132 gave a result of 3 OD_{450} at around 2 nM, whereas approximately 10 nM of rFab-132 was

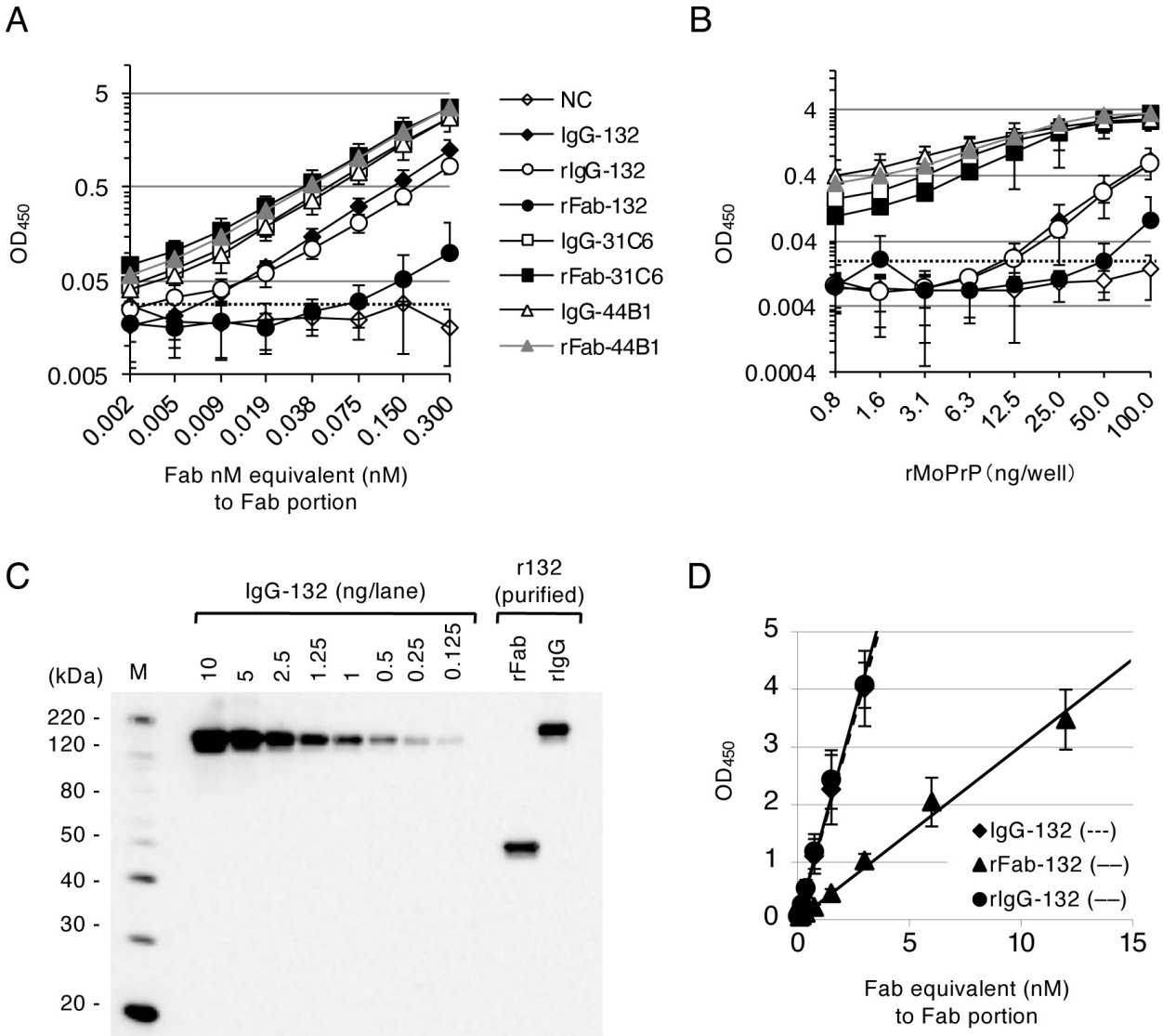

Figure I-3 Reactivity of recombinant antibody fragments in ELISA.

(A) Reactivity of authentic and recombinant Abs (rAbs). Twofold serially diluted Abs (0.002−0.3 nM Fab equivalent) were added to wells coated with 100 μg/well recombinant mouse PrP (rMoPrP). Purified IgG was used for authentic mAbs, whereas the supernatants of HEK293T cells transfected with each expression plasmid was used for rAbs after estimation of concentrations equivalent to the Fab portion by immunoblot analysis using serially diluted purified authentic IgG as a standard. Reactivities of authentic IgG and rIgG of mAbs 132, 31C6 and 44B1 as well as their rFab fragments are shown by plotting mean absorbances at 450 nm of each dilutions. The supernatant of HEK293T cells transfected without any plasmids was used as a negative control (NC). SD calculated from three independent experiments are shown. Dotted line indicates a cutoff values calculated by the mean plus 3 × SD. (B) Reactivity of authentic and rAbs dependent on antigen concentration. Twofold serially diluted rMoPrP (0.8−100 ng/well) was adsorbed to wells and 0.3 nM Abs equivalent to the Fab portion were used for the detection. (C) Quantification of purified rFab-132 and rIgG-132. Concentration of rFab-132 and rIgG-132 was estimated using twofold serially diluted authentic IgG-132 (0.125−10 ng). (D) Difference in reactivity of mono- and bivalent forms of mAb 132. The 100 μg/well rMoPrP and twofold serially diluted purified rFab-132 (0.09−12 nM), IgG-132 and rIgG-132 (0.02−3 nM) were used for the detection.

required to obtain the same level of reaction (Figure I-3D). Since the IgG concentration was estimated according to the Fab portion, the number of IgG molecules was half of that of Fab fragments. Therefore, the reactivity of monovalent rFab-132 was roughly estimated as one-tenth of that of the bivalent IgG form.

3. Production of recombinant mAb 132-EGFP fusion proteins

MAb 132 fused with EGFP could be useful for a direct detection of PrP^{Sc} in multiple immunofluorescence staining. Thus, I attempted to produce four EGFP fusion proteins, rFab-132-EGFP, rF(ab')$_2$-132-EGFP, rIgG(ΔCH3)-132-EGFP lacking the CH3 domain, and rIgG-132-EGFP (Figure I-4A). The EGFP gene was fused to the 3' ends of gene fragments encoding various HC genes of mAb 132 via a DNA fragment encoding a spacer peptide GGGGSGGGGSGGGGS for the bivalent form of mAb 132-EGFP (Figure I-4A) because the spacer would be useful in avoiding an interaction that affects proper folding of the HC region and EGFP (Cutler *et al*., 2009; Weiss and Orfanoudakis, 1994). The mAb 132-EGFP fusion proteins were expressed in HEK293T cells by a single plasmid with IRES or F2A peptide.

The expression and assembly of mAb 132-EGFP was assessed using the culture supernatants of HEK293T cells. Similar to the expression of rFab-132 and rIgG-132 shown in Figure I-2C, bicistronic expression using IRES produced LC, LC_2, and assembly intermediates (Figure I-4B, indicated with arrowheads), which were not observed with expression plasmids with F2A. Bivalent Abs were produced only from the expression plasmid for rIgG-132-EGFP containing CH3 domain in Fc region but not from those for rF(ab')$_2$-132-EGFP, rIgG(ΔCH3)-132-EGFP lacking the CH3 domain (Figure I-4B). These results indicate that the CH3 domain is required for efficient formation of heterotetrameric IgG molecules comprised of two LC and two HC, as reported previously (Ridgway *et al*., 1996).

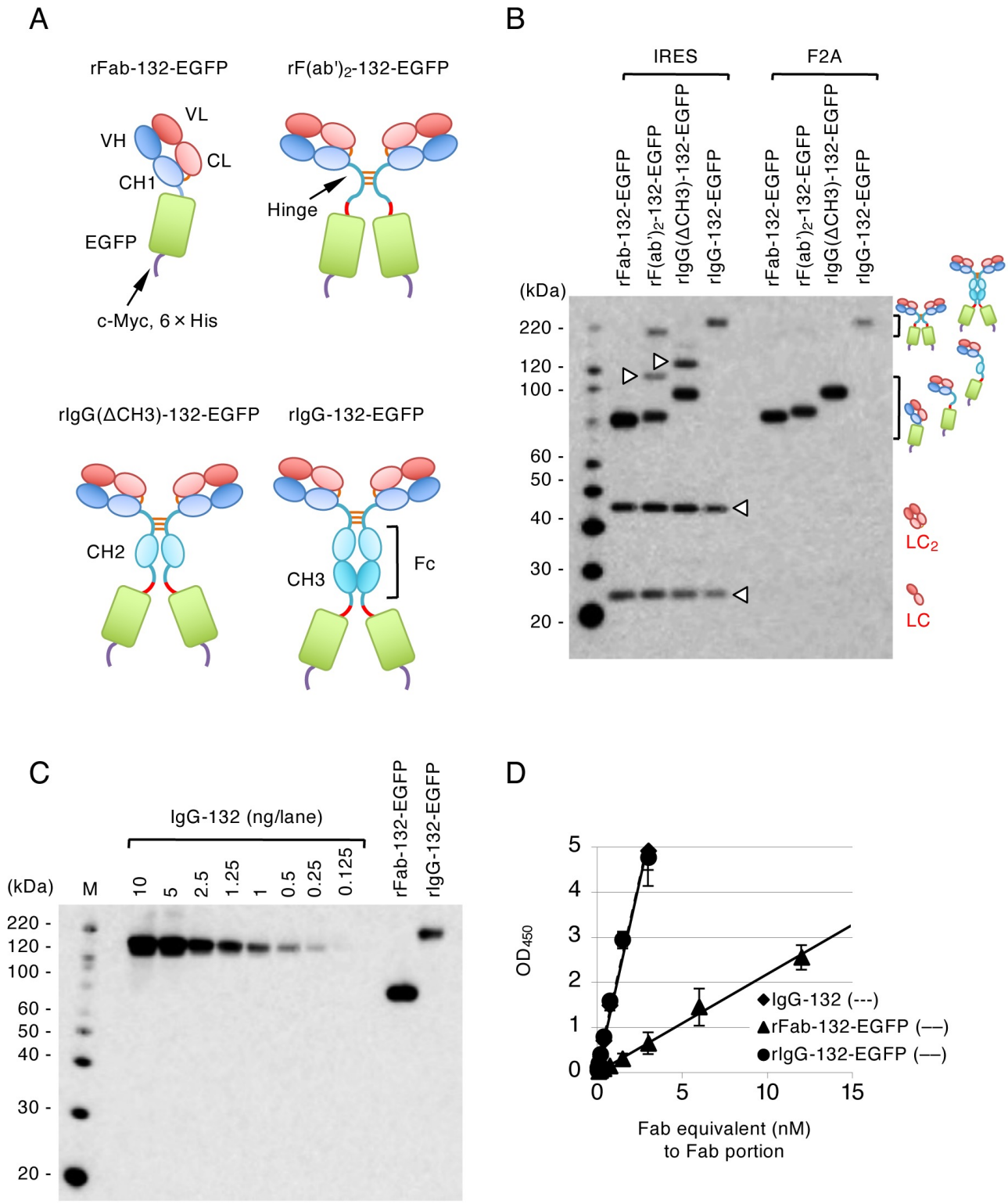

Figure I-4 Reactivity of mAb 132-EGFP fusion protein.

(A) Molecular design of mAb 132-EGFP fusion proteins. The LC and HC are depicted as in Figure I-2A, and the spacer between HC and EGFP is indicated with red lines. The epitope tail comprised of c-Myc and 6 × His (purple line) was added at the C-terminus of EGFP. (B) Analysis of the molecular assembly of mAb 132-EGFP fusion proteins. Transfection of HEK293T cells and immunoblotting were carried out by the same method as shown in Figure I-2. Corresponding illustrations on the right indicate the product of rFab-132-EGFP, rF(ab')$_2$-132-EGFP, rIgG(ΔCH$_3$)-132-EGFP and rIgG-132-EGFP, whereas arrowheads indicate possible assembly intermediates, LC and LC$_2$. The square brackets indicate the molecular weight range of mono- and bivalent fusion proteins. (C) Quantification of purified rFab-132-EGFP and rIgG-132-EGFP. Detection was carried out by the same method as shown in Figure I-3. (D) Difference in reactivity of rFab-132-EGFP and rIgG-132-EGFP. ELISA was performed using 100 μg/well rMoPrP and twofold serially diluted purified rFab-132-EGFP (0.09−12 nM), rIgG-132-EGFP and IgG-132 (0.02−3 nM).

The monovalent rFab-132-EGFP and bivalent rIgG-132-EGFP were purified by Ni^{2+} affinity chromatography from supernatants of HEK293F cells transfected corresponding expression plasmids with F2A (Figure I-4C), and their reactivity to rMoPrP was analyzed. Similar to the difference in the reactivity of rFab-132 and rIgG-132 shown in Figure I-3D, the reactivity of rFab-132-EGFP was much weaker than that of rIgG-132-EGFP (Figure I-4D).

4. Effect of valencies of mAb 132 on PrP^{Sc}-specific detection

Next, the reactivity of the mono- and bivalent forms of recombinant mAb 132-EGFP in PrP^{Sc}-specific immunofluorescence staining was examined using N2a-3 cells persistently infected with 22L prion strain (ScN2a-3-22L) (Figure I-5). rIgG-132-EGFP showed typical perinuclear PrP^{Sc} stains as described previously (Yamasaki *et al*., 2014a; Yamasaki *et al*., 2012), even at the lowest concentration used (Figure I-5G). rFab-132-EGFP reacted very weakly to the perinuclear PrP^{Sc} at 3 nM equivalent to Fab portion (Figure I-5I), whereas intense perinuclear stains were observed if the same concentration of rIgG-132-EGFP was used (Figure I-5H). If cells were stained with a higher concentration of rFab-132-EGFP at 14.2 nM equivalent to Fab portion, at which OD_{450} values of rFab-132-EGFP in ELISA were almost comparable to those of rIgG-132-EGFP at 1.6 nM equivalent to Fab portion (Figure I-4D), perinuclear PrP^{Sc} stains were apparent in ScN2a-3-22L cells (Figure I-5J). These results suggest that bivalent binding of mAb 132 is required for efficient PrP^{Sc}-specific staining.

5. Analysis of the binding characteristics of mAb 132 by SPR

To analyze the effect of antibody valency and Ag density on the reactivity of mAb 132 in more detail, I measured the binding kinetics of mono- and bivalent mAb 132 to rMoPrP using SPR. First, the binding responses of mAbs 31C6 and 132 directly immobilized on the surface of sensorchip as a ligand to injected rMoPrP as an analyte (Figure I-6A) were measured using

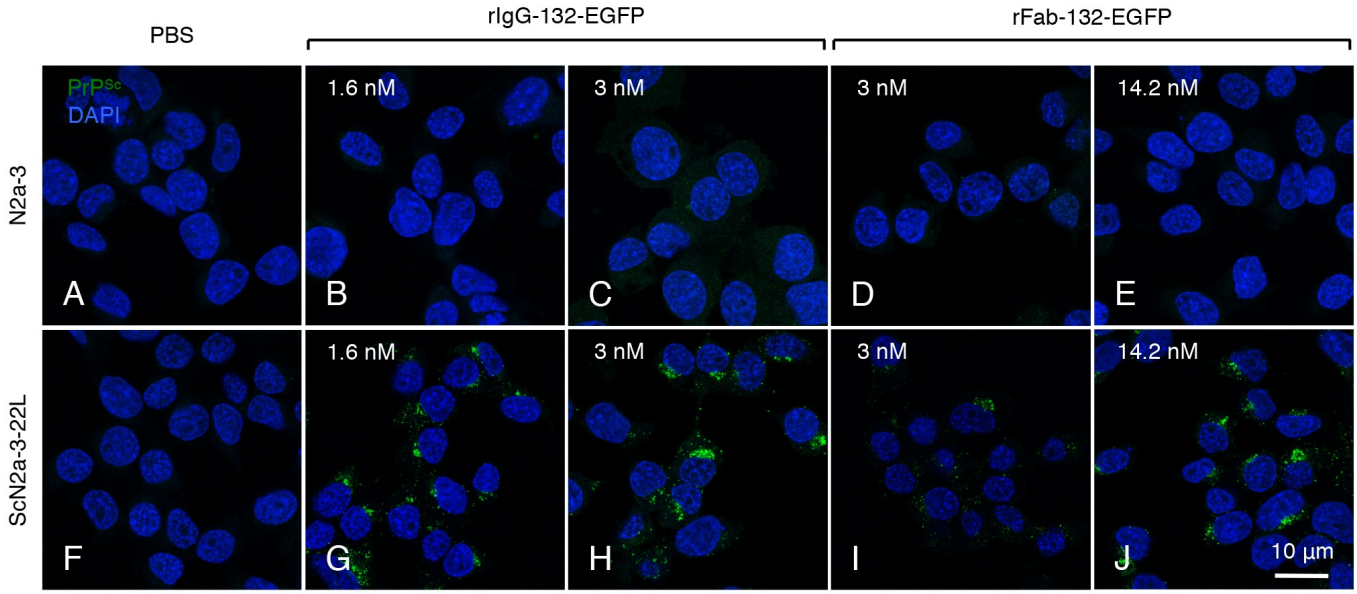

Figure I-5 PrP^{Sc}-specific detection by direct immunofluorescence staining.
Prion-uninfected N2a-3 cells (A−E) and 22L prion strain-infected N2a-2 cells (ScN2a-3-22L) (F−J) were directly stained using rIgG-132-EGFP (B,C, G and H) and rFab-132-EGFP (D, E, I and J) at the indicated concentrations equivalent to the Fab portion. The leftmost images (A, F) show negative controls for EGFP fusion protein. Cell nuclei (blue) were stained with 4', 6'-diamino-2-phenylindole, dilactate (DAPI).

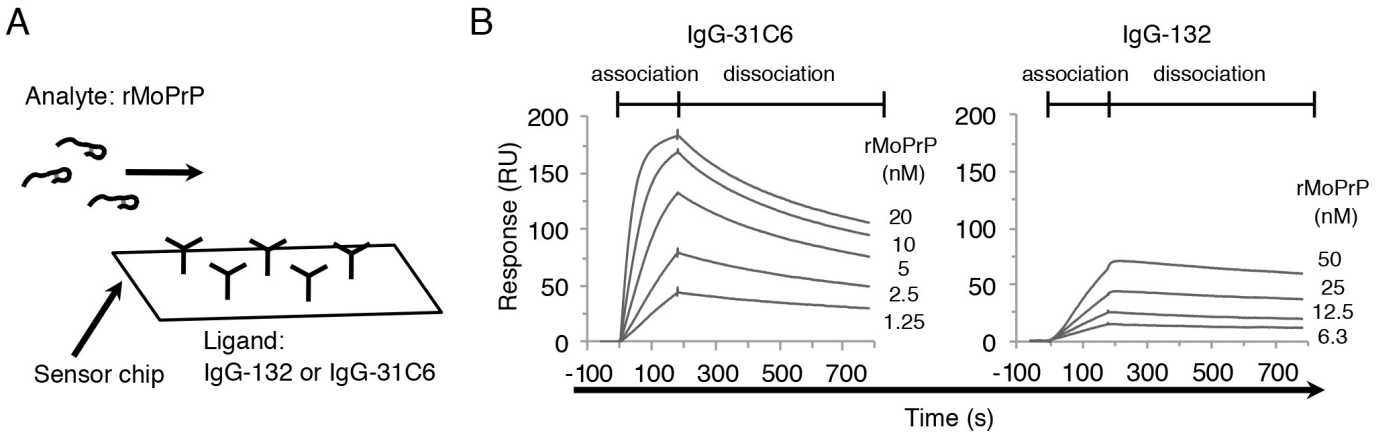

Figure I-6 Binding affinity of authentic mAbs.

(A) Relationship between ligand and analyte in surface plasmon resonance (SPR). IgG-132 or 31C6 was directly immobilized on the surface of a CM5 sensorchip at approximately 1,000 response unit (RU) as a ligand. The injected rMoPrP was passed over on the surface of the chip as an analyte. (B) SPR sensorgrams measured by multi-cycle kinetics analysis. The sensorgrams were obtained using twofold serial dilutions of rMoPrP (1.25−20 nM for IgG-31C6 and 6.3−50 nM for IgG-132).

multi-cycle kinetics analysis (Figure I-6B). In the association phase, the slopes of the sensorgram for IgG-132 were lower than that of IgG-31C6, indicating that the affinity of IgG-132 was lower than that of IgG-31C6. In contrast, the decrease of RU in IgG-132 was slower than that in IgG-31C6, indicating that the binding stability between IgG-132 and rMoPrP is higher than that between IgG-31C6 and rMoPrP. Moreover, IgG-132 required a 20-fold higher concentration of rMoPrP to obtain the comparable levels of RU to IgG-31C6 (Figure I-6B, e.g., compare 1.25 nM rMoPrP for IgG-31C6 with 25 nM rMoPrP for IgG-132), which was consistent with the results that a larger amount of rMoPrP was required to obtain efficient binding of mAb 132 in ELISA (Figure I-3B).

The binding kinetics of mono- and bivalent mAbs 132 and 31C6 were analyzed using single-cycle kinetics analysis (Figure I-7) and rate constants (k_a, k_d), and dissociation constant (K_D) calculated from the sensorgrams are shown in Table I-4. When rMoPrP was immobilized on the surface as a ligand and Abs were used as analytes, under which IgG can bind bivalently to rMoPrP (Figure I-7A, left), the K_D of rFab-132 was two order of magnitude higher than that of IgG-132. The result indicates that the lower reactivity of monovalent mAb 132 than bivalent form (Figure I-7B, Table I-4). However, a similar tendency was observed when the K_D of rFab-31C6 was compared to that of IgG-31C6 (Figure I-7C, Table I-4). These results suggest that the mechanism of PrP^{Sc}-specific detection by mAb 132 is not simply explained by K_D. Consistent with the measurement by multi-cycle kinetics shown in Figure I-6, k_a of IgG-132 to rMoPrP (2.5×10^5) was one order of magnitude lower than that of IgG-31C6 to rMoPrP (5.3×10^6); on the contrary, k_d of IgG-132 from rMoPrP (1.2×10^{-5}) was one order of magnitude lower than that of IgG-31C6 from rMoPrP (2.7×10^{-4}) when IgG was used as analytes. These results suggest that binding reaction of mAb 132 to rMoPrP proceed slowly compared to that of mAb 31C6. Although the K_D of the two rFab fragments or that of the two IgGs were comparable each other, there are some differences in k_a and k_d. The k_a of rFab-132 (6.4×10^5) was 2.6 times

higher than that of IgG-132 (2.5×10^5). This difference was also observed in mAb 31C6: the k_a of rFab-31C6 was 1.6 times higher than that of IgG-31C6. By contrast, the k_d of rFab-132 (3.1×10^{-3}) was approximately 260 times higher than that of IgG-132 (1.2×10^{-5}), suggesting that the binding of rFab-132 is unstable compared to that of IgG-132. The k_d of rFab-31C6 (1.1×10^{-2}) was only 40 times higher than that of IgG-31C6 (2.7×10^{-4}), of which the difference was 6.5 times smaller than that of mAb 132. Taken together, these results indicate that mAbs 132 and 31C6 intrinsically possess the similar binding affinity to rMoPrP. However, the bivalent binding can significantly enhance the binding avidity, a total affinity of multiple binding, of IgG-132 even though the monovalent binding of mAb 132 may be restricted by the kinetics limitation compared to that of mAb 31C6.

The results described above suggest that Ag density influences the binding of mAb 132. To assess this possibility, rMoPrP was immobilized on a CM5 sensorchip at 1.71 and 0.14 ng/mm^2, and 10 nM IgG-132 and 1 nM IgG-31C6 were injected as analytes. The weight of bound Abs was calculated from the RU of sensorgrams (Table I-5). Because of the slow association rate of mAb 132, a 10 times higher concentration of mAb 132 was required to obtain the RU level similar to that of mAb 31C6. When IgG-132 was used as an analyte, 30.8 pg/mm^2 IgG-132 could bind to the sensorchip with 1.71 ng/mm^2 rMoPrP. However, only 21.7% of IgG-132 (6.7 pg/mm^2) could bind to the sensorchip with 0.14 ng/mm^2 rMoPrP. In contrast to mAb 132, nearly 50% of IgG-31C6 still bound to the sensorchip even if the density of rMoPrP on the sensorchip decreased from 1.71 to 0.14 pg/mm^2 (22.7 and 11.3 pg/mm^2). These results indicate that the reaction of mAb 132 is more sensitive to Ag density than that of mAb 31C6.

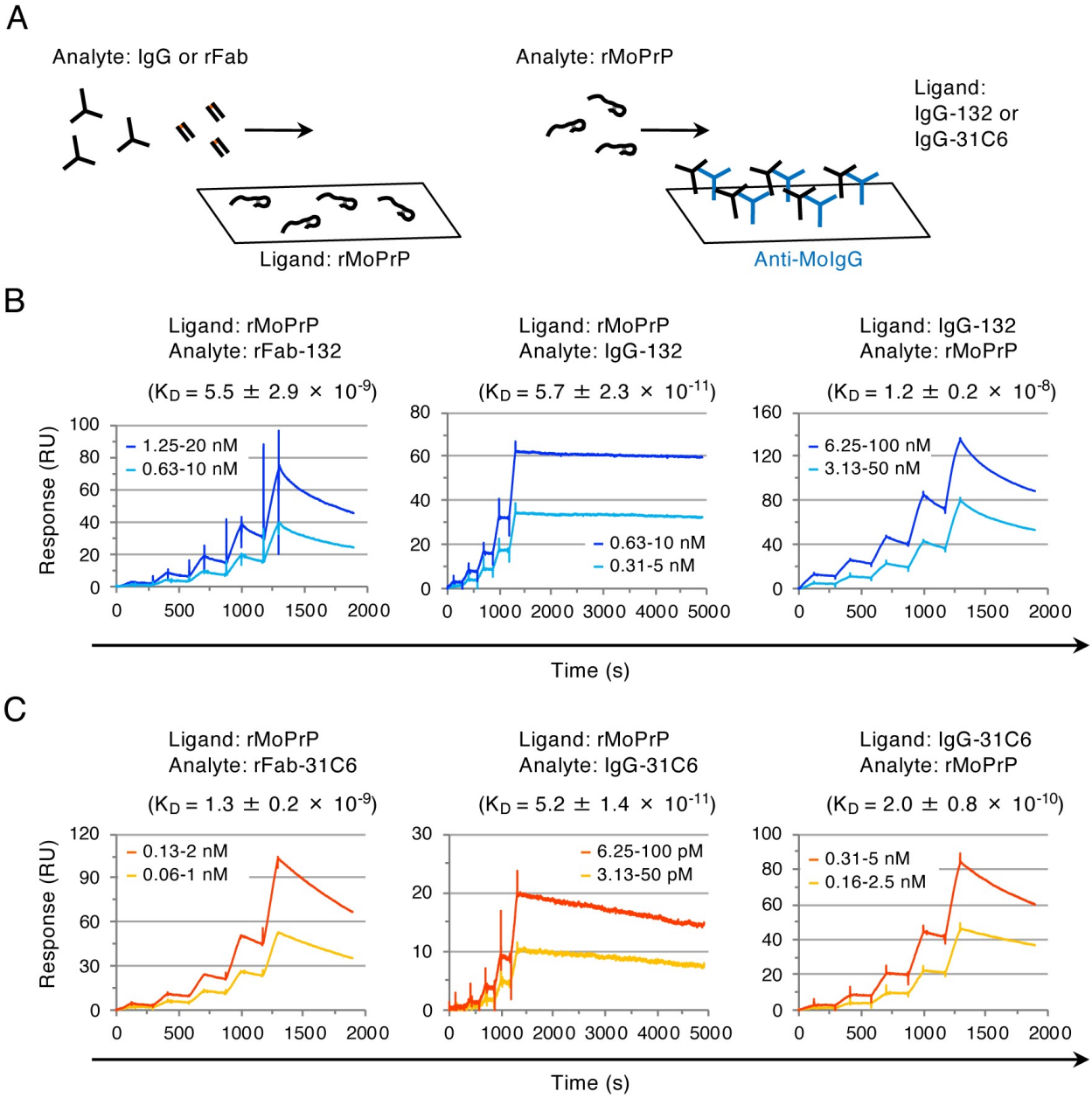

Figure I-7 Binding affinity of mono- and bivalent authentic and recombinant antibody fragment.
(A) Schematic illustrations for analytes and ligands. The SPR sensorgrams were measured using two different binding types: monovalent Ab fragments (rFab) or bivalent authentic Ab (IgG) were injected to the sensorchip with immobilized rMoPrP (left), or rMoPrP was injected to the chip with each IgG captured at approximately 500 RU by anti-MoIgG (blue) immobilized on the surface of the chip (right). (B) Representative sensorgrams for the binding of rFab-132 and IgG-132 to rMoPrP measured by single-cycle kinetics. All sensorgrams were obtained using twofold serial dilutions of antibodies and rMoPrP: rFab-132, 0.63−10 nM and 1.25−20 nM; IgG-132, 0.31−5 and 0.63−10 nM; and rMoPrP, 3.13−50 and 6.25−100 nM. The dissociation constant was calculated from three independent experiments (mean ± SD). (C) Representative sensorgrams for the binding of rFab-31C6 and IgG-31C6 to rMoPrP measured by single-cycle kinetics. All sensorgrams were obtained using twofold serial dilutions of Abs and rMoPrP: rFab-31C6, 0.06−1 nM and 0.13−2 nM; IgG-31C6, 3.13−50 and 6.25−100 pM; and rMoPrP, 0.16−2.5 and 0.31−5 nM.

Table I-4. Summary of equilibrium and kinetic constants [a].

mAb	Ligand	Analyte	K_D (M)	k_a (1/Ms)	k_d (1/s)
mAb 132	rMoPrP	rFab-132	$5.5 \pm 2.9 \times 10^{-9}$	$6.4 \pm 4.7 \times 10^{5}$	$3.1 \pm 1.4 \times 10^{-3}$
	rMoPrP	IgG-132	$5.7 \pm 2.3 \times 10^{-11}$	$2.5 \pm 1.1 \times 10^{5}$	$1.2 \pm 0.9 \times 10^{-5}$
	IgG-132	rMoPrP	$1.2 \pm 0.2 \times 10^{-8}$	$6.3 \pm 0.3 \times 10^{4}$	$7.6 \pm 1.4 \times 10^{-4}$
mAb 31C6	rMoPrP	rFab-31C6	$1.3 \pm 0.2 \times 10^{-9}$	$8.7 \pm 0.3 \times 10^{6}$	$1.1 \pm 0.2 \times 10^{-2}$
	rMoPrP	IgG-31C6	$5.2 \pm 1.4 \times 10^{-11}$	$5.3 \pm 1.4 \times 10^{6}$	$2.7 \pm 0.8 \times 10^{-4}$
	IgG-31C6	rMoPrP	$2.0 \pm 0.8 \times 10^{-10}$	$1.5 \pm 0.2 \times 10^{7}$	$3.1 \pm 1.7 \times 10^{-3}$

a: Calculated from sensorgrams measured by single-cycle kinetics. Mean ± SD from three independent experiments are shown.

Table I-5. Ag density-dependent binding of mAb 132.

Analyte (concentration [a])	Antibodies [b] (pg/mm^2) bound to sensorchip with:	
	1.71 ng rMoPrP /mm^2	0.14 ng rMoPrP /mm^2
IgG-132 (10 nM)	30.8 ± 1.1 [c]	6.7 ± 0.1 [c]
IgG-31C6 (1 nM)	22.7 ± 0.3 [c]	11.3 ± 0.2 [c]

a: Concentration of injected antibodies as analyte.
b: Amounts of antibodies bound to sensorchip were estimated from sensorgrams as 1 RU = 1 pg/mm^2.
c: Mean ± SD from three independent experiments.

6. Reactivity of mAb 132 to PrP^C crosslinked by anti-PrP mAb

The reactivity of mAb 132 and its derivatives suggest that a weak interaction in monovalent binding but the enhancement of binding avidity in bivalent binding accounts for apparent PrP^{Sc}-specific detection in IFA. Therefore, I expected that mAb 132 would detect PrP^C on the cell surface if two PrP^C molecules existed close enough to enable mAb 132 to bind in bivalent form. To address this possibility, PrP^C on the surface of N2a-3 cells was crosslinked by IgG-31C6 or IgG-44B1, which retains PrP^C molecules on the cell membrane possibly by crosslinking two molecules (Kim *et al*., 2004a; Yamasaki *et al*., 2014b), and then stained with Alexa Fluor 647 labeled mAb 132. Interestingly, mAb 132 could detect PrP^C on the cell membrane of N2a-3 cells pretreated with IgG-31C6 or IgG-44B1 regardless of the GdnSCN treatment (Figures I-8B, I-8C, I-8E and I-8F). However, this mAb did not react with PrP^C on the N2a-3 cells under non-treatment condition (Figures I-8A and I-8D). This result indicates that monovalent binding of mAb 132 to monomeric PrP^C is inefficient. However, PrP^{Sc} exists as an oligomer and consequently the epitopes locate close enough to allow mAb 132 binding in a bivalent manner, which confers high binding avidity to mAb 132. This result also suggests that the epitope for mAb 132 is exposed on the surface of the PrP^C molecule regardless of Gdn pretreatment.

7. Detection of PrP^{Sc} in the brain section using mAb 132

The reactivity of mAb 132 suggests that the inefficient monovalent binding decreases the signals from monomeric PrP^C to background level in IFA with cultured cells. To assess if the same mechanism could be applicable to tissue sections, particularly in brain where PrP^C is abundantly expressed, I performed IFA using frozen brain sections from Chandler prion-infected and mock-infected mice (Figure I-9). Compared to mAbs 31C6 (Figures I-9E and I-9G) and 44B1 (Figures I-9I and I-9K), mAb 132 showed weak fluorescence signals (Figures I-

9M and I-9O) that are comparable to those by mAb P2-284 used as negative control (Figures I-9A and I-9C) in the frozen section from mock-infected mouse regardless of Gdn pretreatment. This indicate that mAbs 31C6 and 44B1 can efficiently bind but mAb 132 inefficiently bind to PrP^{C} expressed in the brain. After the Gdn pretreatment, these anti-PrP mAbs showed granular stains of PrP^{Sc} with intense fluorescence in the brain section from the Chandler prion-infected mouse (Figures I-9H, I-9L and I-9P). However, a fine analysis of PrP^{Sc} using mAbs 31C6 and 44B1 appears to be limited because of their reactivity to PrP^{C}. In contrast, mAb 132 provides a better signal-noise-ratio for PrP^{Sc} detection because of the inefficient binding to PrP^{C}. This is an advantage of mAb 132 for the analysis of PrP^{Sc} in tissue sections.

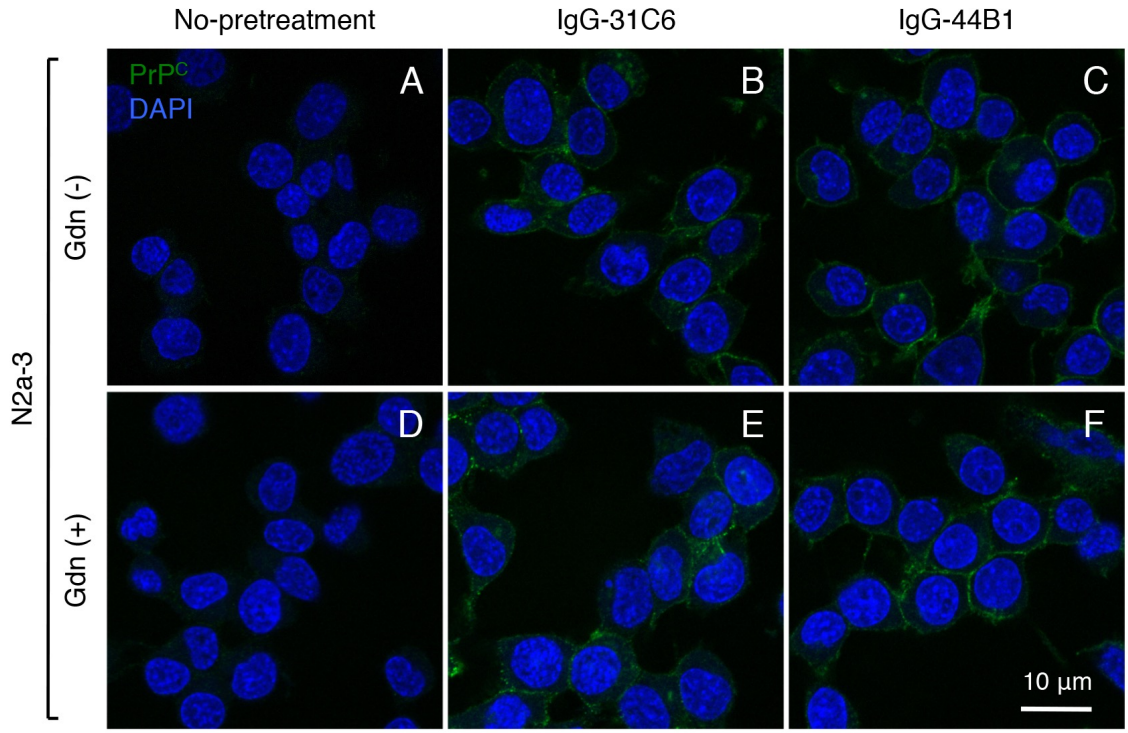

Figure I-8 Detection of PrP^C on the surface of N2a-3 cells.
N2a-3 cells were incubated with DMEM containing 10 nM IgG-31C6 (B, E) and IgG-44B1 (C, F) for 2 days. The cells were stained with 1 μg/ml Alexa Fluor 647-labeled mAb 132 (green) after treatment with (D−F) or without (A−C) 5M guanidinium thiocyanate (GdnSCN). The leftmost images indicate negative controls for Ab-treatment (A, D). Cell nuclei (blue) were stained with DAPI.

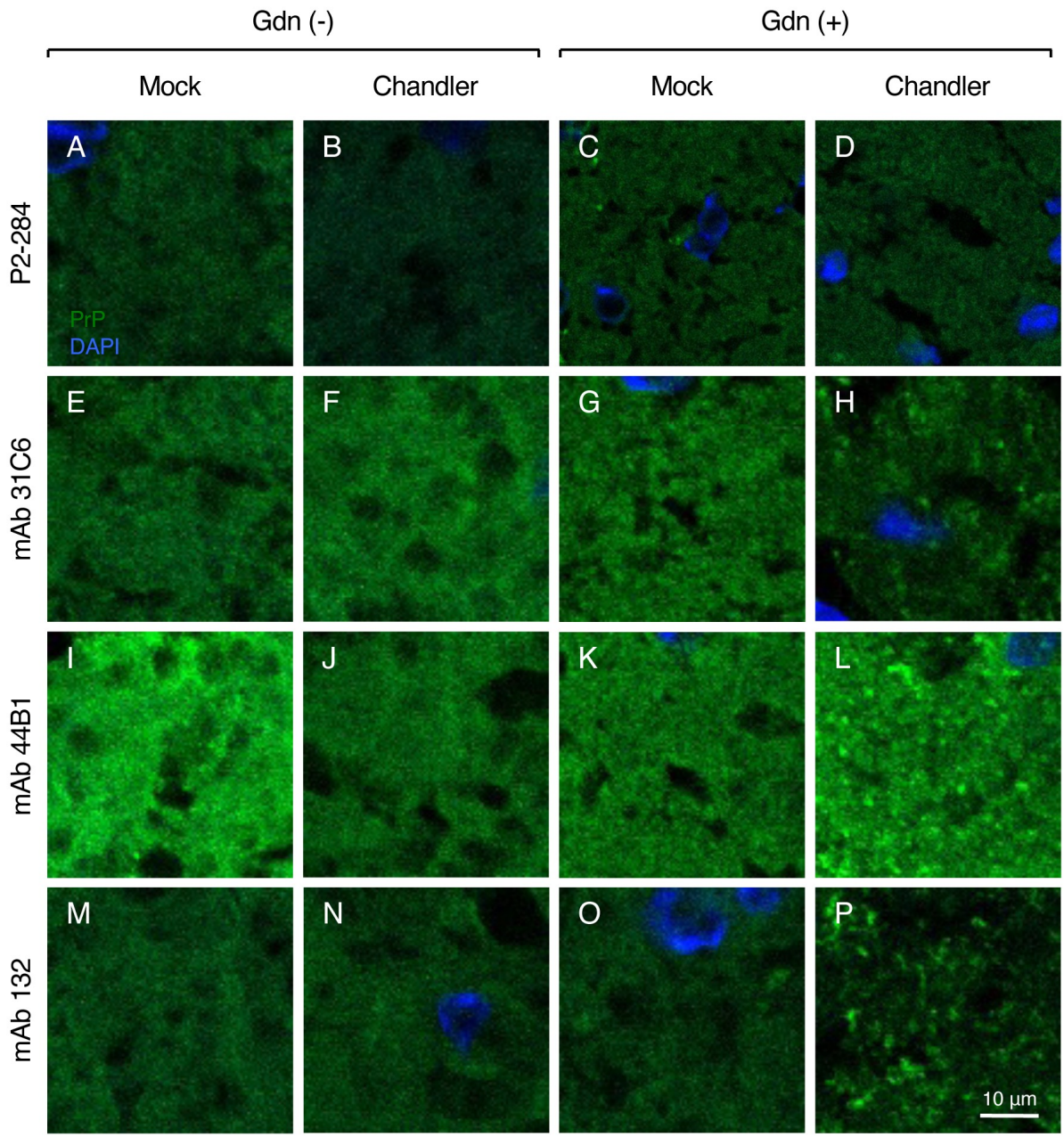

Figure I-9 Detection of PrP^{Sc} in frozen brain sections.
IFA was performed using the frozen brain sections of Chandler strain-infected (Chandler) and mock-infected (Mock) mice at 120 dpi with (Gdn (+)) or without (Gdn (−)) 2.5 M GdnSCN pretreatment. PrP molecules (green) were stained with mAbs 31C6, 44B1 and 132 followed by Alexa Fluor 488 $F(ab')_2$ fragment of goat anti-mouse IgG (H+L) (Invitrogen) as a secondary antibody. Anti-feline panleukopenia virus mAb P2-284 was used as a negative control mAb. Cell nuclei (blue) were stained with DAPI. The fluorescent images were acquired from the coronal sections containing thalamus. Scale bar: 10 µm.

DISCUSSION

Although mAb 132 is a pan-PrP Ab, the use of this mAb facilitates reliable PrP^{Sc}-specific staining in cells or tissue sections pretreated with a chaotropic reagent (Sakai *et al*., 2013; Tanaka *et al*., 2016; Yamasaki *et al*., 2014a; Yamasaki *et al*., 2012). However, the mechanism of PrP^{Sc}-specific detection by mAb 132 is largely unclear. To clarify this mechanism, I analyzed the reactivity and binding kinetics of mono- and bivalent mAb 132 using ELISA and SPR. The monovalent binding of rFab-132 was significantly weaker than that of bivalent IgG-132, whereas that of mAbs 31C6 and 44B1 was as efficient as authentic IgGs (Figures I-3A and I-3B). These results indicate that bivalent binding is required for efficient binding of mAb 132. Consistent with the results of ELISA (Figures I-3 and I-4D), analyses of binding kinetics by SPR showed that Ag density influences the binding of mAb 132 (Table I-5). Crystallographic analysis of IgG revealed that the distance between two Fab domains of intact IgG_1 is around 11.8 nm (Harris *et al*., 1998). The number of rMoPrP molecules in a circle of 11.8 nm in diameter can be estimated as 6.6 and 3.7 molecules in case of 100 ng/well rMoPrP in ELISA (Figure I-3) and 1.71 ng/mm^2 rMoPrP in SPR (Table I-5), respectively. Therefore, theoretically, the rMoPrP density in these conditions appears high enough to allow bivalent binding of mAb 132 (Müller *et al*., 1998). On the other hand, in the case of 12.5 ng/well rMoPrP, the lowest concentration that mAb 132 could bind in ELISA (Figure I-3B), and 0.14 ng/mm^2 rMoPrP in SPR (Table I-5), the number of rMoPrP molecules can be estimated as 0.9 and 0.3, respectively, in a circle of 11.8 nm in diameter. Consequently, it is expected that the binding of IgG-132 to rMoPrP occurred mainly in a monovalent manner under these conditions (Figure I-10A). The estimated numbers of rMoPrP molecules are consistent with the idea that bivalent binding confers a higher binding stability to mAb 132 (Figure I-10B). Indeed, the binding of rFab-132 to rMoPrP in ELISA was not so efficient even at the highest Ag concentration (Figures I-3 and I-4D). This trend was not observed with other pan-PrP mAbs, 31C6 and 44B1, and their rFab

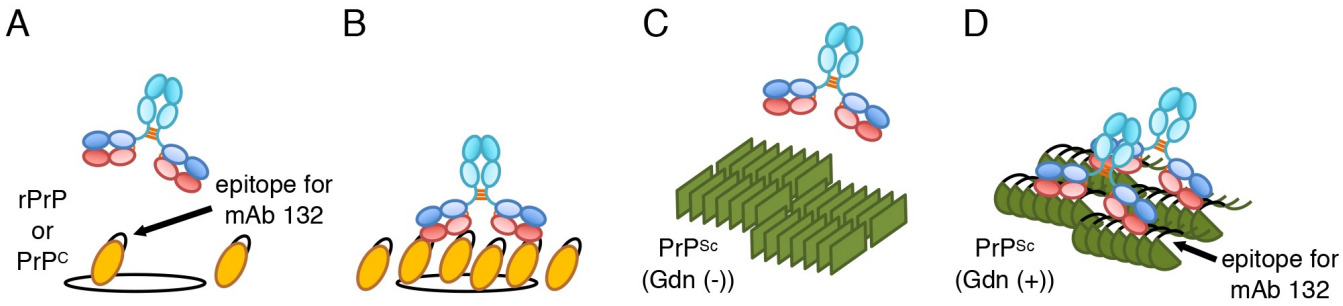

Figure I-10 Mechanism for PrP^{Sc}-specific detection by mAb 132.
(A, B) Binding of mAb 132 to rPrP and PrP^{C} molecule. mAb 132 inefficiently binds to PrP molecule if density of PrP molecules is lower than that allows bivalent binding because of low affinity of monovalent binding of mAb 132 (A), whereas mAb 132 binds stably to PrP molecules by avidity effect if the density of PrP molecules is high enough to allow bivalent binding (B). Orange ovals: rPrP or PrP^{C}; black line on the orange ovals: epitope for mAb 132. Circles indicates the area where bivalent binding of intact mouse IgG_1 take place. (C, D) Binding of mAb 132 to PrP^{Sc} oligomer/aggregate. mAb 132 does not bind to PrP^{Sc} without Gdn salt pretreatment (C, Gdn (−)), whereas epitopes for mAb 132 are exposed by the pretreatment (D, Gdn (+)), multiple epitopes for mAb 132 on the PrP^{Sc} oligomer/aggregate allow bivalent binding of mAb 132.

fragments (Figures I-3A and I-3B). Furthermore, the amount of IgG-132 bound on the sensorchip with 0.14 ng/mm^2 rMoPrP was only 20% of that bound to the senserchip with 1.71 ng/mm^2 rMoPrP. Taken together, these results indicate that monovalent mAb 132 binding is less stable than the bivalent binding.

In the present study, monovalent and bivalent forms of mAbs 132 and 31C6 showed similar K_D values when they were used as analytes. However, mAb 132 possessed the smaller k_a and k_d values in one order of magnitude than those of mAb 31C6 regardless of the valency (Table I-4). A small k_a value indicates slow binding rate of mAb to its Ag. It has been reported that mAb with a smaller k_a required longer reaction time and relatively high concentration compared to that with a larger k_a (Olson *et al*., 1989). Thus, the inefficient binding of rFab-132 (Figures I-3, I-4D and I-5) may be explained by the kinetic limitation at the lower concentration and/or in the short time incubation. However, rFab-132 showed only 2.6 times higher k_a values than IgG-132 (Table I-4), suggesting the PrP^{Sc}-specific staining of mAb 132 is not explained by association kinetics in different valency. On the other hand, a small k_d value indicates slow dissociation rate of mAb binding on its Ag. The k_d of rFab-132 was approximately 260 times larger than that of IgG-132, whereas rFab-31C6 showed 40 times larger k_d than IgG-31C6 (Table I-4). The difference in the k_d between mono- and bivalent mAb 132 was 6.5 times higher than that of mAb 31C6. Avidity is applied to the sum of the binding affinity of Ab to its epitopes crosslinked by bivalent binding, which is an ability inherent to the epitope and depends on the density (Harms *et al*., 2012; Müller *et al*., 1998; Olson *et al*., 1989). Thus, it is expected that the bivalent binding of IgG-132 may strongly enhance the retention on the surface of Ags compared to that of IgG-31C6. Indeed, the enhancement of the antitumor and antiviral activity through the bivalent binding have been shown in anti-EGFR nimotuzumab (Garrido *et al*., 2011), anti-influenza virus mAb S139/1 (Lee *et al*., 2012) and anti-Dengue virus mAb E106 (Edeling *et al*., 2014). Taken together, the Ag density-dependent enhancement of the binding

by avidity effect may be a key mechanism of PrP^{Sc}-specific detection by mAb 132.

MAb 132 bound to PrP^{C} expressed in N2a-3 cells when PrP^{C} molecules were crosslinked by anti-PrP Abs (Figure I-8). This result clearly indicates that bivalent binding confers a high binding avidity to mAb 132. Additionally, detection does not require the pretreatment of cells with Gdn salt, indicating that the epitope for mAb 132 locates an accessible surface of the PrP^{C} molecule (Figure I-10A and I-10B). In contrast, pretreatment with Gdn salt is essential for PrP^{Sc} detection. This means that the epitope for mAb 132 in the PrP^{Sc} molecule is inaccessible to Ab before denaturation (Fig. I-10C). However, PrP^{Sc} exists as an oligomer of the PrP molecule so that more than two epitopes for mAb 132, which have become accessible after denaturation, allow Abs to bind to PrP^{Sc} oligomers in a bivalent manner (Figure I-10D). Thus, weak monovalent binding of mAb 132 to monomeric PrP^{C} diminishes the signals from PrP^{C} to background level, whereas after exposure of the epitope, mAb 132 selectively binds to oligomeric PrP^{Sc} in a bivalent manner (Figures I-9, I-10A and I-10D). This combination provides a better signal-noise-ratio and therefore enables reliable PrP^{Sc} detection in cells and section by IFA, cell-based ELISA and flow cytometry (Figure I-9) (Sakai *et al*., 2013; Shan *et al*., 2016; Tanaka *et al*., 2016; Yamasaki *et al*., 2018; Yamasaki *et al*., 2012). However, considering the mechanism of PrP^{Sc}-specific detection of mAb 132 described above, mAb 132 will react with PrP^{C} if more than two PrP^{C} molecules exist within the distance that allow bivalent binding of IgG (Figure I-10B).

MAb 132 cannot bind with the epitope on PrP^{Sc} molecules without the Gdn salt pretreatment (Yamasaki *et al*., 2012). A group of anti-PrP Abs that recognize the region around aa 90−120 of PrP molecules exhibit a similar property (Peretz *et al*., 1997; Serban *et al*., 1990; Williamson *et al*., 1996). Thus, the region is partially or completely buried in PrP^{Sc} molecules. Moreover, H/D exchange mass spectrometry showed that the solvent exposure of the hydrophobic region comprised aa 111−120, including the epitope for mAb 132 on PrP^{Sc}, was

significantly decreased compared to that of rMoPrP or PrP^{Sc} intermediates (Miller *et al*., 2013). These results are consistent with the fact that mAb 132 cannot directly access the epitope on PrP^{Sc} molecules. Most of PrP^{Sc}-specific mAb recognize the conformational epitopes that are exposed on PrP^{Sc} molecules, and thus those Abs react with PrP^{Sc} without denaturation. In contrast to the reactivity of mAb 132 to PrP^{Sc}, the reactivity of PrP^{Sc}-specific mAbs decreased after denaturation of PrP^{Sc} molecules (Horiuchi *et al*., 2009; Masujin *et al*., 2013; Saijo *et al*., 2016; Ushiki-Kaku *et al*., 2010).

In this chapter, I described the mechanism of PrP^{Sc}-specific detection by mAb 132. This mAb belongs to a group of pan-PrP Abs that cannot distinguish PrP^{Sc} from PrP^{C}. However, the Ag density-dependent enhancement of binding stability via bivalent binding facilitates the detection of PrP^{Sc} that exists as oligomer and/or aggregates of PrP molecules. PrP^{Sc} oligomers consisting of small numbers of PrP molecules are sensitive to PK treatment (Silveira *et al*., 2005). Thus, the finding in this study provides a mechanistic rationale for the detection of PrP^{Sc}-sen in prion-infected cells by mAb 132 (Shan *et al*., 2016); Gdn salt treatment exposed epitopes for mAb 132 on PrP^{Sc} molecule, which are close enough to allow the bivalent binding. Furthermore, the detection pattern of PrP^{Sc} fibril by mAb 132 is partly different from that by the PrP^{Sc}-specific mAb 8D5 (Tanaka *et al*., 2016), suggesting that this mAb may be a useful tool for precise understanding of the mechanism of localization and propagation of PrP^{Sc}. The epitope for mAb 132 is widely conserved across species from animals to chicken (van Rheede *et al*., 2003; Wopfner *et al*., 1999). Therefore, mAb 132 will be useful for the detection of PrP^{Sc} in various species including human.

BRIEF SUMMARY

Anti-PrP mAb 132 recognizing MoPrP aa 119−127 facilitates reliable PrP^{Sc}-specific detection in cells or frozen tissue sections by IFA, although pretreatment with Gdn salts is required. Despite the benefit of this mAb, the mechanism of PrP^{Sc}-specific detection remains unclear. Therefore, I attempted to analyze the reactivity and binding kinetics of mAb 132. I found that monovalent binding of mAb 132 was significantly weaker than bivalent binding. Consistent with this, the k_d value of the monovalent binding was approximately 260 times larger than that of the bivalent form, suggesting that the monovalent binding is less stable than bivalent binding. Furthermore, compared to the other anti-PrP mAbs tested, the amount of mAb 132 bound to rMoPrP decreased if the Ag density was too low to allow the bivalent binding. If two PrP^{C} exist close enough to allow the bivalent binding, mAb 132 binds to PrP^{C}. These results indicate that weak monovalent binding of mAb132 diminishes PrP^{C} signals to background level, whereas the stable bivalent binding enables PrP^{Sc}-specific detection after exposure of the epitope.

CHAPTER II

Analyses for the unique reactivity and its responsible regions of recombinant cervid PrP in real-time quaking-induced conversion reaction in the presence of high concentration of tissue homogenates.

INTRODUCTION

Prion diseases in animals are generally transmitted via prion-contaminated tissues or body fluid of prion-infected animals (Andreoletti *et al*., 2002; Mathiason *et al*., 2006; Pattison *et al*., 1972; Tamguney *et al*., 2009) or environment contaminated with prions (Georgsson *et al*., 2006; Miller *et al*., 2004; Pritzkow *et al*., 2015). The emergence of animal prion diseases such as BSE (Wells *et al*., 1987) and CWD (Haley and Hoover, 2015; Koutsoumanis *et al*., 2019; Osterholm *et al*., 2019; Vikoren *et al*., 2019; Williams and Miller, 2002) may raise concerns about a potential risk for interspecies transmission including humans. Therefore, sensitive and accurate methods are necessary for disclosing the potential existence of prions in animals and environments.

CWD was first identified in 1967 in a group of captive mule deer and was classified as a transmissible spongiform encephalopathies in 1980 (Williams and Young, 1980). To date, CWD-affected cervids, such as elk, moose and reindeer, have been found in the US, Canada, South Korea (Haley and Hoover, 2015; Williams and Miller, 2002), and Scandinavian countries (Koutsoumanis *et al*., 2019; Osterholm *et al*., 2019; Vikoren *et al*., 2019). Different from other prions, infectious CWD prions have been detected in secreted body fluids and excretions such as saliva, urine, and feces (Williams and Miller, 2002). CWD did not transmit to mice expressing human PrP (Kong *et al*., 2005; Tamguney *et al*., 2006). However, a potential risk of transmission to human cannot be ignored, as CWD prions are known as experimentally transmissible to several animals including squirrel monkey (Hamir *et al*., 2006; Race *et al*., 2009; Sigurdson *et al*., 2006), and prion properties change during interspecies transmission (Baron *et al*., 2011; Capobianco *et al*., 2007; Huor *et al*., 2019; Simmons *et al*., 2016).

C-BSE was first recognized in the United Kingdom in 1986 (Wells *et al*., 1987), and since then has spread globally. C-BSE is known as a cause of zoonotic prion diseases because it is transmitted to human via BSE-contaminated products, which has caused the emergence of

variant CJD (Will *et al*., 1996). C-BSE is now under control due to worldwide implementation of control measures such as feed bans. However, two atypical BSEs were identified in 2004 (Biacabe *et al*., 2004; Casalone *et al*., 2004), and classified as H- and L-BSE based on the higher and lower apparent molecular weight of un-glycosylated PrP^{Sc} detected in immunoblotting (Jacobs *et al*., 2007). Atypical BSE cases were mainly disclosed in cattle over the age of 8-year-old, and found worldwide including in Brazil wherein no C-BSE case has been reported. Thus, atypical BSEs are thought as sporadic diseases that occur in aged cattle, similar to sporadic CJD in human (Biacabe *et al*., 2008). L-BSE is known to be experimentally transmissible to primates and mice expressing human PrP (Beringue *et al*., 2008; Comoy *et al*., 2008; Mestre-Frances *et al*., 2012), whereas the evidence for zoonotic potential of H-BSE has yet been insufficient. However, a potential risk of transmission of atypical BSE prions to human via food consumption cannot be neglected because low levels of prion infectivity and seeding activity of atypical BSE prions were detected in skeletal and intercostalis muscles (Sawada *et al*., 2019; Suardi *et al*., 2012) and in tonsillar tissue (Balkema-Buschmann *et al*., 2011).

Real-time quaking-induced conversion (RT-QuIC) is known as one of specific and highly sensitive method detecting low levels of prions (Atarashi *et al*., 2011; Orru *et al*., 2015; Peden *et al*., 2012; Wilham *et al*., 2010). However, the reaction is easily interfered by the inhibitory factor(s) included in the tissue homogenates and body fluids, which hampers the detection of prions in the presence of high concentration of tissue homogenates (Hoover *et al*., 2017; Orru *et al*., 2011; Wilham *et al*., 2010). Concentration of PrP^{Sc} form tissues and body fluids by immunoprecipitation or iron oxide beads, or lipid removal by alcohol extraction partly reduced the interference of RT-QuIC reaction (Denkers *et al*., 2016; Hoover *et al*., 2017; Orru *et al*., 2011). However, a simpler method is desirable for practical application of RT-QuIC. In the recent study, rCerPrP is reportedly useful for the detection atypical BSE prions in tissues of cattle affected with atypical BSEs even reactions were performed in the presence of high

concentration of tissue homogenates (Sawada *et al*., 2019). The reason why RT-QuIC with rCerPrP is less affected by the inhibitory factor(s) in tissue homogenates than other rPrPs will facilitate to improve RT-QuIC reaction.

In Chapter II, I extensively analyzed the reactivity of rCerPrP to CWD and atypical BSE prions in RT-QuIC in the presence of high concentration of tissue homogenates. I confirmed that the reactivity of rCerPrP was not severely affected in the presence of high concentration of uninfected brain homogenates compared to the other rPrPs tested. Furthermore, I found the involvement of N- and extreme C-terminal regions of rCerPrP in the unique reactivity on rCerPrP in RT-QuIC reaction.

MATERIALS & METHODS

1. Brain materials

Brain tissues from six CWD-affected deer were pooled and used as a source of CWD prions. Two brains unaffected white-tailed deer in USA were pooled and used as negative control (McNulty *et al*., 2019). Each tissue was homogenized in PBS at a concentration of 20% and were frozen at −80˚C until use. Brain homogenate of H-BSE-affected cattle (Okada *et al*., 2011) was kindly provided by Dr. Iwamaru Y, National Institute of Animal Health, Japan. The 10% brain homogenates from C-BSE (Shindoh *et al*., 2009) and L-BSE (Hagiwara *et al*., 2007) -affected cattle were prepared with PBS and stored at −80˚C.

2. Construction of the expression system of recombinant PrPs

Expression plasmids for the full-length rMoPrP and rHaPrP comprised of aa 23−231 were kindly provided by Dr. Atarashi R, Miyazaki University, Japan. An expression plasmid for the full-length rBvPrP comprised of aa 23−230 was kindly provided by Dr. Caughey B, National Institute of Health, USA. Genes encoding for full-length bovine (BoPrP; aa 25−242), CerPrP (aa 25−233, genotype: $G_{96}M_{132}S_{225}Q_{226}$ (Moreno and Telling, 2018)) and sheep ($A_{136}R_{154}Q_{171}$) PrP (ShPrP) (aa 25−233) were amplified from the corresponding genomic DNA (Table II-1). The gene fragment encoding N-terminal truncated rCerPrP (aa 94−233) was amplified from that of the full-length rCerPrP using primers shown in Table II-2. Each gene fragment was subcloned using the Zero Blunt TOPO PCR Cloning Kit (Invitrogen). Nucleotide sequences were determined using BigDye v3.1 (Applied Biosystems) and ABI-3130 Avant sequencer (Applied Biosystems). Each gene fragment with the correct nucleotide sequence was inserted into *Nde* I and *Bam*H I sites of pET11a (Novagen, USA).

Genes encoding the N-terminal replaced chimera of rCerPrP and rMoPrP (rMo^{N}−CerPrP, $rCer^{N}$−MoPrP) were generated using assembly PCR (Stemmer *et al*., 1995;

Suzuki *et al*., 2019) with primer sets described in the Table II-2. Genes encoding the C-terminal replaced chimeras (rCer−Mo^{C}PrP, rMo−Cer^{C}PrP) were generated through two consecutive PCRs with primers shown in Table II-2. Genes encoding rCerPrP and rMoPrP with two amino acid substitutions (rCerPrP−173S_{Mo}/177N_{Mo}, rMoPrP−169N_{Cer}/173T_{Cer}) were generated by assembly PCR using primer sets listed in Table II-2. Each gene was inserted into pET11a for the expression and purification of rPrPs.

Table II-1. Primers for cloning of the full-length rPrPs.

Constructs	Primer names	Nucleotide sequences [b]
rBoPrP	CerPrP-F [a]	5'-TTCATATGAAGAAGCGACCAAAACCTG-3'
	BoPrP-R	5'-TTGGATCCTCATGCCCCTCGTTGGTAATA-3'
rCerPrP	CerPrP-F [a]	5'-TTCATATGAAGAAGCGACCAAAACCTG-3'
	CerPrP-R	5'-TTGGATCCTCATGCCCCTCTTTGGTAA-3'
rShPrP	CerPrP-F [a]	5'-TTCATATGAAGAAGCGACCAAAACCTG-3'
	ShPrP-R	5'-TTGGATCCTCATGCCCCCCTTTGGTAA-3'

a: Same forward primer was used for the amplification because the nucleotide sequence encoding aa 25−30 of PrP from three artiodactyls is identical.
b: Underlines in forward primers indicate *Nde* I site, whereas those in reverse primers indicate *Bam*H I site.

Table II-2. Primers for constructing Cer/Mo chimeric PrPs.

Constructs	Primer names	Nucleotide sequences [b]
$rCerPrP_{94–233}$	CerPrP94-F	5'-TTCATATGGGTCAAGGTGGTACCCAC-3'
	CerPrP-R	5'-TTGGATCCTCATGCCCCTCTTTGGTAA-3'
rMo^{N}–CerPrP	MoPrP-F [a, b]	5'-TTCATATGAAAAAGCGGCCAAAGCCTG-3'
	Mo-CerPrP-R [a]	5'-GGGGTACGGTACATGTTTTCACG-3'
	Cer-MoPrP-F [a]	5'-CGTTACCCCAACCAAGTGACT-3'
	CerPrP-R [a, b]	5'-TTGGATCCTCATGCCCCTCTTTGGTAA-3'
$rCer^{N}$–MoPrP	CerPrP-F [a, b]	5'-TTCATATGAAGAAGCGACCAAAACCTG-3'
	Mo-CerPrP-R [a]	5'-GGGGTACGGTACATGTTTTCACG-3'
	Cer-MoPrP-F [a]	5'-CGTTACCCCAACCAAGTGACT-3'
	MoPrP-R [a, b]	5'-TTGGATCCTAGGATCTTCTCCCGTCGTAATA-3'
rCer–Mo^{C}PrP	CerPrP-F [c, d]	5'-TTCATATGAAGAAGCGACCAAAACCTG-3'
	$MoPrP^{C}$-R [c]	5'-GTCGTAATAAGCCTGGGATTCTTTCTGGTAC-3'
	MoPrP-R [d]	5'-TTGGATCCTAGGATCTTCTCCCGTCGTAATA-3'
rMo–Cer^{C}PrP	MoPrP-F [c, d]	5'-TTCATATGAAAAAGCGGCCAAAGCCTG-3'
	$CerPrP^{C}$-R [c]	5'- TTGGTAATAGGCCTGGGACTCCCTCTGGTAC -3'
	rCerPrP-R [d]	5'-TTGGATCCTCATGCCCCTCTTTGGTAA-3'
rCerPrP–$173S_{Mo}/177N_{Mo}$	CerPrP-F [a, b]	5'-TTCATATGAAGAAGCGACCAAAACCTG-3'
	CerN173ST177N-F [a]	5'-AGCAACCAGAACAACTTTGTGCATGACTG-3'
	CerN173ST177N-R [a]	5'-GTTGTTCTGGTTGCTATACTGATCCACT-3'
	CerPrP-R [a, b]	5'-TTGGATCCTCATGCCCCTCTTTGGTAA-3'
rMoPrP–$169N_{Cer}/173T_{Cer}$	MoPrP-F [a, b]	5'-TTCATATGAAAAAGCGGCCAAAGCCTG-3'
	MoS169NN173T-F [a]	5'-AATAACCAGAACACCTTCGTGCACGACTGC-3'
	MoS169NN173T-R [a]	5'-GGTGTTCTGGTTATTGTACTGATCCACT-3'
	MoPrP-R [a, b]	5'-TTGGATCCTAGGATCTTCTCCCGTCGTAATA-3'

a: Primers used for the amplifying the gene fragments in the first step of the assembly PCR.
b: Primers for assembling gene fragments in the second step of the assembly PCR.
c: Primes used for the first step reaction to replace the C-terminus of rPrP.
d: Primers used for the addition of *Bam*H I site for cloning into pET11a in the second step reaction to replace the C-terminus of rPrP. GGTACC, *Bam*H I site; CATATG, *Nde* I site.

3. Expression and purification of rPrPs

Expression and purification of rPrPs were performed as described elsewhere (Atarashi *et al*., 2007) with minor modifications. Briefly, BL21(DE3)pLysS cells (Invitrogen) transformed with the each expression plasmid were pre-cultured in 5 ml L-Broth medium overnight at 37˚C, and were further cultured in 200 ml MagicMedia E. coli expression medium (Invitrogen) for 30 h at 37˚C. Bacterial cells were harvested and lysed using CelLytic B cell lysis reagent (Sigma) with lysozyme (Sigma) and benzonase (Millipore) for 30 min at r.t. Inclusion bodies were collected by centrifugation at 14,400 ×g for 10 min at 4˚C. The resulting pellets were washed three times using the 10% CelLytic B cell lysis reagent and stored at −80˚C until use. Pellets were thawed and solubilized in denaturing buffer (100 mM sodium phosphate [pH 8.0], 10 mM tris(hydroxymethyl)aminomethane [tris], 6M GdnHCl) by rotating for 2 h at r.t. After centrifugation at 5,170 ×g for 30 min at 4˚C, the supernatant was mixed with Ni-NTA superflow resin (Qiagen, Germany), equilibrated with the denaturing buffer by washing three times, and the Ni-NTA superflow resin was loaded onto the XK16 column (GE Healthcare). The rPrP was refolded using a linear gradient of 6 to 0 M GdnHCl in refolding buffer (100 mM sodium phosphate [pH 8.0], 10 mM tris) using the ÄKTAexplore 10S system (GE Healthcare) and eluted by a linear gradient of 0 to 500 mM imidazole in 10 mM tris (pH 5.8). The fractions were pooled and dialyzed against ultra-pure water. After filtration, rPrP concentration was determined by measuring absorbance at 280 nm.

4. RT-QuIC reaction

RT-QuIC with rMoPrP, rBvPrP, rBoPrP, rShPrP and rCerPrP were performed using reaction condition with 100 μg/ml substrate and 500 mM NaCl with 0.001% SDS as described elsewhere (Sawada *et al*., 2019). The reaction using rHaPrP was performed with 60 μg/ml substrate and 350 mM NaCl without SDS. The 20% brain homogenates from prion-uninfected

deer and cattle (hereafter referred to as normal brain homogenate [NBH]) were diluted to 2% with PBS and were used as the negative control or diluent for the seed of the corresponding species. Then, 2% BHs of prion-infected animals were prepared from stock solutions (10% or 20%) (Figure II-1) and were serially diluted with PBS or species-matched 2% NBH, and 5 µl of each dilution was added into the three wells as seed. Final concentrations of brain tissue homogenates of the seed in the reaction mixture were from 10^{-4} [0.01%] to 10^{-9} [0.0000001%] after diluting with PBS. When the seeds were diluted with 2% NBH, the final concentration of the NBH in the reaction was 0.1%. RT-QuIC reactions were performed using the Infinite F200 microplate reader (TECAN, Switzerland) at 37˚C, or at 42˚C for rBvPrP, using the same cycles as described elsewhere (Sawada *et al*., 2019).

5. Date analysis

Threshold of the reactions were calculated as mean thioflavin T (ThT) fluorescence intensity plus 5 × SD from the negative control wells without seed (PBS). The reactions were considered as positive when the ThT fluorescence intensity exceeded the threshold (Henderson *et al*., 2015), with the following exception. If ThT fluorescence intensity temporarily exceeded the threshold within the first 1 h, the data from the first 1 h were excluded from calculations. If the oscillated waveforms were continuously observed throughout the reaction, it was considered as negative even the intensity exceeded the threshold. If oscillated waveforms were observed prior to the appearance of the typical ThT fluorescence curve observed from rPrP fibrils, the reaction was judged as positive once the typical fluorescence curve exceeded the threshold. The endpoint of the reaction was determined as the highest seed dilution that gave a positive reaction in three independent experiments with three replicates. If positive reactions were observed at 10^{-9} dilution, the endpoint was set as $<10^{-9}$. The lag phase (h) was defined as the time required for the fluorescence intensity to exceed the threshold.

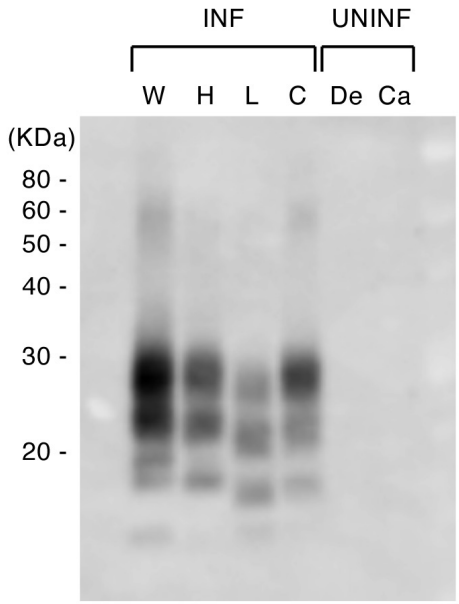

Figure II-1 Presence of proteinase-resistant PrP in the brain homogenates.
The 250 µl of 2% brain homogenates (BHs) of chronic wasting disease (CWD) (W), atypical bovine spongiform encephalopathy (BSE) (H-BSE (H), L-BSE (L)), and classical BSE (C-BSE) (C) infected animals (INF), and those of uninfected deer (De) and cattle (Ca) (UNINF), were digested with 40 µg/ml proteinase K (PK) at 37˚C for 30 min in the final reaction volume of 500 µl. PK-digested samples (250 µg brain tissue equivalent) were applied to each well. Immunoreaction was performed using monoclonal antibody T2 (Shimizu *et al*., 2010) directly conjugated with a horse radish peroxidase. Molecular weight markers are shown on the left in kDa.

RESULTS

1. Detection of CWD prions in the presence of high concentration of brain tissue homogenates

The reactivity of six rPrPs to CWD prions in the presence and absence of 0.1% deer NBH (Figure II-2) was analyzed by comparing the endpoints and lag phases. The endpoints of the reactions using five rPrPs, rMoPrP, rBvPrP, rHaPrP, rShPrP and rCerPrP, were from 10^{-8} to $<10^{-9}$ when reactions were performed in the absence of NBH (Figure II-2, PBS). However, the lag phases were varied with the rPrPs. Among the five rPrPs, the lag phases of rCerPrP were shortest at each seed dilution. On the other hand, rBoPrP was ineffective in detecting CWD prions, as the endpoint of the reaction was 10^{-4} (Figure II-2). Interestingly, the reactions of rHaPrP, rMoPrP, and rShPrP were affected by 0.1% deer NBH: the reaction of rHaPrP was completely inhibited, and the endpoints of the reactions using rMoPrP and rShPrP were worsened by 3 and 1 logs, respectively (Figure II-2). Additionally, lag phases of the reactions with each rPrP were significantly prolonged: the lag phases of rMoPrP, rBvPrP, and rShPrP were prolonged by 43.5, 27.8, and 29.6 h, respectively, at 10^{-5} seed dilutions in the presence of 0.1% deer NBH (Figure II-2). In contrast, only the reaction of rCerPrP was not severely affected by 0.1% deer NBH; the endpoint was unchanged, and the lag phase at 10^{-5} seed dilution was only prolonged by 7.7 h (Figure II-2).

2. Detection of atypical and classical BSE prions in the presence of high concentration of brain tissue homogenates

I also analyzed the reactivity of six rPrPs to atypical BSE (H- and L-BSE) and C-BSE in RT-QuIC. rBoPrP showed longer lag phases compared to the other rPrPs. However, all rPrPs showed similar endpoints of the detection of H-BSE prions in the absence of NBH (10^{-8} or $<10^{-9}$, Table II-3). rBoPrP and rHaPrP seemed to be less effective than the other four rPrP in the detecting L-BSE prions: endpoints of reactions using the former rPrPs (10^{-6} and 10^{-7}) were

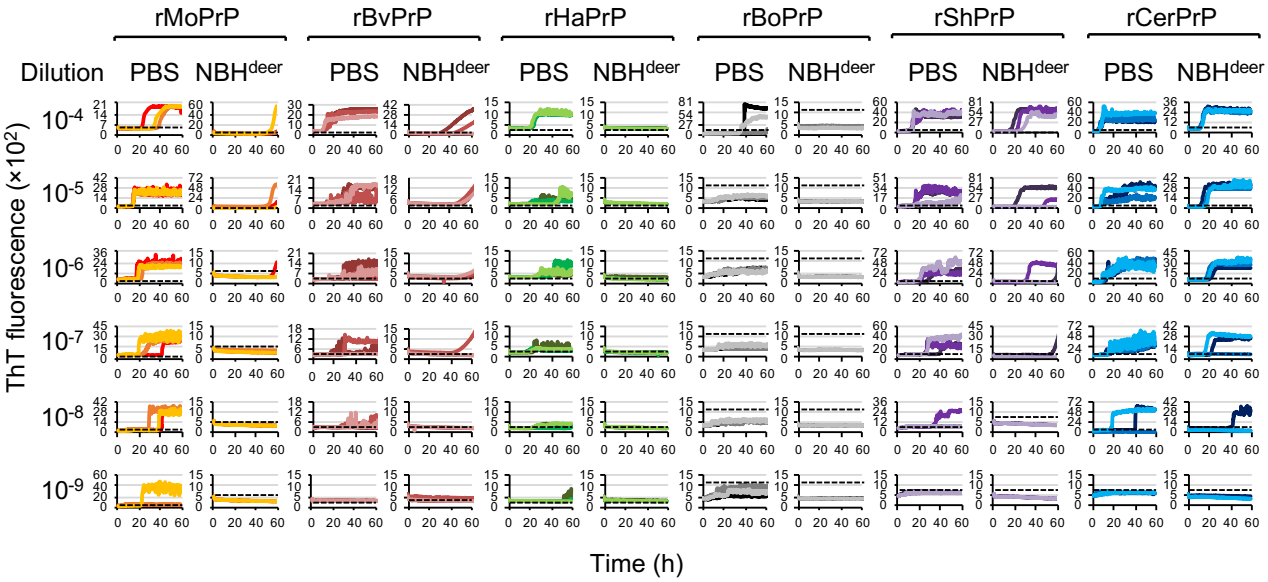

Seed	rPrP	Dil-uent	Lag phase (h) 10^{-4}	10^{-5}	10^{-6}	10^{-7}	10^{-8}	10^{-9}	End-point	Ratio
CWD	Mo	PBS	19.1 ± 11.1	14.7 ± 2.1	19.3 ± 7.7	28.5 ± 12.0	47.4 ± 15.4	55.8 ± 12.7	$<10^{-9}$	$<10^{-3}$
		NBH	59.0 ± 3.1**	58.2 ± 3.6**	59.7 ± 1.0**	>60.0**	>60.0*	>60.0	10^{-6}	
	Bv	PBS	10.1 ± 1.5	17.8 ± 3.9	17.5 ± 6.7	25.8 ± 9.1	38.5 ± 15.5	>60.0	10^{-8}	>10
		NBH	37.4 ± 10.5**	45.6 ± 6.5**	54.1 ± 5.1**	58.6 ± 4.1**	>60.0**	58.5 ± 4.4	$<10^{-9}$	
	Ha	PBS	18.1 ± 4.5	34.4 ± 15.6	28.7 ± 12.0	25.8 ± 14.1	43.5 ± 15.9	59.0 ± 2.4	$<10^{-9}$	$<10^{-5}$
		NBH	>60.0**	>60.0**	>60.0**	>60.0**	>60.0**	>60.0	$>10^{-4}$	
	Bo	PBS	45.1 ± 14.7	>60.0	>60.0	>60.0	>60.0	>60.0	10^{-4}	<1
		NBH	>60.0**	>60.0	>60.0	>60.0	>60.0	>60.0	$>10^{-4}$	
	Sh	PBS	12.3 ± 0.6	15.7 ± 1.9	19.8 ± 3.8	26.0 ± 7.6	50.1 ± 14.8	>60.0	10^{-8}	10^{-1}
		NBH	22.5 ± 6.1**	45.3 ± 13.7**	56.1 ± 10.3**	59.4 ± 1.8**	>60.0	>60.0	10^{-7}	
	Cer	PBS	7.4 ± 0.7	10.0 ± 1.4	10.9 ± 0.9	17.7 ± 3.2	35.9 ± 14.4	>60.0	10^{-8}	1
		NBH	14.6 ± 2.9**	17.7 ± 4.0**	32.0 ± 14.2**	30.0 ± 14.8*	47.7 ± 16.6	>60.0	10^{-8}	

Figure II-2 Reactivity of rPrPs to CWD prions in real-time quaking-induced conversion in the presence and absence of normal brain homogenates.

(A) Representative line graphs for the detection of CWD prions serially diluted with PBS (left column) or 2% BHs of CWD-negative white-tailed deer (NBH) (final concentration in the reaction mixture: 0.1%) (right column). Detections performed using recombinant mouse PrP (rMoPrP) (red to yellow), bank vole PrP (rBvPrP) (brown), hamster PrP (rHaPrP) (green), bovine PrP (rBoPrP) (black), sheep PrP (rShPrP) (purple), and cervid PrP (rCerPrP) (blue) are shown. thioflavin T (ThT) intensities from triplicate wells were plotted against reaction time using different brightness or colors. Dotted lines indicate the thresholds of reaction calculated from the mean ThT fluorescence intensity plus 5 × SD of negative control wells (without brain homogenates). Lag phases (mean ± SD), endpoints, and ratios of the endpoints [Ratio, endpoint (PBS)/endpoint (NBH)] are summarized in the table. *: $p < 0.05$, **: $p < 0.01$ by welch t-test.

lower than the latter four rPrPs (10^{-8} or $<10^{-9}$). A similar tendency was observed for the detection of C-BSE prions: rBoPrP and rHaPrP (endpoints: 10^{-4} and 10^{-5}) appeared to be less effective than the other four rPrPs (endpoints: 10^{-6}). Although no difference was observed in the detection endpoints of H-BSE prions among rMoPrP, rBvPrP, rShPrP, and rCerPrP, rCerPrP was able to detect H-BSE prions with shorter lag phases than the other rPrPs, especially at 10^{-5}–10^{-7} seed dilutions (Table II-3). Interestingly, 0.1% cattle NBH completely interfered with the detection of H-BSE prions with rBvPrP and rHaPrP, detection of L-BSE prions with rMoPrP, rBvPrP, rHaPrP, and rBoPrP, and detection of C-BSE prions with the five rPrP except for rCerPrP (Table II-3). Notably, the detection of atypical BSE prions with rCerPrP was not severely affected by 0.1% cattle NBH: endpoints of the reaction were unchanged and lag phases were prolonged at some seed dilutions, e.g. at 10^{-5}–10^{-7} for H-BSE, and 10^{-4} for L-BSE, but the difference were under 10 h except for 10^{-7} seed dilution of H-BSE (Table II-3). These results suggest that rCerPrP is a good substrate for the detection of atypical BSE as well as CWD prions in the presence of high concentrations of brain tissue homogenates. Moreover, detection of C-BSE prions was affected by 0.1% cattle NBH, which the endpoints of the reaction worsened by 2 logs and the lag phases were significantly prolonged (Table II-3). Also, 0.1% cattle NBH did not interfere with the detection of atypical BSE prions but interfered with the detection of C-BSE prions, suggesting that RT-QuIC using rCerPrP can discriminate atypical BSE from C-BSE prions.

Table II-3. Reactivity of rPrPs to atypical and classical BSE prions in RT-QuIC.

Seed	rPrP	Dil-uent [a]	Lag phase (h) [b]						End-point	Ratio [c]
			10^{-4}	10^{-5}	10^{-6}	10^{-7}	10^{-8}	10^{-9}		
H-BSE	Mo	PBS	21.2 ± 6.6	29.0 ± 12.3	28.8 ± 3.5	35.0 ± 13.4	49.1 ± 10.4	57.2 ± 8.3	$<10^{-9}$	$<10^{-2}$
		NBH	50.4 ± 9.9**	56.0 ± 5.4**	59.2 ± 2.4**	59.5 ± 1.4**	>60.0**	>60.0	10^{-7}	
	Bv	PBS	10.6 ± 1.5	21.9 ± 7.7	21.9 ± 3.8	27.6 ± 6.2	35.4 ± 10.5	55.5 ± 9.2	$<10^{-9}$	$<10^{-5}$
		NBH	>60.0**	>60.0**	>60.0**	>60.0**	>60.0**	>60.0	$>10^{-4}$	
	Ha	PBS	11.2 ± 1.1	26.3 ± 7.7	28.8 ± 8.5	43.5 ± 16.6	54.1 ± 8.8	>60.0	10^{-8}	$<10^{-4}$
		NBH	>60.0**	>60.0**	>60.0**	>60.0**	>60.0	>60.0	$>10^{-4}$	
	Bo	PBS	34.1 ± 3.0	41.2 ± 3.2	46.8 ± 7.4	56.9 ± 4.6	59.2 ± 2.3	58.7 ± 4.0	$<10^{-9}$	$<10^{-4}$
		NBH	59.0 ± 2.6**	59.7 ± 0.8**	>60.0**	>60.0	>60.0	>60.0	10^{-5}	
	Sh	PBS	12.0 ± 1.1	14.5 ± 1.5	18.7 ± 3.1	19.9 ± 2.2	31.0 ± 12.6	56.2 ± 10.1	$<10^{-9}$	1
		NBH	13.3 ± 1.8	14.4 ± 1.4	16.4 ± 0.9	19.2 ± 2.9	24.6 ± 7.9	52.3 ± 12.6	$<10^{-9}$	
	Cer	PBS	10.8 ± 1.9	10.9 ± 1.6	14.7 ± 2.8	16.9 ± 4.1	30.2 ± 7.9	58.2 ± 3.4	$<10^{-9}$	1
		NBH	20.4 ± 15.6	17.4 ± 3.0**	19.0 ± 3.3**	29.7 ± 15.7*	29.9 ± 13.0	51.8 ± 12.7	$<10^{-9}$	
L-BSE	Mo	PBS	19.9 ± 2.8	31.2 ± 4.7	42.7 ± 7.7	58.6 ± 2.9	58.4 ± 4.7	>60.0	10^{-8}	$<10^{-4}$
		NBH	>60.0**	>60.0**	>60.0**	>60.0	>60.0	>60.0	$>10^{-4}$	
	Bv	PBS	12.3 ± 0.7	23.0 ± 7.6	28.7 ± 9.5	37.6 ± 9.7	48.6 ± 10.6	56.6 ± 4.5	$<10^{-9}$	$<10^{-5}$
		NBH	>60.0**	>60.0**	>60.0**	>60.0**	>60.0**	> 60.0*	$>10^{-4}$	
	Ha	PBS	21.4 ± 2.9	47.7 ± 9.0	44.8 ± 12.8	55.1 ± 8.6	>60.0	>60.0	10^{-7}	$<10^{-3}$
		NBH	>60.0**	>60.0**	>60.0**	>60.0	>60.0	>60.0	$>10^{-4}$	
	Bo	PBS	51.3 ± 10.4	52.4 ± 5.9	58.8 ± 3.7	>60.0	>60.0	>60.0	10^{-6}	$<10^{-2}$
		NBH	>60.0*	>60.0**	>60.0	>60.0	>60.0	>60.0	$>10^{-4}$	
	Sh	PBS	19.3 ± 4.1	30.7 ± 6.9	32.8 ± 9.9	52.0 ± 9.0	57.7 ± 4.9	> 60.0	10^{-8}	10^{-1}
		NBH	31.1 ± 12.3*	47.2 ± 15.6*	50.9 ± 18.0*	59.1 ± 2.8*	> 60.0	> 60.0	10^{-7}	
	Cer	PBS	13.7 ± 2.1	19.5 ± 4.0	25.1 ± 6.1	36.8 ± 11.9	57.5 ± 5.9	57.5 ± 7.4	$<10^{-9}$	1
		NBH	18.6 ± 4.3**	22.5 ± 3.7	25.2 ± 7.2	36.2 ± 12.8	56.9 ± 6.2	58.6 ± 4.1	$<10^{-9}$	
C-BSE	Mo	PBS	26.2 ± 10.9	33.7 ± 14.8	50.0 ± 13.0	>60.0	>60.0	59.8 ± 0.5	10^{-6}	$<10^{-2}$
		NBH	>60.0**	>60.0**	>60.0*	>60.0	>60.0	>60.0	$>10^{-4}$	
	Bv	PBS	23.8 ± 7.5	54.7 ± 8.6	59.9 ± 0.3	>60.0	>60.0	>60.0	10^{-6}	$<10^{-2}$
		NBH	>60.0**	>60.0	>60.0	>60.0	>60.0	>60.0	$>10^{-4}$	
	Ha	PBS	52.1 ± 13.2	53.4 ± 9.9	>60.0	>60.0	>60.0	>60.0	10^{-5}	$<10^{-1}$
		NBH	>60.0	>60.0	>60.0	>60.0	>60.0	>60.0	$>10^{-4}$	
	Bo	PBS	53.6 ± 6.5	>60.0	>60.0	>60.0	>60.0	>60.0	10^{-4}	<1
		NBH	>60.0**	>60.0	>60.0	>60.0	>60.0	>60.0	$>10^{-4}$	
	Sh	PBS	34.5 ± 3.9	49.1 ± 9.5	59.6 ± 1.2	>60.0	>60.0	>60.0	10^{-6}	$<10^{-2}$
		NBH	>60.0**	>60.0**	>60.0	>60.0	>60.0	>60.0	$>10^{-4}$	
	Cer	PBS	20.7 ± 2.5	38.7 ± 7.5	56.5 ± 8.0	>60.0	>60.0	>60.0	10^{-6}	10^{-2}
		NBH	53.5 ± 12.9**	>60.0**	>60.0	>60.0	>60.0	>60.0	10^{-4}	

a: Seeds (brain homogenates [BHs] from prion-infected animal) were serially diluted 10-fold with either PBS or 2% NBH (final concentration in the reaction mixture was 0.1%) of the same species as the seeds.

b: Mean ± SD from three independent experiments with three replicates are shown (*: $p < 0.05$, **: $p < 0.01$, welch t-test).

c: The ratio was calculated as endpoint (PBS)/endpoint (NBH).

3. Involvement of N-terminal region of rCerPrP in its reactivity in the presence of NBH

RT-QuIC reaction is reported to be easily inhibited by high concentrations of tissue homogenates and body fluids (Orru *et al*., 2011; Wilham *et al*., 2010). In the present study, I found that the reaction of rCerPrP to CWD and atypical BSE prions was not largely affected by NBH as shown above. To clarify the mechanism of the unique property of rCerPrP in RT-QuIC reaction, I further analyzed the reactivities of rPrPs shown in Figure II-3. Compared to the full-length rCerPrP, the reactions of N-terminal truncated rCerPrP comprised aa 94−233 ($rCerPrP_{94–233}$) to CWD and atypical BSE prions were completely inhibited in the presence of NBH in the reaction (Table II-4). Furthermore, lag phases for detecting CWD and L-BSE prions using $rCerPrP_{94–233}$ at 10^{-4} seed dilution in PBS corresponding to 0.01% brain homogenates present in the reaction were obviously longer than those using full-length rCerPrP. Replacement of the N-terminal region of rCerPrP (aa 25−153) with the corresponding region of rMoPrP (aa 23−149) (rMo^{N}−CerPrP) showed modest influence on the detection endpoints for CWD and atypical BSE prions: the detection endpoints of rMo^{N}−CerPrP for CWD, H-BSE, and L-BSE (10^{-8}, 10^{-8}, and 10^{-7}, respectively, without NBH, Table II-5) were slightly lower than those of rCerPrP (10^{-8}, $<10^{-9}$, $<10^{-9}$, respectively, Figure II-2 and Table II-3). Additionally, the reaction of rMo^{N}−CerPrP to L-BSE prions was completely inhibited, and the reactions of rMo^{N}−CerPrP to CWD and H-BSE were severely affected by 0.1% NBH; the detection endpoints for CWD, H-BSE, and L-BSE prions worsened by 4, 2, >3 logs, respectively, with significant prolongation of lag phases at each seed dilution (Table II-5). The reactivities of rMo^{N}−CerPrP were quite similar to those of rMoPrP; the reaction of rMoPrP to L-BSE prions were completely inhibited (Table II-3), and the reactions of rMoPrP to CWD (Figure II-2) and H-BSE (Table II-3) were severely affected as observed in the significant prolongation of lag phases in the presence of 0.1% NBH.

On the other hand, replacement of the N-terminal region of rMoPrP (aa 23−149) with

the corresponding CerPrP (aa 25−153) (rCer^{N}−MoPrP) partially restored reactivity to a similar level to that of rCerPrP. Detection endpoints of CWD, H-BSE, and L-BSE prions using rCer^{N}−MoPrP without NBH (10^{-8}, $<10^{-9}$, and 10^{-8}, respectively, Table II-5) were almost comparable to those using rCerPrP (10^{-8}, $<10^{-9}$, and $<10^{-9}$, respectively, Figure II-2 and Table II-3). In addition, the reactivity of rCer^{N}−MoPrP to the three prions was not affected by NBH when endpoints were compared in the absence (PBS) and presence of NBH (Table II-5). However, the prolongation of lag phases in the detection of CWD, H-BSE, and L-BSE prions using rCer^{N}−MoPrP (11.8, 20.9, and 12.0 h, respectively, at 10^{-5} seed dilution, Table II-5) appeared to be longer than those caused by rCerPrP in the presence of NBH (7.7, 6.5, and 3.0 h, respectively, at 10^{-5} seed dilution, Figure II-2 and Table II-3), suggesting that rCer^{N}−MoPrP is more affected by NBH than rCerPrP. Taken together, these results suggest that the N-terminal region of rCerPrP is necessary for its unique property in RT-QuIC reaction in the presence of NBH.

rPrP		Efficiency for RT-QuIC substrate		Reactivity in the presence of NBH		
		Good	Moderate	Slightly affected	Moderately affected	Severely affected
rCerPrP	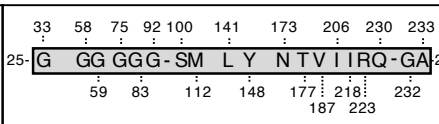	W, H, L		W, H, L		
rMoPrP	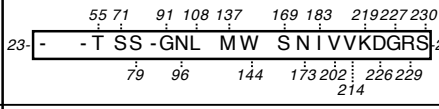	W	H, L		H	W, L
rCerPrP$_{94–233}$		H	W, L			W, H, L
rMo^{N}–CerPrP	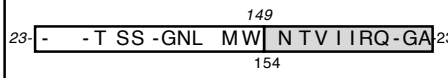	W, H	L			W, H, L
rCer^{N}–MoPrP	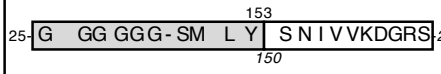	W, H	L		W, H, L	
rCer–Mo^{C}PrP		W, H, L		L		W, H
rMo–Cer^{C}PrP	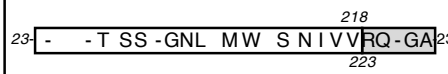		W, H, L	W, H, L		
rCer^{N}–Mo–Cer^{C}PrP	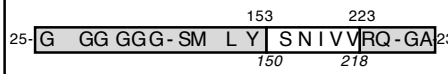	W, H, L		W, H, L		
rMo^{N}–Cer–Mo^{C}PrP	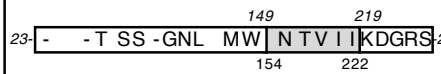	H	W, L			W, H, L
rCerPrP–173S$_{Mo}$/177N$_{Mo}$	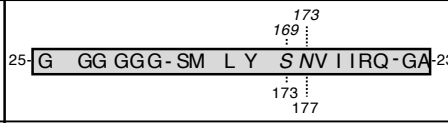	W, H, L			W, H	L
rMoPrP–169N$_{Cer}$/173T$_{Cer}$	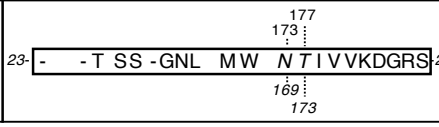	W	H, L		W, H, L	

Figure II-3 Summary of the reactivity of recombinant chimeric PrPs between CerPrP and MoPrP.
rCerPrP, rMoPrP, and their chimeras are indicated with their amino acid (aa) differences. Numbers with capital letters are the aa of CerPrP, while those with italics indicate the aa of MoPrP. "-" indicates gaps. A single-letter notation of aa with italics indicate the substituted aa between CerPrP and MoPrP. The real-time quaking-induced conversion (RT-QuIC) substrate efficiencies were classified as follows: Good, detection endpoints are $\leqq 10^{-8}$ and lag phases at 10^{-4} and 10^{-5} seed dilutions were <20 h for seeds diluted with PBS; Moderate, detection endpoints were $>10^{-8}$ or lag phases at 10^{-4} or 10^{-5} seed dilutions were ≧20 h. The criteria of the reactivity in the presence of NBH were defined as follows: slightly affected, endpoint ratio was $\geqq 10^{-2}$ and prolongation of the lag phase at 10^{-5} seed dilution [lag phase (NBH) − lag phase (PBS)] was <10 h; moderately affected: endpoint ratio is 10^{-2} to 10^{-3} and/or prolongation of the lag phase at 10^{-5} was from 10–25 h; severely affected, endpoint ratio was $<10^{-3}$ and/or prolongation of the lag phase at 10^{-5} seed dilution is >25 h. H, H-BSE; L, L-BSE; W, CWD.

Table II-4. Reactivity of N-terminal truncated rCerPrP in RT-QuIC.

rPrP	Seed	Dil-uent [a]	Lag phase (h) [b]						End-point	Ratio [c]
			10^{-4}	10^{-5}	10^{-6}	10^{-7}	10^{-8}	10^{-9}		
rCerPrP 94–233	CWD	PBS	38.1 ± 16.7	21.0 ± 10.4	23.6 ± 13.1	30.7 ± 19.9	48.1 ± 15.1	56.2 ± 11.3	$<10^{-9}$	$<10^{-5}$
		NBH	>60.0**	>60.0**	>60.0**	>60.0**	>60.0*	>60.0	$>10^{-4}$	
	H-BSE	PBS	14.1 ± 7.3	10.8 ± 5.5	11.6 ± 1.2	14.1 ± 7.2	29.7 ± 19.8	>60.0	10^{-8}	$<10^{-4}$
		NBH	>60.0**	>60.0**	>60.0**	>60.0**	>60.0**	>60.0	$>10^{-4}$	
	L-BSE	PBS	23.8 ± 17.1	18.3 ± 3.2	29.2 ± 11.9	47.3 ± 15.6	57.9 ± 4.8	>60.0	10^{-8}	$<10^{-4}$
		NBH	>60.0**	>60.0**	>60.0**	>60.0*	>60.0	>60.0	$>10^{-4}$	

a-c: Descriptions are the same as Table 1.

Table II-5. Reactivity of recombinant chimeric PrP between CerPrP and MoPrP in RT-QuIC.

rPrP	Seed	Dil-uent [a]	Lag phase (h) [b]						End-point	Ratio [c]
			10^{-4}	10^{-5}	10^{-6}	10^{-7}	10^{-8}	10^{-9}		
rMo^{N}–CerPrP	CWD	PBS	10.8 ± 1.9	14.3 ± 2.2	19.2 ± 5.5	23.6 ± 9.6	53.2 ± 13.7	>60.0	10^{-8}	10^{-4}
		NBH	46.8 ± 9.1**	>60.0**	>60.0**	>60.0**	>60.0	>60.0	10^{-4}	
	H-BSE	PBS	7.8 ± 1.4	10.5 ± 2.2	12.6 ± 2.3	17.4 ± 2.8	34.6 ± 21.0	>60.0	10^{-8}	10^{-2}
		NBH	52.4 ± 13.5**	58.1 ± 4.5**	58.8 ± 3.6**	>60.0**	>60.0**	>60.0	10^{-6}	
	L-BSE	PBS	13.5 ± 2.7	18.2 ± 2.2	28.1 ± 5.6	44.9 ± 14.0	>60.0	>60.0	10^{-7}	$<10^{-3}$
		NBH	>60.0**	>60.0**	>60.0**	>60.0**	>60.0	>60.0	$>10^{-4}$	
$rCer^{N}$–MoPrP	CWD	PBS	8.1 ± 1.2	10.0 ± 1.5	11.8 ± 2.1	17.4 ± 6.0	45.1 ± 17.3	>60.0	10^{-8}	1
		NBH	20.6 ± 2.0**	21.8 ± 3.0**	23.9 ±2.5**	34.4 ± 8.6**	51.5 ± 12.0	>60.0	10^{-8}	
	H-BSE	PBS	14.2 ± 2.1	17.6 ± 1.4	19.8 ± 2.0	25.0 ± 3.3	29.0 ± 3.3	51.1 ± 10.4	$<10^{-9}$	1
		NBH	28.4 ± 9.2**	38.5 ± 12.9**	35.7 ± 12.5**	44.7 ± 9.2**	54.2 ± 11.2**	57.1 ± 8.8	$<10^{-9}$	
	L-BSE	PBS	13.8 ± 2.1	20.1 ± 3.8	28.8 ± 11.3	45.1 ± 12.8	58.2 ± 5.5	>60.0	10^{-8}	1
		NBH	35.3 ± 16.9**	32.1 ± 15.3*	44.0 ± 18.9	47.1 ± 13.0	58.2 ± 3.9	>60.0	10^{-8}	
rCer–Mo^{C}PrP	CWD	PBS	10.6 ± 1.6	12.5 ± 2.0	13.6 ± 2.7	19.6 ± 3.6	33.6 ± 12.6	58.0 ± 4.5	$<10^{-9}$	$<10^{-3}$
		NBH	41.0 ± 15.9**	44.6 ± 14.5**	57.9 ± 6.2**	>60.0**	>60.0**	>60.0	10^{-6}	
	H-BSE	PBS	9.5 ± 1.3	10.6 ± 2.8	13.0 ± 2.5	26.7 ± 12.8	33.3 ± 15.9	54.7 ± 10.7	$<10^{-9}$	$<10^{-1}$
		NBH	43.8 ± 15.2**	54.5 ± 10.6**	57.8 ± 6.7**	58.5 ± 4.6**	57.0 ± 9.1**	>60.0	10^{-8}	
	L-BSE	PBS	12.6 ± 1.8	19.7 ± 1.8	24.0 ± 2.5	41.5 ± 8.4	57.6 ± 2.4	58.9 ± 2.4	$<10^{-9}$	1
		NBH	28.8 ± 4.9**	27.6 ± 6.5**	36.7 ± 11.8*	52.5 ± 9.6*	57.8 ± 6.6	57.8 ± 6.7	$<10^{-9}$	
rMo–Cer^{C}PrP	CWD	PBS	20.5 ± 3.5	24.5 ± 7.1	29.7 ± 6.7	33.4 ± 7.5	52.2 ± 11.6	58.9 ± 2.5	$<10^{-9}$	1
		NBH	20.4 ± 2.2	23.7 ± 2.9	30.3 ± 12.4	33.6 ± 5.6	45.5 ± 9.5	59.6 ± 1.2	$<10^{-9}$	
	H-BSE	PBS	22.9 ± 10.9	26.5 ± 6.2	29.7 ± 11.0	28.9 ± 6.4	51.6 ±9.6	58.5 ± 3.0	$<10^{-9}$	1
		NBH	22.3 ± 1.4	35.8 ± 12.8	37.6 ± 12.8	41.7 ± 13.3*	48.5 ± 8.5	59.1 ± 2.7	$<10^{-9}$	
	L-BSE	PBS	22.0 ± 5.0	25.7 ± 6.8	35.9 ± 9.1	44.6 ± 9.1	51.6 ± 18.4	>60.0	10^{-8}	1
		NBH	25.4 ± 6.7	33.3 ± 6.3*	43.8 ± 8.1	50.1 ± 7.9	59.3 ± 1.5	>60.0	10^{-8}	
$rCer^{N}$–Mo–Cer^{C}PrP	CWD	PBS	12.5 ± 2.6	14.7 ± 2.0	20.1 ± 5.2	28.9 ± 12.4	52.6 ± 15.6	>60.0	10^{-8}	1
		NBH	17.2 ± 2.3**	20.3 ± 3.5**	22.9 ± 4.3	34.5 ± 4.8	53.7 ± 6.8	>60.0	10^{-8}	
	H-BSE	PBS	13.3 ± 0.8	16.6 ± 2.0	17.4 ± 1.1	22.6 ± 3.8	38.8 ± 12.0	56.5 ± 9.4	$<10^{-9}$	1
		NBH	17.2 ± 2.5**	22.1 ± 3.9**	27.0 ± 3.3**	32.8 ± 4.5**	42.0 ± 6.6	52.9 ± 7.9	$<10^{-9}$	
	L-BSE	PBS	11.7 ± 0.9	19.5 ± 3.5	23.6 ± 2.9	37.9 ± 12.8	55.7 ± 6.9	59.8 ± 0.7	$<10^{-9}$	$<10^{-1}$
		NBH	17.3 ± 3.2**	25.4 ± 5.0**	33.7 ± 6.5**	41.4 ± 14.0	59.5 ± 1.6	>60.0	10^{-8}	
rMo^{N}–Cer–Mo^{C}PrP	CWD	PBS	13.8 ± 2.4	21.8 ± 5.4	22.7 ± 3.0	29.6 ± 8.6	57.3 ± 5.7	59.6 ± 1.2	$<10^{-9}$	$<10^{-5}$
		NBH	>60.0**	>60.0**	>60.0**	>60.0**	>60.0	>60.0	$>10^{-4}$	
	H-BSE	PBS	9.4 ± 1.6	14.6 ± 5.1	19.5 ± 7.0	31.2 ± 13.5	47.0 ± 15.3	>60.0	10^{-8}	$<10^{-4}$
		NBH	>60.0**	>60.0**	>60.0**	>60.0**	>60.0*	>60.0	$>10^{-4}$	
	L-BSE	PBS	17.6 ± 4.1	22.3 ± 3.0	29.2 ± 9.6	46.9 ± 11.4	55.7 ± 5.7	56.4 ± 6.1	$<10^{-9}$	$<10^{-5}$
		NBH	>60.0**	>60.0**	>60.0**	>60.0**	>60.0*	>60.0	$>10^{-4}$	

Table II-5. continued.

rPrP	Seed	Dil-uent [a]	Lag phase (h) [b]						End-point	Ratio [c]
			10^{-4}	10^{-5}	10^{-6}	10^{-7}	10^{-8}	10^{-9}		
rCerPrP–173S_{Mo}/177N_{Mo}	CWD	PBS	9.5 ± 0.7	11.3 ± 1.0	14.4 ± 3.1	26.3 ± 12.8	49.6 ± 14.6	57.2 ± 5.9	$<10^{-9}$	$<10^{-2}$
		NBH	32.8 ± 8.2**	36.1 ± 13.9**	47.5 ± 10.8**	55.5 ± 8.0*	>60.0*	>60.0	10^{-7}	
	H-BSE	PBS	9.5 ± 1.0	11.3 ± 0.9	13.5 ± 1.2	18.8 ± 3.1	27.4 ± 14.4	48.1 ± 11.1	$<10^{-9}$	$<10^{-2}$
		NBH	30.7 ± 11.3**	42.8 ± 15.2**	54.5 ± 12.9**	54.4 ± 9.8**	>60.0**	>60.0**	10^{-7}	
	L-BSE	PBS	12.1 ± 3.1	17.6 ± 7.6	29.9 ± 17.8	32.4 ± 12.2	>60.0	56.5 ± 5.1	10^{-9}	10^{-1}
		NBH	31.1 ± 9.3**	48.1 ± 13.7**	49.6 ± 14.0*	>60.0**	56.8 ± 9.7	>60.0	10^{-8}	
rMoPrP–169N_{Cer}/173T_{Cer}	CWD	PBS	12.6 ± 2.4	13.2 ± 1.7	18.5 ± 3.9	34.8 ± 19.5	53.1 ± 15.9	59.5 ± 1.4	$<10^{-9}$	$<10^{-1}$
		NBH	28.2 ± 4.9**	37.4 ± 7.9**	49.3 ± 12.0**	58.4 ± 4.3**	59.1 ± 2.7	>60.0	10^{-8}	
	H-BSE	PBS	11.9 ± 3.8	27.0 ± 14.9	31.9 ± 5.2	45.1 ± 14.9	55.3 ± 9.3	>60.0	10^{-8}	1
		NBH	20.1 ± 8.8*	42.6 ± 16.4	53.5 ± 10.5**	56.8 ± 9.6	55.7 ± 13.0	>60.0	10^{-8}	
	L-BSE	PBS	23.5 ± 5.2	24.9 ± 9.3	32.8 ± 13.2	46.9 ± 16.6	59.7 ± 0.9	>60.0	10^{-8}	10^{-1}
		NBH	21.6 ± 7.2	49.4 ± 10.3**	59.7 ± 1.0**	59.5 ± 1.6	> 60.0	>60.0	10^{-7}	

a-c: Descriptions are the same as Table 1.

4. Involvement of C-terminal region of rCerPrP in its reactivity in the presence of NBH

It has been reported that the aa sequence at the extreme C-terminus of PrP^C is varied among animal species (Billeter *et al*., 1997), and aa substitution in this region could influence the efficiency of PrP^C conformational conversion (Erana *et al*., 2017; Kurt *et al*., 2017) and transmission kinetics (Watts *et al*., 2015). Therefore, I analyzed the involvement of the C-terminal region of CerPrP in its reactivity in RT-QuIC. The rCer−Mo^{C}PrP, which possesses MoPrP aa 219−231 in the corresponding region of CerPrP aa 223−233, with 5 aa difference in this region from rCerPrP reacted well with CWD, H-BSE, and L-BSE prions (endpoints: $<10^{-9}$, Table II-5) in the absence of NBH compared to the reactivity of rCerPrP (10^{-8}, $<10^{-9}$, and $<10^{-9}$, respectively, Figure II-2 and Table II-3). Lag phases for the detection of CWD, H-BSE, and L-BSE prions using rCer−Mo^{C}PrP (12.5, 10.6, 19.7 h, respectively, at 10^{-5} seed dilution, Table II-5) were comparable to those using rCerPrP (10.0, 10.9, and 19.5 h, respectively, Figure II-2 and Table II-3). However, the detection endpoint of CWD prions using rCer−Mo^{C}PrP worsened by >3 logs in the presence of 0.1% NBH with prolonged lag phases (Table II-5). This reactivity is rather similar to that of rMoPrP to CWD prions (Figure II-2). Although the detection endpoint of H-BSE using rCer−Mo^{C}PrP worsened only by 1 log in the presence of 0.1% NBH, lag phases of the detection of H-BSE prions were significantly prolonged, e.g. lag phases of the detection using rCerPrP were prolonged only by 6.5 h at 10^{-5} seed dilution (Table II-3), but those using rCer−Mo^{C}PrP were prolonged by 43.9 h at 10^{-5} seed dilution in the presence of 0.1% NBH (Table II-5). On the contrary, the reactivity of rCer−Mo^{C}PrP to L-BSE was not severely affected, and no differences in the detection endpoints with marginally prolonged lag phases (around 10 h) at each seed dilution (Table II-5). Thus, the reactivity of rCer−Mo^{C}PrP to CWD and H-BSE prions in the presence of NBH resembles that of rMoPrP, whereas its reactivity to L-BSE prions resembles that of rCerPrP.

On the other hand, replacement of MoPrP aa 219−231 with the corresponding CerPrP

aa 223−233 (rMo−Cer^{C}PrP) did not affect the detection endpoint of CWD, H-BSE, and L-BSE prions diluted with PBS ($<10^{-9}$, $<10^{-9}$, and 10^{-8}, respectively, Table II-5). However, lag phases in the detection of three prions diluted with PBS using rMo−Cer^{C}PrP (about 20.5−26.5 h at 10^{-4} and 10^{-5} seed dilutions, Table II-5) were longer than those using rCerPrP (less than 19.5 h at 10^{-4} and 10^{-5} seed dilutions, Figure II-2 and Table II-3), but were comparable to those using rMoPrP (14.7−31.2 h at 10^{-4} and 10^{-5} seed dilutions, Figure II-2 and Table II-3), suggesting that rMo−Cer^{C}PrP is less efficient than rCerPrP as a substrate for RT-QuIC reaction. Interestingly, however, the reactivity of rMo−Cer^{C}PrP to three prions were less affected by 0.1% NBH; their detection endpoints were not changed, but slightly prolonged lag phases were observed (0, 9.3, and 7.6 h, respectively, at 10^{-5} seed dilution, Table II-5). In contrast, those of rMoPrP were severely interfered in the presence of 0.1% NBH; detection endpoints worsened by 2−4 logs with significantly prolonged lag phases (43.5, 27.0, and >28.8 h for CWD, H-BSE, and L-BSE, respectively, at 10^{-5} seed dilution, Figure II-2 and Table II-3). These results indicate that replacing only eleven aa in the C-terminal region of CerPrP appeared to confer the unique property of rCerPrP to rMoPrP that made it such that the presence of NBH interferes less the same as the RT-QuIC reaction using rCerPrP.

To confirm the involvement of N- and C-terminal regions of CerPrP in its reactivity in RT-QuIC, I further analyzed the reactivity of chimeric PrPs shown in Figure II-3. rCer^{N}−Mo−Cer^{C}PrP, which is composed of CerPrP aa 25−153, MoPrP aa 150−218, and CerPrP aa 223−233, could detect CWD, H-BSE, and L-BSE well without worsening the detection endpoints but had marginally prolonged lag phases, most of them which were less than 10 h long in the presence of NBH (Table II-5). These results were consistent with the finding that both N- and C-terminal regions of CerPrP are involved in its unique property in RT-QuIC reaction in the presence of NBH. On the contrary, rMo^{N}−Cer−Mo^{C}PrP, which has an opposite structure to rCer^{N}−Mo−Cer^{C}PrP, showed similar reactivity to rMoPrP, and detections of CWD,

H-BSE, and L-BSE prions were severely affected by NBH (Table II-5).

5. Effect of CerPrP-specific aa in the β2−α2 loop on its reactivity in the presence of NBH

Several studies reported that the CerPrP-specific aa Asn173 and Thr177 in the β2−α2 loop (aa 168−178) (Gossert *et al*., 2005) influence cross-species prion transmission in transgenic mice and affect the reaction in PMCA (Harrathi *et al*., 2019; Sigurdson *et al*., 2010). To clarify the influence of these aa residues on the unique reactivity of rCerPrP in RT-QuIC reaction, I analyzed the reactivities of rCerPrP carrying the corresponding MoPrP aa Ser169 and Asn173 (rCerPrP−173S_{Mo}/177N_{Mo}). Substitution of two CerPrP-specific aa did not affect the detection endpoints of the CWD and atypical BES prions (10^{-9} or $<10^{-9}$, in Table II-5) compared to rCerPrP (10^{-8}, $<10^{-9}$, and $<10^{-9}$, for CWD, H-BSE, and L-BSE, respectively, Figure II-2 and Table II-3) in the absence of NBH. However, substitution of the two aa affected the reactivity of rCerPrP in the presence of NBH: the detection endpoints worsened by more than >2 logs for CWD and H-BSE prions and by 1 log for L-BSE prions, with >20 h prolonged lag phases at most seed dilutions (Table II-5). The substitution of MoPrP Ser169 and Asn173 with the corresponding CerPrP Ans173 and Thr177 (rMoPrP−169N_{Cer}/173T_{Cer}) reduced the reactivity to H- and L-BSE prions by 1 log in the absence of NBH (Table II-5). The reactivity of rMoPrP to CWD, H-BSE, and L-BSE prions were extremely affected in the presence of NBH as described above (Figure II-2 and Table II-3). However, the detection of the three prions using rMoPrP−169N_{Cer}/173T_{Cer} in the presence of NBH was moderately affected compared to rMoPrP; the detection endpoints were reduced only by 1 log for CWD and L-BSE prions with moderately prolonged lag phases (8.2−24.5 h at 10^{-4} a 10^{-5} seed dilutions, Table II-5).

DISCUSSION

rPrPs from Bv, Ha, and Hu have been widely used as substrates to detect the seeding activity of prions by the RT-QuIC reaction (Atarashi *et al*., 2011; Orru *et al*., 2015; Peden *et al*., 2012; Wilham *et al*., 2010). However, the reaction is known to be sensitive to inhibitory factor(s) present in tissue homogenate and body fluids (Hoover *et al*., 2017; Orru *et al*., 2011; Wilham *et al*., 2010). In this Chapter, I demonstrated that rCerPrP reacted with CWD and atypical BSE prions even in the presence of the highest concentration of NBH (0.1%) in the reaction mixture. Since reactivity of rCerPrP was stable and reproducible without any influence of lot differences, I attempted to determine the region(s) responsible for the unique reactivity of rCerPrP. The unique reactivity of rCerPrP disappeared when the N-terminal region (aa 25−93) was truncated. Moreover, replacement of the N-terminal half of MoPrP (23−149) with the corresponding region of CerPrP partly restored this reactivity, whereas replacing the N-terminal half of CerPrP (aa 25−153) with the corresponding region of MoPrP abolished the unique reactivity of rCerPrP as summarized in Figure II-3. These results indicate that the N-terminal region of the rCerPrP is one of the determinants modulating the reactivity of rCerPrP in RT-QuIC reaction in the presence of NBH (Figure II-4). N-terminal truncated rPrPs have been known to act as better substrates for detecting the amyloid seeding activity of PrP^{Sc} (Orru *et al*., 2016; Peden *et al*., 2012). However, it has been reported that the N-terminal region is one of essential regions for the binding between PrP^{C} and PrP^{Sc}, and PrP^{Sc} production (Abalos *et al*., 2008; Erana *et al*., 2017; Hara *et al*., 2018; Lawson *et al*., 2001). Deletion of the octapeptide repeat region (aa 51−90 of MoPrP) delayed accumulation of PrP^{Sc} and prolonged the survival of mice inoculated with C-BSE prions (Hara *et al*., 2018), suggesting the involvement of the N-terminal region in the efficacy of conformational conversion in certain combinations of PrP^{C} and PrP^{Sc}. In addition, aa polymorphisms of CerPrP at Gln95 and Gly96 are known to modulate the susceptibility of deer to CWD prions (Duque Velasquez *et al*., 2015; Johnson *et al*., 2011),

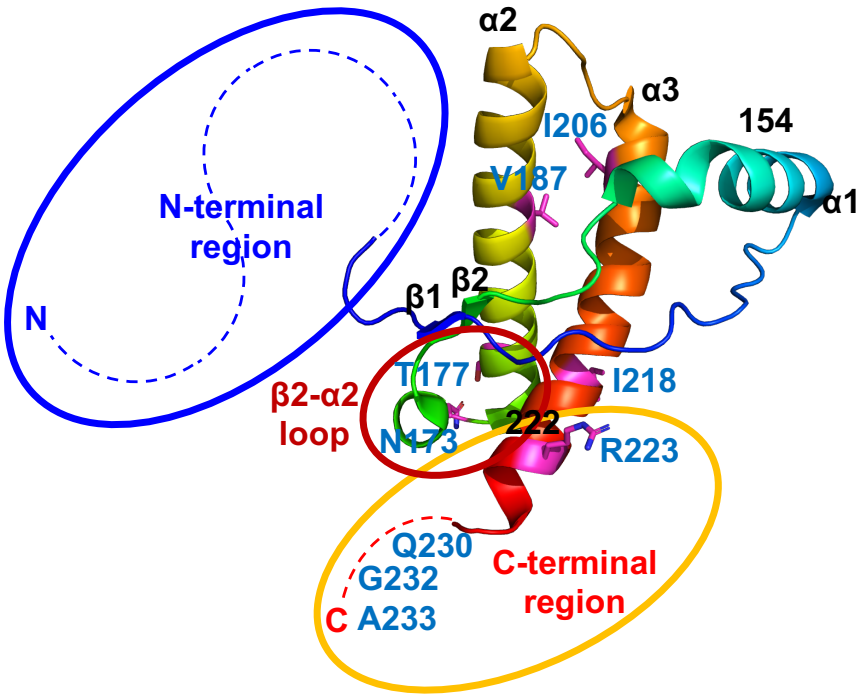

Figure II-4. Regions responsible for the unique reactivity of rCerPrP in RT-QuIC.
The three-dimensional structure of CerPrP (PDB ID: 4YXH) was drawn using open-source PyMOL. The regions responsible for the unique reactivity of rCerPrP, N- and C-terminal regions and the β2–α2 loop are shown using blue, yellow, and red circles, respectively. The aa of rCerPrP in the β2–α2 loop and C-terminus are shown in the single-letter notation. Hydrophobic aa differed between $rCer^{N}$–Mo–Cer^{C}PrP and rCerPrP–$173S_{Mo}/177N_{Mo}$ and regions in which rCerPrP are replaced with (aa 153–222) are shown around the structure. The side chains of aa with aa numbers except for three aa at C-terminal end were drawn with sticks and the aa residues were colored indicated with magenta.

also suggesting the involvement of the N-terminal region of CerPrP^{C} on the efficacy of its conformational conversion. There are two possibilities regarding the role of the N-terminal region of CerPrP in its unique reactivity in the presence of NBH. First, the presence of the N-terminal region may stabilize intra- or intermolecular interaction of rCerPrP, which enhances the efficacy of amyloid formation. Alternatively, the N-terminal region effectively inhibits the interaction of inhibitory factor(s) in tissue homogenates with rCerPrP. However, the latter is unlikely because the reactivity of rCerPrP to C-BSE was affected in the presence of NBH.

Although rMo−Cer^{C}PrP was not a good substrate for the RT-QuIC reaction, i.e., the lag phases for detecting CWD and atypical BSE prions in the absence of NBH were >20 h at 10^{-4} and 10^{-5} seed dilutions (Table II-5), the C-terminal region of rCerPrP is also involved in the unique reactivity of rCerPrP, and the reactivity of rMo−Cer^{C}PrP was less affected by NBH than that of rMoPrP (Figure II-3 and Table II-5). Nevertheless, the unique reactivity of rCerPrP in the presence of NBH disappeared due to the N-terminal truncation even in the presence of the C-terminal region of CerPrP (rCerPrP$_{94–233}$) (Figure II-3 and Table II-4), suggesting that a cooperative effect of the C-terminal region with the N-terminal region. Indeed, rCer^{N}−Mo−Cer^{C}PrP showed better reactivity than rCer−Mo^{C}PrP when used as a substrate for RT-QuIC and was less affected in the presence of NBH compared to rCer−Mo^{C}PrP, suggesting that an additive effect of the N- and C-terminal regions of CerPrP (Figure II-3). The NMR structure of rHuPrP and rMoPrP revealed the intermolecular interaction between the C-terminal region (aa 219−226) and the N-terminal flexible region (Zahn *et al*., 2000) or the C-terminal region (aa 215−223) and the β2−α2 loop (aa 164−174) (Billeter *et al*., 1997). These intramolecular interaction could be destabilized by substituting Gln217$_{Mo}$ with Arg, which is a mutation associated with GSS (Liemann and Glockshuber, 1999), and HuPrP Glu219 with Lys, which is a protective polymorphism against CJD (Biljan *et al*., 2012). Thus, intra- and intermolecular interactions between the N- and C-terminal regions of rCerPrP may be strong

enough to overcome the influence of possible inhibitory factor(s) in NBH and to promote the conformational conversion of rCerPrP.

Since rCer^{N}−Mo−Cer^{C}PrP possessed five aas from MoPrP including aa substitutions at aa 173 and 177, the reactivity to CWD and atypical BSE prions of rCerPrP−173S$_{Mo}$/177N$_{Mo}$, which possesses only two aa difference from CerPrP, seems to be closer to that of rCerPrP compared to that of rCer^{N}−Mo−Cer^{C}PrP. The detection endpoints of rCerPrP−173S$_{Mo}$/177N$_{Mo}$ for detecting CWD and atypical BSE prions were comparable to that of rCer^{N}−Mo−Cer^{C}PrP when the seeds were diluted with PBS (Table II-5). However, the reactivity of rCerPrP−173S$_{Mo}$/177N$_{Mo}$ was more susceptible to the inhibitory effect of NBH than that of rCer^{N}−Mo−Cer^{C}PrP even though the N- and C-terminal regions of both rPrPs were composed of CerPrP (Figure II-3). One possible explanation for this may be an incompatibility of aa in the region comprised of aa 154−222 in CerPrP, which contains five aa differences between Cer- and MoPrP. Indeed, aa 173 and 177 of rCerPrP−173S$_{Mo}$/177N$_{Mo}$ were substituted by Ser169 and Asn173 of MoPrP, respectively, which are locate within the β2−α2 loop (aa 168−178 of CerPrP) (Gossert *et al*., 2005), whereas the remaining three aa are Val187 (α2-helix: aa 176-197 of CerPrP), Ile206 and Ile218 (α3-helix: aa 202−226 of CerPrP) (Figure II-4). An aa substitution at Ser170 of HuPrP with the corresponding Asn from BvPrP, which is corresponding to aa 173 of CerPrP, increased the conversion of HuPrP^{C} into the PrP-res by CWD prions during PMCA analysis (Kurt *et al*., 2017). Rabbit (Rb) PrP is known to be resistant to convert into PrP-res. However, substitution at Ile202 of RbPrP using the corresponding Val from MoPrP, which corresponds to aa 206 of CerPrP, increased the conversion of RbPrP^{C} into PrP-res by RML prions during PMCA (Erana *et al*., 2017). Additionally, substitution of Ile215 of HuPrP with the Val from BvPrP, which corresponds to aa 218 of CerPrP, worsened the conversion efficiency of HuPrP^{C} by the RML prions (Kurt *et al*., 2017). The β2−α2 loop is known to interact with the α3-helix through hydrophobic interactions and a disulfide bridge,

but single aa substitutions within these regions decreased the hydrophobic interaction (Lee *et al*., 2019). Therefore, heterologous aa combinations in the β2−α2 loop and α3-helix may influence PrP stability and affect the conversion efficiency of rPrP during RT-QuIC reaction.

In this chapter, I showed that the RT-QuIC reaction using full-length rCerPrP as a substrate is useful for detecting low levels of CWD and atypical BSE prions in tissues homogenates, since the reaction of rCerPrP was not highly affected by high NBH concentrations. Additionally, I found that at least the N- and C-terminal regions of CerPrP are involved in the unique reactivity of the rCerPrP in RT-QuIC. These results will be useful for optimizing artificial rPrP for RT-QuIC reaction.

BRIEF SUMMARY

RT-QuIC reaction is known as a sensitive and specific method for detecting prions. However, the reaction is easily affected by the inhibitory factor(s) present in tissue homogenates. To identify the RT-QuIC condition that can detect low levels of CWD and BSE prions in the presence of high concentration of brain tissue homogenates, I tested the reactivities of various rPrPs. Among rPrPs tested, only the reaction of rCerPrP to CWD and atypical BSE prions was less affected by the high concentration of NBH. This unique reactivity disappeared when the N-terminal region aa 25−93 was truncated. In addition, replacement of MoPrP aa 23−149 with CerPrP aa 25−153, and C-terminal region of MoPrP aa 219−231 with CerPrP aa 223-233 partly conferred the unique reactivity of CerPrP to rMoPrP, suggesting the involvement of both N- and C-terminal regions in the unique reactivity of rCerPrP. Additionally, the reactivity of rCer^{N}−Mo−Cer^{C}PrP, a chimeric PrP comprising CerPrP aa 25−153, MoPrP aa 150−218, and CerPrP 223−233, showed an additive effect of the N- and C-terminal regions. These results provide a mechanistic implication for detecting CWD and atypical BSE prions by RT-QuIC using rCerPrP and are useful for further improvement of RT-QuIC.

CHAPTER III

Monitoring for CWD status in Japan by RT-QuIC assay using rCerPrP as an application of its unique reactivity.

INTRODUCTION

Recently, venison consumption in Japan is getting popular year by year. From 2017 to 2019, the amount of processed sika deer (*Cervus Nippon*) meat at the slaughterhouses increased by nearly 150 tons every year in Japan (Ministry of Agriculture Forestry and Fisheries (MAFF), 2020). Therefore, clarifying CWD status in cervid in Japan is important for ensuring the safety and security of deer products. There are two reports on surveillance in Japan that were conducted more than 15 years ago, and no CWD cases were identified at that time (Kataoka *et al*., 2005; Masujin *et al*., 2007). However, the recent emergence and spread of CWD in Scandinavian countries remind us the importance of continuous monitoring to clarify the CWD status. Therefore, I attempted to clarify a recent CWD status in Japan using RT-QuIC assay.

The RT-QuIC assay is a specific and highly sensitive method used in detecting the seeding activity of PrP^{Sc} (Atarashi *et al*., 2011). The assay can detect low levels of PrP^{Sc} from tissues and body fluids of prion-infected animals within a short time. Despite its specificity and sensitivity, the reaction is easily interfered with inhibitory factor(s) present in the tissue homogenates or body fluids (Orru *et al*., 2011; Wilham *et al*., 2010), that impedes the detection of PrP^{Sc} from the high concentration of tissue homogenates. In the Chapter II, I demonstrated that the rCerPrP is a suitable substrate for detecting low levels of CWD prions in a high concentration of brain tissue homogenates. Since the reaction of rCerPrP is less affected by the tissue homogenates present in the reaction mixture than other rPrPs (Suzuki *et al*., 2020), RT-QuIC assay using rCerPrP will be useful as a practical and reliable method for the monitoring of CWD.

In Chapter III, I describe the monitoring of CWD status in Japan by the RT-QuIC assay.

MATERIALS & METHODS

1. Brain materials

A total of 690 obex region of the medulla oblongata from captured or hunted deer in Japan during 2016−2020 were tested in this study (Fig. III-1 and Table III-1). The 634 obex tissues were obtained from three and one game meat processing companies in Hokkaido and Hyogo prefecture, respectively, and 56 obex tissues of Reeves's muntjac in Kanto area were kindly provided by Tokyo metropolitan Oshima Park Office. The tested deer included 332 males and 275 females; gender information was unavailable for the 83 samples. The estimated age ranged from 0 to 8 year-old, while the 70 samples was unknown (Table III-1). The 100 mg obex tissues were homogenized in sterile PBS at a concentration of 10% as described elsewhere (Sawada *et al*., 2019) and stored at −30˚C until use. Preparation of 20% BHs of pooled six and two CWD-affected and unaffected, respectively, white-tailed deer were described in Chapter II.

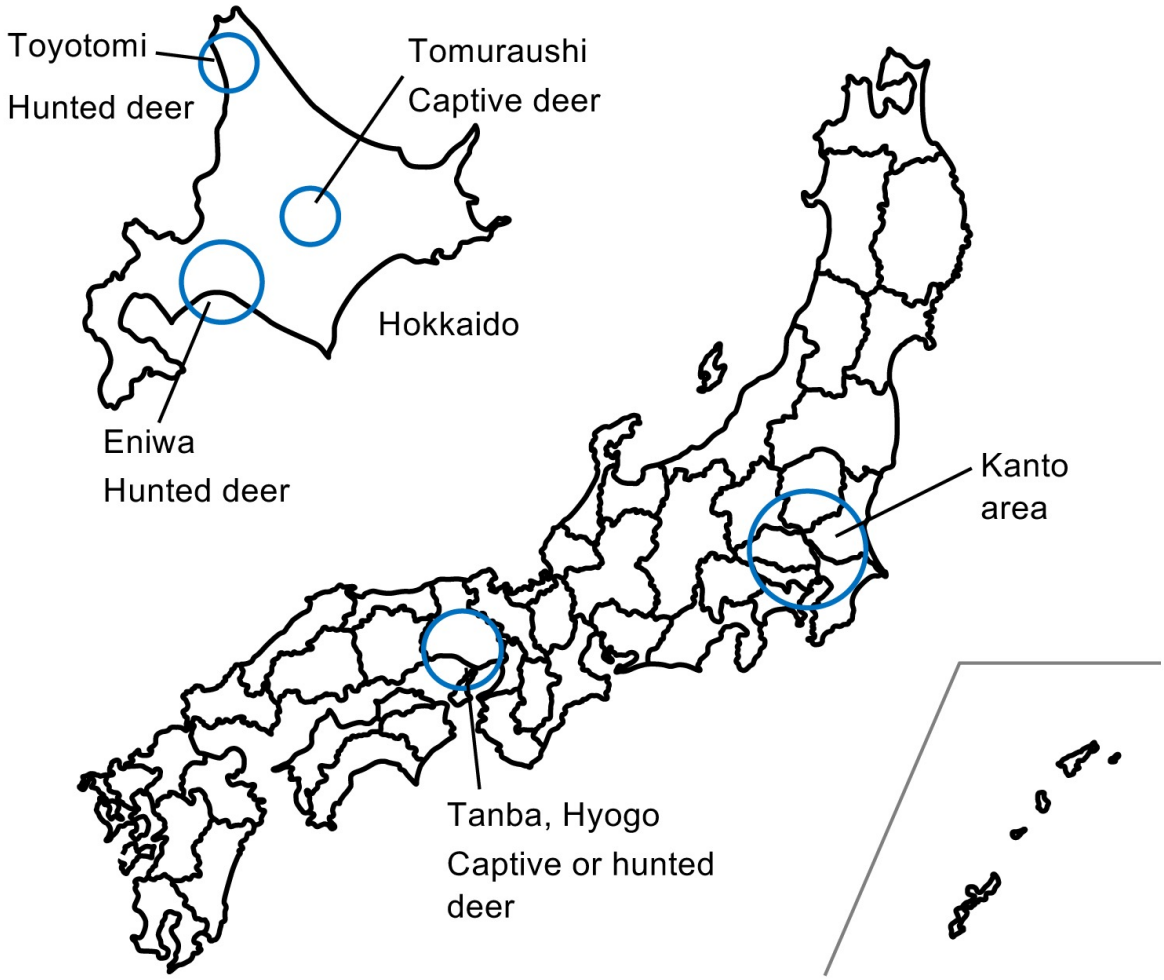

Figure III-1 Captured and hunted area of cervids in the present study.
Areas of sampling. The areas where deer were captured or hunted were shown in blue circles on the map. Names of area, and prefecture, and capture methods were shown around the circles. The capture area in Kanto area is still undisclosed. Detailed information were provided in Table 1.

Table 1. Summary of deer obex samples.

Capture areas	Number	Sex			Age									
		Male	Female	Un-known	0	1	2	3	4	5	6	7	8	Un-known
Hokkaido														
Eniwa	340	186	154	0	8	35	80	80	60	38	31	5	1	2
Tomuraushi	53	9	21	23	0	0	4	17	21	0	5	0	0	6
Toyotomi	61	41	19	1	0	0	27	17	14	1	1	0	0	1
Kanto area [a]	56			56										56
Hyogo														
Tanba	180	96	81	3	0	4	21	62	52	21	12	3	0	5
Total	690	332	275	83	8	39	132	176	147	60	49	8	1	70

a: Sex and age of Reeves's muntjac in Kanto area were not applicable.

2. Preparation for RT-QuIC assay

2-1. Pretreatment of BH samples

Prior to the first RT-QuIC assay, the BH samples except for those from Tomuraushi were pretreated using a fully automatic cross-ultrasonic protein activating apparatus Elestein 070-GOT (Elekon Science, Japan) with 10 cycles of intermittent sonication and agitation in the cold water. One cycle was comprised of 6 repetitions of 30 sec pulse on and 10 sec pulse off followed by 2 min agitation. The BH samples from Tomuraushi were pretreated solely by the sonication for 2 min at 35% amplitude using Ultrasonic Cup-horn Digital Sonifier (Branson, USA). Then, 2% BH was prepared with PBS.

2-2. RT-QuIC assay

The methods for expression and purification of rCerPrP were described in Chapter II. RT-QuIC assay was performed as described elsewhere (Sawada *et al*., 2019) and in Chapter II, using infinite F200 and M200 microplate readers (TECAN). The duration of the RT-QuIC assay was set for a maximum of 40 h. Two-percent BH of pooled six CWD-affected white-tailed deer from the USA was serially diluted 10-fold with PBS from 0.02% to 0.0000002% and 5 μl of each dilution was used as seeds for positive control (final dilution in the reaction mixture: 10^{-5}–10^{-10}, corresponding to 0.001% to 0.00000001%) (hereafter referred as CWD ctrl). The 2% BH of pooled two CWD-unaffected white-tailed deer in USA was used as negative control (NC) (McNulty *et al*., 2019). The first RT-QuIC tests were conducted with quadruplicate wells.

2-3. Date analysis

Data from CWD ctrl and NC were analyzed as described in Chapter II. The sample was evaluated as positive if ThT fluorescence intensity exceeded the threshold calculated as mean ThT intensity plus 5 × SD from the wells without seed (PBS) (Henderson *et al*., 2015).

As described in Chapter II, the lag phase (h) was defined as the time of reaction needed to cross the threshold. If the ThT intensity exceeded the threshold, but the ThT fluorescence curve showed atypical forms in more than one out of four wells, such a sample was considered false-positive and was subjected to re-examination in the next RT-QuIC assay with an increased number of wells.

3. Nucleotide sequence determination of PrP gene

For nucleotide sequence determination of PrP gene, genomic DNA was isolated from 25 mg brain tissues or 100 μl of 10% BHs using DNeasy Blood and Tissue Kit (Qiagen). The gene fragment including *PRNP* was amplified using primers, MD582F and MD1479R described elsewhere (Jewell *et al*., 2005), and the nucleotide sequences were determined using four primers, MD582F, MD1479R, DPrPF1: 5'-TGGCTACATGCTGGGAAGTG-3', and DPrPR1: 5'-TTTTCACGATAGTAACGGTC-3'.

RESULTS

1. First RT-QuIC tests for CWD monitoring

The first RT-QuIC tests were performed with quadruplicate wells of PBS, NC, CWD ctrl (10^{-5}–10^{-10}) and samples examined, which were arranged in the same plate. A total of 136 wells for each control was used at the first RT-QuIC tests. Figure III-2A shows the representative ThT fluorescence curves from one RT-QuIC assay and the summarized results of RT-QuIC assay of the first RT-QuIC tests. Although typical prolongation of lag phases was observed with the dilution of CWD ctrl, reactions were positive up to 10^{-9} dilution in the representative RT-QuIC assay. In a total first RT-QuIC tests for monitoring, typical ThT fluorescence curves that exceeded the threshold were observed in 100% wells of 10^{-5}–10^{-7}, 42.6% wells at 10^{-8}, 5.9% wells at 10^{-9}, and 0.7% at 10^{-10} CWD ctrl dilutions. No positive or false-positive reaction was observed in the wells of NC throughout the examinations. Atypical ThT fluorescence curves such as oscillated waveforms and gradual elevation of the base line were occasionally observed. Representative atypical fluorescence curves are indicated in Figure III-2B. These curves exceeded the threshold but were clearly distinguished from the ThT fluorescence curve of CWD ctrl (Figure III-2A) based on a lack of significant increase of the ThT fluorescence and their appearance at a very early time point. False-positive reactions were observed in 2, 5, and 9 wells at 10^{-8}, 10^{-9}, and 10^{-10} dilution of CWD ctrl, and 3 wells for PBS (Figure III-2A). In the first RT-QuIC tests, the atypical fluorescence curves were observed from 71 out of 690 samples (10.3%) and those samples were judged as false-positive (Table III-2). During the first RT-QuIC tests, more than half of the false-positive samples showed atypical curves only in one of four wells (Figure III-2B). Compared to the incidence of atypical fluorescence curves in the samples from Tomuraushi that were pretreated with sonication using a regular cup-horn sonicator (41.5%, Table III-2), the incidence of atypical fluorescence curves apparently decreased in samples pretreated with the intermittent 10 cycles of sonication and

agitation (7.7%). These results indicate that the intermittent sonication and agitation performed prior to the assays could efficiently reduce the appearance of atypical fluorescence curves if not all.

2. Re-examination of false-positive samples by RT-QuIC assay

A total of 71 samples that showed atypical fluorescence curves were subjected to the second RT-QuIC tests with octuplicate wells to confirm the results. Of 71 samples, the atypical fluorescence curves were observed in 6 samples (0.9%) (Table III-2). These samples were confirmed in the third RT-QuIC tests with twelve replicated wells, and all were judged as negative (Table III-2).

A

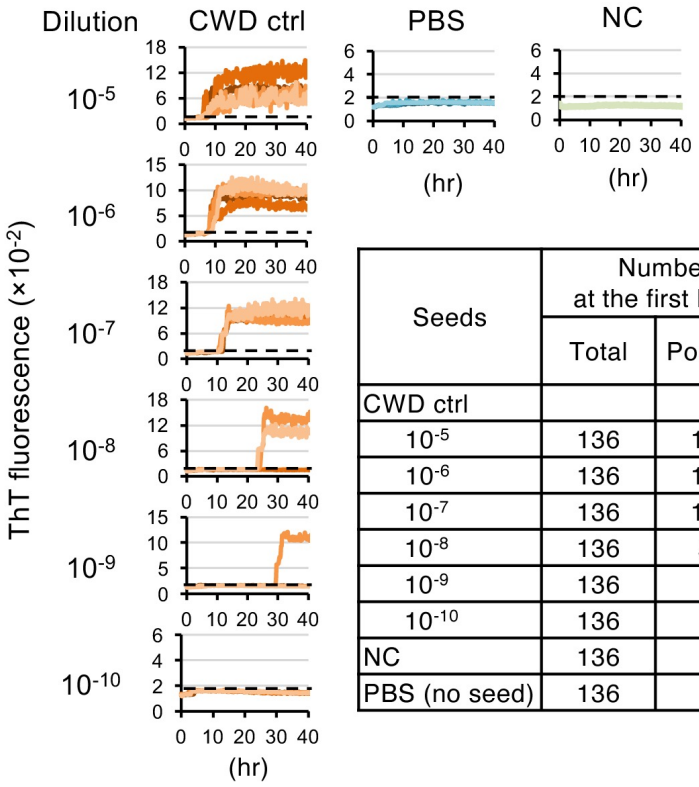

Seeds	Number of wells at the first RT-QuIC test			Ratio of positive wells (%)
	Total	Positive	False-positive	
CWD ctrl				
10^{-5}	136	136	0	100
10^{-6}	136	136	0	100
10^{-7}	136	136	0	100
10^{-8}	136	58	2	42.6
10^{-9}	136	8	5	5.9
10^{-10}	136	1	9	0.7
NC	136	0	0	0
PBS (no seed)	136	0	3	0

B

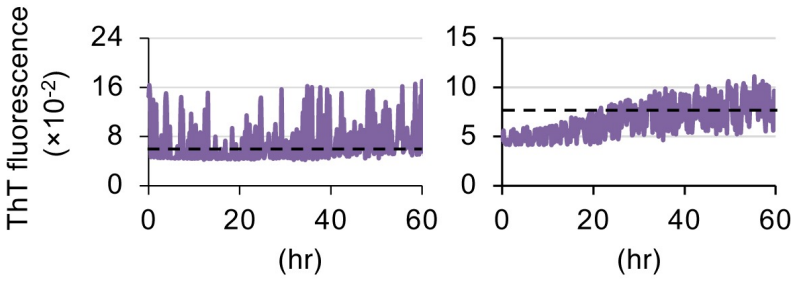

Number of false-positive samples		Number of wells with non-specific waveforms (Ratio to the false-positive samples)			
		4 wells	3 wells	2 wells	1 well
Eniwa, Toyotomi, Kanto area, and Tamba	49	4 (8.2%)	3 (6.1%)	9 (18.4%)	33 (67.3%)
Tomuraushi	22	5 (22.7%)	2 (9.1%)	3 (13.6%)	12 (54.4%)

Figure III-2 Representative Thioflavin T fluorescence curves from CWD-positive control and false-positive samples.

(A) Representative fluorescence curves of CWD-positive and negative control from one RT-QuIC assay (left) and summarized results at the first RT-QuIC tests (right). Brain homogenates of CWD-infected and uninfected deer (CWD ctrl (orange) and NC (light green), respectively) were used as positive and negative controls. The quadruplicate wells without seed (PBS (light blue)) were used to calculate the threshold (dashed lines). Data shown here were collected using infinite M200 microplate reader. The numbers of the total wells used in the first RT-QuIC tests, and positive and false-positive wells are summarized in the table. (B) Summary of false-positive samples at the first RT-QuIC tests. Representative atypical ThT fluorescence curves (purple), oscillated waveform (left), and gradually elevated baseline (right) are shown. Dashed lines indicate the threshold level. Data shown here were collected using infinite F200 microplate reader, which gave 3.6 times higher base line than that of M200 used in the present study. The numbers of false-positive samples, number of wells that showed non-specific waveforms among quadruplicate wells, and the percentage of false-positive samples which showed non-specific waveforms in 1 to 4 wells, are summarized in the table.

Table III-2. Summary of the RT-QuIC tests for CWD monitoring.

Capture areas (number of samples)	Rounds of RT-QuIC test [a]					
	First		Second		Third	
	Negative	False-positive	Negative	False-positive	Negative	False-positive
BH samples pretreated with intermittent sonication and agitation						
Hokkaido						
Eniwa (340)	320 (94.1%)	20 (5.9%)	18 (5.3%)	2 (0.6%)	2 (0.6%)	0 (0%)
Toyotomi (61)	55 (90.2%)	6 (9.8%)	6 (9.8%)	0 (0%)	0 (0%)	0 (0%)
Kanto area (56)	52 (92.9%)	4 (7.1%)	4 (7.1%)	0 (0%)	0 (0%)	0 (0%)
Hyogo						
Tanba (180)	161 (89.4%)	19 (10.6%)	18 (10.0%)	1 (0.6%)	1 (0%)	0 (0%)
Total (637)	588 (92.3%)	49 (7.7%)	46 (7.2%)	3 (0.5%)	3 (0.2%)	0 (0%)
BH samples pretreated with a regular cup-horn sonicator						
Tomuraushi (53)	31 (58.5%)	22 (41.5%)	19 (35.8%)	3 (5.7%)	3 (5.7%)	0 (0%)
Sum total (690)	619 (89.7%)	71 (10.3%)	65 (9.6%)	6 (0.9%)	6 (0.9%)	0 (0%)

a: The values in parentheses indicate the percentage of samples judged as negative or false-positive relative to the total number of samples from each district or total numbers of corresponding samples.

3. Genotype analysis of *PRNP*

It has been reported that the aa polymorphisms of CerPrP influence the susceptibility to CWD (Moreno and Telling, 2018). In the white-tailed deer, mule deer, and elk, polymorphisms at codon 96 (G/S), 225 (S/F), and 132 (M/L), respectively, influence CWD susceptibility; codon S96 of white-tailed deer, F225 of mule deer, and L132 reduce the susceptibility to CWD (Arifin *et al*., 2021). Thus, I estimated the deduced aa sequences of PrP in deer used in this study. A total of 50 sika deer samples, 10 from Tomuraushi, 10 from Eniwa, 20 from Toyotomi, and 10 from Tamba were used for nucleotide sequence analysis. Nucleotide sequences of the PrP gene of sika deer tested in this study were identical to that of the Chinese domestic sika deer reported previously (Meng *et al*., 2005); all deer tested were homozygous for $Q_{96}M_{132}S_{225}$ allele, which is thought to be a CWD-susceptible allele. Although further analyses for wider regions in Japan will be necessary, these results suggest that sika deer inhabiting Japan comprise CWD-susceptible populations.

DISCUSSION

RT-QuIC assay is an easy and sensitive method for detecting PrP^{Sc} and its utility in the diagnosis of human prion diseases has been demonstrated (Atarashi *et al*., 2011). RT-QuIC assay using N-terminal truncated rHaPrP as a substrate is useful for detecting CWD prions from lymphoid tissues (Haley and Hoover, 2015), brain tissue, saliva and urine (Henderson *et al*., 2015). In this study, full-length rCerPrP was used instead of rHaPrP, which can detect low levels of CWD prions in the presence of a high concentration of brain homogenates (Suzuki *et al*., 2020). Samples considered false-positive due to the atypical fluorescence curves are easily expected to be negative for PrP^{Sc}. Indeed, such samples turned out negative after the following RT-QuIC tests with increased multiplicate wells (Table III-2). However, RT-QuIC assay is sensitive enough to detect PrP^{Sc} below the detection limit of immunoblotting and ELISA, a gold standard for PrP^{Sc} detection. Therefore, if samples show typical fluorescence curves with the long lag phase that suggests very low PrP^{Sc} level, it is difficult to confirm the result with immunoblotting and ELISA. PMCA is the sole candidate that validates such samples for the presence of prions, since a sequential PMCA is also highly sensitive for detecting the low levels of PrP^{Sc} (Saborio *et al*., 2001).

Since atypical BSE cases have been mainly identified in cattle over 8-year-old, atypical BSE is hypothesized to be a sporadic disease in aged cattle, as is sporadic CJD in humans (Houston and Andreoletti, 2019). As the prion diseases in ruminant, the possibility of CWD occurring naturally in aged deer cannot be ruled out. Additionally, Japan imports large amounts of dry pasture and hay cube from the USA and Canada every year (Agriculture & Livestock Industries Corporation (ALIC), 2021). CWD prions from carcasses of CWD-affected deer that died outside and/or excreted into the environment can contaminate pastures and soil, and they persist for many years once excreted into the environment (Haley and Hoover, 2015; Pritzkow *et al*., 2015). Therefore, even if no live deer are imported, if hay production areas overlap with

CWD outbreak areas, there is a possibility that CWD prions will enter Japan with the imported hay. In this study, CWD status was monitored about 10 years after the previous report (Masujin *et al*., 2007). No CWD cases were again disclosed in Japan. CWD spreads horizontally from deer to deer, whichever in the field or in the ranch (Escobar *et al*., 2020). Additionally, there is an increase in demands on venison in Japan (Ministry of Agriculture Forestry and Fisheries (MAFF), 2020). Thus, continuous monitoring is necessary for an earlier response and securing the safety of deer products.

In this chapter, I described that RT-QuIC assay using full-length rCerPrP is practical and reliable for monitoring the potential existence of CWD prions. No CWD cases was disclosed in Japan so far. However, the nucleotide sequence analyses of deer PrP gene indicated that the sika deer inhabiting Japan possess CWD-susceptible allele, suggesting that CWD prions may easily spread among sika deer in Japan if CWD prions were emerged or imported. Therefore, continuous monitoring of CWD from wider regions in Japan will be required.

BRIEF SUMMARY

Although there has been no report on CWD cases in Japan to date, there is concern about the unpredictable occurrence and geographic spread of CWD. To clarify the CWD status in Japan, I conducted CWD monitoring using RT-QuIC assay, which can detect the low levels of CWD prions. A total of 690 obex samples from sika deer and Reeves's muntjac were tested for CWD prions. No CWD cases were found, suggesting that CWD may be nonexistent in Japan. The results also indicate that RT-QuIC assay is useful for continuous monitoring of CWD. Furthermore, nucleotide sequence analysis of the PrP gene revealed sika deer in Japan harbor CWD-susceptible allele.

CONCLUSION

Prions, the causative agent of prion diseases, are mainly composed of an abnormal isoform of prion protein (PrP^{Sc}), which is produced from host-encoded cellular isoform of prion protein (PrP^{C}) by post-translational modification including conformational transformation. The binding of PrP^{C} to PrP^{Sc} and following conversion of α-helix-rich PrP^{C} into β-structure-rich PrP^{Sc} are thought to be a key event in prion propagation. After prion infection, production of PrP^{Sc} begins, and PrP^{Sc} gradually accumulates in the central nervous system during a long latency period. Eventually, neuronal cell death is caused by the accumulation of PrP^{Sc} and/or alteration of the neural niche as a response to PrP^{Sc} formation and accumulation. Since PrP^{Sc} is a major component of prions and the process of PrP^{Sc} production is regarded as prion propagation, PrP^{Sc}-specific detection is important in analyzing of the mechanisms of prion propagation and neuropathobiology of prion diseases. Furthermore, PrP^{Sc}-specific detection is important for the diagnosis and surveillance of prion diseases. Therefore, in my doctoral dissertation, I studied the mechanism of PrP^{Sc}-specific detection using monoclonal antibody (mAb) 132, which is extremely useful for PrP^{Sc}-specific staining, and the utility of real-time quaking-induced conversion (RT-QuIC) using recombinant cervid PrP (rCerPrP) as a substrate for detecting PrP^{Sc}.

In Chapter I, to address the mechanism of PrP^{Sc}-specific detection by mAb 132, the reactivities of mono- and bi-valent mAb 132 to recombinant mouse PrP (rMoPrP) were analyzed using enzyme-linked immunosorbent assay (ELISA) and surface plasmon resonance (SPR). In ELISA, the monovalent binding of mAb 132 was significantly weaker than that of the bivalent form, indicating that the bivalent binding confers higher binding stability to mAb 132. Compared to the other anti-PrP mAbs tested, the reactivity of bivalent mAb 132 was easily affected by a decrease in the antigen concentration. In SPR, the binding kinetics of mAb 132 were consistent with the results of ELISA. The k_d value of the monovalent binding was

approximately 260 times larger than that of the bivalent form, suggesting that the monovalent binding is less stable than the bivalent binding. Furthermore, the amount of mAb 132 bound to rMoPrP decreased if the antigen density was too low to allow bivalent binding. On the other hand, if two PrP^C exist close enough to allow bivalent binding, mAb 132 binds to PrP^C. These results indicate that weak monovalent binding to monomeric PrP^C diminishes PrP^C signals to the background level, whereas mAb 132 binds stably to PrP^{Sc} in a bivalent manner after exposure of the epitope.

In Chapter II, I tested the reactivities of various rPrPs including rCerPrP to identify the RT-QuIC condition under which low levels of chronic wasting disease (CWD) and bovine spongiform encephalopathy (BSE) prions can be detected, when in the concentration of brain tissue homogenates is high. Among rPrP tested, only rCerPrP exhibited unique reactivity: the reactivity of rCerPrP to CWD and atypical BSE prions was less affected by the high concentration of normal brain homogenates. The unique reactivity of rCerPrP disappeared when the N-terminal region comprising amino acid (aa) 25−93 was truncated. In addition, the replacement of MoPrP aa 23−149 with the corresponding region of CerPrP partly restored the unique reactivity of CerPrP in RT-QuIC reaction. Furthermore, replacement of the extreme C-terminal region of MoPrP aa 219−231 to the corresponding region of CerPrP partly conferred the unique reactivity of rCerPrP to rMoPrP, suggesting the involvement of both N- and C-terminal regions in the unique reactivity. Additionally, $rCer^N$−Mo−Cer^CPrP, a chimeric PrP comprising CerPrP aa 25−153, MoPrP aa150−218, and CerPrP aa 223−233, showed an additive effect of the N- and C-terminal regions. These results provide a mechanistic implication for detecting CWD and atypical BSE prions using rCerPrP and are useful for further improvement of RT-QuIC.

In Chapter III, I conducted the CWD monitoring by RT-QuIC assay using full-length rCerPrP to clarify the CWD status in Japan. A total of 690 obex samples from captured or hunted

sika deer and Reeves's muntjac in Hokkaido and Honshu were tested using RT-QuIC assay. No CWD-positive cases were found, suggesting that CWD may be nonexistent in Japan. Furthermore, nucleotide sequence analysis of the PrP gene suggests that sika deer inhabiting in wide area in Japan comprise CWD-susceptible populations. Therefore, continuous monitoring of deer from wider regions in Japan will be necessary for earlier detection and response for the emergence of CWD cases and securing the safety of deer products.

In my doctoral dissertation, I elucidated the mechanism of PrP^{Sc}-specific staining with anti-PrP mAb 132. The findings provide the rationale for using mAb 132 in elucidation of mechanism for prion propagation and neuropathobiology. I also showed the utility of rCerPrP in RT-QuIC reaction for detecting CWD and BSE prions. The results demonstrate the practical use of RT-QuIC and are useful for further improvement of RT-QuIC reaction. The findings on PrP^{Sc}-specific detection and its application contributes to the elucidation of pathobiology of prion diseases and further improvement of diagnosis and monitoring of prion disease.

ACKNOWLEDGEMENTS

I would like to express my sincere gratitude to my supervisor, Professor Motohiro Horiuchi (Laboratory of Veterinary Hygiene, Department of Preventive Veterinary Medicine, Faculty of Veterinary Medicine, Graduate School of Infectious Diseases, Hokkaido University) for providing me the valuable opportunity to engage in this study and work, and for his great support and encouragement and his perceptive advise on my research life in his laboratory.

I would like to express deep appreciation to deputy examiners, Professor Hiroaki Kariwa (Laboratory of Public Health, Department of Preventive Veterinary Medicine, Faculty of Veterinary Medicine, Graduate School of Infectious Diseases, Hokkaido University), Associate Professor Satoru Konnai (Laboratory of Infectious Diseases, Department of Disease Control, Faculty of Veterinary Medicine, Graduate School of Infectious Diseases, Hokkaido University), and Associate Professor Atsushi Kobayashi (Laboratory of Comparative Pathology, Department of Clinical Sciences, Faculty of Veterinary Medicine, Graduate School of Veterinary Medicine, Hokkaido University), for joining my research as the examiners in my doctoral dissertation and giving many pieces of their insightful comments and kind advice on my dissertation.

I would like to express my deep gratitude to Professor Ryuichiro Atarashi (Division of Microbiology, Department of Infectious Diseases, Faculty of Medicine, University of Miyazaki) and Ms. Atsuko Matsuo (Department of Molecular Microbiology and Immunology, Graduate School of Biomedical Sciences, Nagasaki University) for kind instruction and advice about the methods for RT-QuIC.

I deeply grateful to Dr. Takeshi Yamasaki and Dr. Rie Hasebe for their daily discussion and continuous help for my study. I would like to show my greatest appreciation to Dr. Yusuke Komatsu, Ms. Mari Ohsawa, Ms. Megumi Oikawa, and Ms. Tomomi Miyakoshi for their helpful support. Also, I am grateful for all members of the Laboratory of Veterinary Hygiene for their warm friendship and help.

Also, I am grateful to Professor Ryuichiro Atarashi for kindly providing expression plasmids for full-length rHaPrP and rMoPrP, to Dr. Byron W. Caughey (National Institute of Health, USA) for kindly providing an expression plasmid for full-length rBvPrP, to Dr. Yoshifumi Iwamaru (National Institute of Animal Health, National Agriculture and Food Research Organization, Japan) for kindly providing BH of H-BSE affected cattle, to Dr. Edward A. Hoover (Prion Research Center, Department of Microbiology, Immunology, and Pathology, College of Veterinary Medicine and Biomedical Sciences, Colorado State University, USA), Dr. Candace K. Mathiason (Prion Research Center, Department of Microbiology, Immunology, and Pathology, College of Veterinary Medicine and Biomedical Sciences, Colorado State University, USA), and Dr. Nathaniel D. Denkers (Prion Research Center, Department of Microbiology, Immunology, and Pathology, College of Veterinary Medicine and Biomedical Sciences, Colorado State University, USA) for kindly providing pooled CWD-infected and uninfected white-tailed deer BHs, to Mr. Auki Konishi (Sarobetsu Venison, Hokkaido, Japan), Mr. Yutaka Takakura (Dream Hill Tomuraushi, Hokkaido, Japan), Mis. Kinuyo Suga (Hyogo Prefecture Nishiharima Meat Hygiene Inspection Office, Hyogo, Japan), Mr. Masao Yanagawase (Tamba Himemomiji, Hyogo, Japan), and Mr. Kazuyuki Yumine (Apuka-no-mori, Hokkaido, Japan) for kindly providing the obex samples of sika deer, and to Dr. Minoru Tobiume (National Institute of Infectious Diseases) and Dr. Shinji Ozawa (Tokyo metropolitan Oshima Park) for

kindly providing the obex samples of Reeves's muntjac from Kanto area. I also thank Zensho Co., Ltd, for the BSL3 facility.

REFERENCES

Abalos, G.C., Cruite, J.T., Bellon, A., Hemmers, S., Akagi, J., Mastrianni, J.A., Williamson, R.A., Solforosi, L. (2008) Identifying key components of the PrP^{C}-PrP^{Sc} replicative interface. *J Biol Chem,* 283: 34021-34028.

Agriculture & Livestock Industries Corporation (ALIC), 2021. Statistical Data, Livestock and Livestock Products. https://www.alic.go.jp/joho-c/joho05_000073.html [accessed on May 31].

Andreoletti, O., Lacroux, C., Chabert, A., Monnereau, L., Tabouret, G., Lantier, F., Berthon, P., Eychenne, F., Lafond-Benestad, S., Elsen, J.M., Schelcher, F. (2002) PrP^{Sc} accumulation in placentas of ewes exposed to natural scrapie: influence of foetal PrP genotype and effect on ewe-to-lamb transmission. *J Gen Virol,* 83: 2607-2616.

Arifin, M.I., Hannaoui, S., Chang, S.C., Thapa, S., Schatzl, H.M., Gilch, S. (2021) Cervid Prion Protein Polymorphisms: Role in Chronic Wasting Disease Pathogenesis. *Int J Mol Sci,* 22.

Atarashi, R., Moore, R.A., Sim, V.L., Hughson, A.G., Dorward, D.W., Onwubiko, H.A., Priola, S.A., Caughey, B. (2007) Ultrasensitive detection of scrapie prion protein using seeded conversion of recombinant prion protein. *Nat Methods,* 4: 645-650.

Atarashi, R., Satoh, K., Sano, K., Fuse, T., Yamaguchi, N., Ishibashi, D., Matsubara, T., Nakagaki, T., Yamanaka, H., Shirabe, S., Yamada, M., Mizusawa, H., Kitamoto, T., Klug, G., McGlade, A., Collins, S.J., Nishida, N. (2011) Ultrasensitive human prion detection in cerebrospinal fluid by real-time quaking-induced conversion. *Nat Med,* 17: 175-178.

Balkema-Buschmann, A., Eiden, M., Hoffmann, C., Kaatz, M., Ziegler, U., Keller, M., Groschup, M.H. (2011) BSE infectivity in the absence of detectable PrP^{Sc} accumulation in the tongue and nasal mucosa of terminally diseased cattle. *J Gen Virol,* 92: 467-476.

Baron, T., Vulin, J., Biacabe, A.G., Lakhdar, L., Verchere, J., Torres, J.M., Bencsik, A. (2011) Emergence of classical BSE strain properties during serial passages of H-BSE in wild-type mice. *PLoS One,* 6: e15839.

Bendhein, P.E., Barry, R.A., DeArmond, S.J., Stites, D.P., Prusiner, S.B. (1984) Antibodies to a scrapie prion protein. *Nature,* 310: 418-421.

Beringue, V., Herzog, L., Reine, F., Le Dur, A., Casalone, C., Vilotte, J.L., Laude, H. (2008) Transmission of atypical bovine prions to mice transgenic for human prion protein. *Emerg Infect Dis,* 14: 1898-1901.

Biacabe, A.G., Laplanche, J.L., Ryder, S., Baron, T. (2004) Distinct molecular phenotypes in bovine prion diseases. *EMBO Rep,* 5: 110-115.

Biacabe, A.G., Laplanche, J.L., Ryder, S., Baron, T. (2008) Atypical Bovine Spongiform

Encephalopathies, France, 2001-2007. *EMBO Rep,* 5: 110-115.

Biljan, I., Giachin, G., Ilc, G., Zhukov, I., Plavec, J., Legname, G. (2012) Structural basis for the protective effect of the human prion protein carrying the dominant-negative E219K polymorphism. *Biochem J,* 446: 243-251.

Billeter, M., Riek, R., Wider, G., Hornemann, S., Glockshuber, R., Wuthrich, K. (1997) Prion protein NMR structure and species barrier for prion diseases. *Proc Natl Acad Sci U S A,* 94: 7281-7285.

Bolton, D.C., Seligman, S.J., Bablanian, G., Windsor, D., Scala, L.J., Kim, K.S., Chen, C.M., Kascsak, R.J., Bendhein, P.E. (1991) Molecular location of a species-specific epitope on the hamster scrapie agent protein. *J Virol,* 65: 3667-3675.

Buschmann, A., Groschup, M. (2005) Highly bovine spongiform encephalopathy-sensitive transgenic mice confirm the essential restriction of infectivity to the nervous system in clinically diseased cattle. *J Infect Dis,* 192: 934-942.

Capobianco, R., Casalone, C., Suardi, S., Mangieri, M., Miccolo, C., Limido, L., Catania, M., Rossi, G., Di Fede, G., Giaccone, G., Bruzzone, M.G., Minati, L., Corona, C., Acutis, P., Gelmetti, D., Lombardi, G., Groschup, M.H., Buschmann, A., Zanusso, G., Monaco, S., Caramelli, M., Tagliavini, F. (2007) Conversion of the BASE prion strain into the BSE strain: the origin of BSE? *PLoS Pathog,* 3: e31.

Casalone, C., Zanusso, G., Acutis, P., Ferrari, S., Capucci, L., Tagliavini, F., Monaco, S., Caramelli, M. (2004) Identification of a second bovine amyloidotic spongiform encephalopathy: molecular similarities with sporadic Creutzfeldt-Jakob disease. *Proc Natl Acad Sci U S A,* 101: 3065-3070.

Castilla, J., Saa, P., Hetz, C., Soto, C. (2005) *In vitro* generation of infectious scrapie prions. *Cell,* 121: 195-206.

Comoy, E.E., Casalone, C., Lescoutra-Etchegaray, N., Zanusso, G., Freire, S., Marce, D., Aurve, F., Ruchoux, L.E., Monaco, S., Sales, N., Caramelli, M., Leboulch, P., Brown, P., Lasmezas, C., Deslys, J.P. (2008) Atypical BSE (BASE) transmitted from asymptomatic aging cattle to a primate. *PLoS One,* 3: e3017.

Cutler, T.A., Mills, B.M., Lubin, D.J., Chong, L.T., Loh, S.N. (2009) Effect of interdomain linker length on an antagonistic folding-unfolding equilibrium between two protein domains. *J Mol Biol,* 386: 854-868.

Dassanayake, R.P., Orru, C.D., Hughson, A.G., Caughey, B., Graca, T., Zhuang, D., Madsen-Bouterse, S.A., Knowles, D.P., Schneider, D.A. (2016) Sensitive and specific detection of classical scrapie prions in the brains of goats by real-time quaking-induced conversion. *J Gen Virol,* 97: 803-812.

Deleault, N., Harris, B., Rees, J., Supattapone, S. (2007) Formation of native prions from minimal components *in vitro*. *Proc Natl Acad Sci U S A,* 104: 9741-9746.

Denkers, N.D., Henderson, D.M., Mathiason, C.K., Hoover, E.A. (2016) Enhanced prion detection in biological samples by magnetic particle extraction and real-time quaking-induced conversion. *J Gen Virol,* 97: 2023-2029.

Donnelly, M.L., Luke, G., Mehrotra, A., Li, X., Hughes, L.E., Gani, D., Ryan, M.D. (2001) Analysis of the aphthovirus 2A/2B polyprotein 'cleavage' mechanism indicates not a proteolytic reaction, but a novel translational effect: a putative ribosomal 'skip'. *J Gen Virol,* 82: 1013-1025.

Duque Velasquez, C., Kim, C., Herbst, A., Daude, N., Garza, M.C., Wille, H., Aiken, J., McKenzie, D. (2015) Deer Prion Proteins Modulate the Emergence and Adaptation of Chronic Wasting Disease Strains. *J Virol,* 89: 12362-12373.

Edeling, M.A., Austin, S.K., Shrestha, B., Dowd, K.A., Mukherjee, S., Nelson, C.A., Johnson, S., Mabila, M.N., Christian, E.A., Rucker, J., Pierson, T.C., Diamond, M.S., Fremont, D.H. (2014) Potent dengue virus neutralization by a therapeutic antibody with low monovalent affinity requires bivalent engagement. *PLoS Pathog,* 10: e1004072.

Erana, H., Fernandez-Borges, N., Elezgarai, S.R., Harrathi, C., Charco, J.M., Chianini, F., Dagleish, M.P., Ortega, G., Millet, O., Castilla, J. (2017) *In Vitro* Approach To Identify Key Amino Acids in Low Susceptibility of Rabbit Prion Protein to Misfolding. *J Virol,* 91.

Escobar, L.E., Pritzkow, S., Winter, S.N., Grear, D.A., Kirchgessner, M.S., Dominguez-Villegas, E., Machado, G., Townsend Peterson, A., Soto, C. (2020) The ecology of chronic wasting disease in wildlife. *Biol Rev Camb Philos Soc,* 95: 393-408.

Fischer, M., Rulicke, T., Raeber, A., Sailer, A., Moser, M., Oesch, B., Brander, S., Aguzzi, A., Weissman, C. (1996) Prion protein (PrP) with amino-proximal deletions restoring susceptibility of PrP knockout mice to scrapie. *EMBO J,* 15: 1255-1264.

Garrido, G., Tikhomirov, I.A., Rabasa, A., Yang, E., Gracia, E., Iznaga, N., Fernández, L.E., Crombet, T., Kerbel, R.S., Pérez, R. (2011) Bivalent binding by intermediate affinity of nimotuzumab: A contribution to explain antibody clinical profile. *Cancer Biology & Therapy,* 11: 373-382.

Georgsson, G., Sigurdarson, S., Brown, P. (2006) Infectious agent of sheep scrapie may persist in the environment for at least 16 years. *J Gen Virol,* 87: 3737-3740.

Gossert, A.D., Bonjour, S., Lysek, D.A., Fiorito, F., Wuthrich, K. (2005) Prion protein NMR structures of elk and of mouse/elk hybrids. *Proc Natl Acad Sci U S A,* 102: 646-650.

Hagiwara, K., Yamakawa, Y., Sato, Y., Nakamura, Y., Tobiume, M., Shinagawa, M., Sata, T.

(2007) Accumulation of Mono-Glycosylated Form-Rich, Plaque-Forming PrP^{Sc} in the Second Atypical Bovine Spongiform Encephalopathy Case in Japan. *Jpn J Infect Dis,* 60: 305-308.

Haley, N.J., Hoover, E.A. (2015) Chronic wasting disease of cervids: current knowledge and future perspectives. *Annu Rev Anim Biosci,* 3: 305-325.

Haley, N.J., Richt, J.A. (2017) Evolution of Diagnostic Tests for Chronic Wasting Disease, a Naturally Occurring Prion Disease of Cervids. *Pathogens,* 6.

Hamir, A.N., Kunkle, R.A., Cutlip, R.C., Miller, J.M., Williams, E.S., Richt, J.A. (2006) Transmission of Chronic Wasting Disease of Mule Deer to Suffolk Sheep following Intracerebral Inoculation. *J Vet Diagn Invest,* 18: 558-565.

Hara, H., Miyata, H., Das, N.R., Chida, J., Yoshimochi, T., Uchiyama, K., Watanabe, H., Kondoh, G., Yokoyama, T., Sakaguchi, S. (2018) Prion protein devoid of the octapeptide repeat region delays bovine spongiform encephalopathy pathogenesis in mice. *J. Virol.,* 92: e01368-01317.

Harms, B.D., Kearns, J.D., Su, S.V., Kohli, N., Nielsen, U.B., Schoeberl, B. (2012) Optimizing properties of antireceptor antibodies using kinetic computational models and experiments. *Methods Enzymol,* 502: 67-87.

Harrathi, C., Fernandez-Borges, N., Erana, H., Elezgarai, S.R., Venegas, V., Charco, J.M., Castilla, J. (2019) Insights into the Bidirectional Properties of the Sheep-Deer Prion Transmission Barrier. *Mol Neurobiol,* 56: 5287-5303.

Harris, L.J., Skaletsky, E., McPherson, A. (1998) Crystallographic structure of an intact IgG1 monoclonal antibody. *J Mol Biol,* 275: 861-872.

Henderson, D.M., Davenport, K.A., Haley, N.J., Denkers, N.D., Mathiason, C.K., Hoover, E.A. (2015) Quantitative assessment of prion infectivity in tissues and body fluids by real-time quaking-induced conversion. *J Gen Virol,* 96: 210-219.

Holscher, C., Delius, H., Burkle, A. (1998) Overexpression of nonconvertible PrP^{C} delta114−121 in scrapie-infected mouse neuroblastoma cells leads to trans-dominant inhibition of wild-type PrP^{Sc} accumulation. *J Virol,* 72: 1153-1159.

Hoover, C.E., Davenport, K.A., Henderson, D.M., Zabel, M.D., Hoover, E.A. (2017) Endogenous Brain Lipids Inhibit Prion Amyloid Formation *In Vitro*. *J Virol,* 91.

Horiuchi, M., Ishiguro, N., Nagayama, K., Toyoda, Y., Shinagawa, M. (1997) Alternative usage of exon 1 of bovine PrP mRNA. *Biochem Biophys Res Commun,* 233: 650-654.

Horiuchi, M., Ishiguro, N., Nagayama, K., Toyoda, Y., Shinagawa, M. (1998) Genomic structure of the bovine PrP gene and complete nucleotide sequence of bovine PrP cDNA. *Anim Genet,* 29: 37-40.

Horiuchi, M., Karino, A., Furuoka, H., Ishiguro, N., Kimura, K., Shinagawa, M. (2009) Generation of monoclonal antibody that distinguishes PrP^{Sc} from PrP^{C} and neutralizes prion infectivity. *Virology,* 394: 200-207.

Houston, F., Andreoletti, O. (2019) Animal prion diseases: the risks to human health. *Brain Pathol,* 29: 248-262.

Huor, A., Espinosa, J.C., Vidal, E., Cassard, H., Douet, J.Y., Lugan, S., Aron, N., Benestad, S.L., Orge, L., Trackray, A.M., Bujdoso, R., Torres, J.M. (2019) The emergence of classical BSE from atypical/Nor98 scrapie. *Proc Natl Acad Sci U S A,* 116: 26853-26862.

Jacobs, J.G., Langeveld, J.P., Biacabe, A.G., Acutis, P.L., Polak, M.P., Gavier-Widen, D., Buschmann, A., Caramelli, M., Casalone, C., Mazza, M., Groschup, M., Erkens, J.H., Davidse, A., van Zijderveld, F.G., Baron, T. (2007) Molecular discrimination of atypical bovine spongiform encephalopathy strains from a geographical region spanning a wide area in Europe. *J Clin Microbiol,* 45: 1821-1829.

Jewell, J.E., Conner, M.M., Wolfe, L.L., Miller, M.W., Williams, E.S. (2005) Low frequency of PrP genotype 225SF among free-ranging mule deer (*Odocoileus hemionus*) with chronic wasting disease. *J Gen Virol,* 86: 2127-2134.

Johnson, C.J., Duque Velasquez, C., Vanderllo, J.P., Bochsler, P., Chappell, R., McKenzie, D. (2011) Prion protein polymorphisms affect chronic wasting disease propgression. *PLoS One,* 6: e17450.

Jostock, T., Vanhove, M., Brepoels, E., Van Gool, R., Daukandt, M., Wehnert, A., Van Hegelsom, R., Dransfield, D., Sexton, D., Devlin, M., Ley, A., Hoogenboom, H., Mullberg, J. (2004) Rapid generation of functional human IgG antibodies derived from Fab-on-phage display libraries. *J Immunol Methods,* 289: 65-80.

Kascsak, R.J., Rubenstein, R., Merz, P.A., Tonna-DeMasi, M., Fresko, R., Carp, R.I., Wisniewski, H.M., Dirnger, H. (1987) Mouse polyclonal and monoclonal antibody to scrapie-associated fibril proteins. *J Virol,* 61: 3688-3693.

Kataoka, N., Nishimura, M., Horiuchi, M., Ishiguro, N. (2005) Surveillance of Chronic Wasting Disease in Sika Deer, *Cervus Nippon*, From Tokachi District in Hokkaido. *J Vet Med Sci,* 67: 349-351.

Kettleborough, C.A., Saldanha, J., Ansell, K.H., Bendig, M.M. (1993) Optimization of primers for cloning libraries of mouse immunoglobulin genes using the polymerase chain reaction. *Eur J Immunol,* 23: 206-211.

Khalili-Shirazi, A., Quaratino, S., Londei, M., Summers, L., Tayebi, M., Clarke, A.R., Hawke, S.H., Jackson, G.S., Collinge, J. (2005) Protein conformation significantly influences immune responses to prion protein. *J Immunol,* 174: 3256-3263.

Kim, C.L., Karino, A., Ishiguro, N., Shinagawa, M., Sato, M., Horiuchi, M. (2004a) Cell-surface retention of PrP^C by anti-PrP antibody prevents protease-resistant PrP formation. *J Gen Virol,* 85: 3473-3482.

Kim, C.L., Umetani, A., Matsui, T., Ishiguro, N., Shinagawa, M., Horiuchi, M. (2004b) Antigenic characterization of an abnormal isoform of prion protein using a new diverse panel of monoclonal antibodies. *Virology,* 320: 40-51.

Kitamoto, T., Muramoto, T., Mohri, S., Doh-Ura, K., Tateishi, J. (1991) Abnormal isoform of prion protein accumulates in follicular dendritic cells in mice with Creutzfeldt-Jakob disease. *J Virol,* 65: 6292-6295.

Kong, Q., Huang, S., Zou, W., Vanegas, D., Wang, M., Wu, D., Yuan, J., Zheng, M., Bai, H., Deng, H., Chen, K., Jenny, A.L., O'Rourke, K., Belay, E.D., Schonberger, L.B., Petersen, R.B., Sy, M.S., Chen, S.G., Gambetti, P. (2005) Chronic wasting disease of elk: transmissibility to humans examined by transgenic mouse models. *J Neurosci,* 25: 7944-7949.

Kong, Q., Zheng, M., Casalone, C., Qing, L., Huang, S., Chakraborty, B., Wang, P., Chen, F., Cali, I., Corona, C., Martucci, F., Iulini, B., Acutis, P., Wang, L., Liang, J., Wang, M., Li, X., Monaco, S., Zanusso, G., Zou, W.Q., Caramelli, M., Gambetti, P. (2008) Evaluation of the human transmission risk of an atypical bovine spongiform encephalopathy prion strain. *J Virol,* 82: 3697-3701.

Korth, C., Stierli, B., Streit, P., Moser, M., Schaller, O., Fischer, R., Schulz-Schaeffer, W., Kretzschmar, H., Raeber, A., Braun, U., Ehrensperger, F., Hornemann, S., Glockshuber, R., Riek, R., Billeter, M., Wuthrich, K., Oesch, B. (1997) Prion (PrP^{Sc})-specific epitope defined by a monoclonal antibody. *Nature,* 390: 74-77.

Koutsoumanis, K., Allende, A., Alvarez-Ordonez, A., Bolton, D., Bover-Cid, S., Chemaly, M., Davies, R., De Cesare, A., Herman, L., Hilbert, F., Lindqvist, R., Nauta, M., Peixe, L., Ru, G., Skandamis, P., Suffredini, E., Andreoletti, O., Benestad, S.L., Comoy, E., Nonno, R., da Silva Felicio, T., Ortiz-Pelaez, A., Simmons, M.M. (2019) Update on chronic wasting disease (CWD) III. *EFSA J,* 17: e05863.

Krasemann, S., Jugens, T., Bodemer, W. (1999) Generation of monoclonal antibodies against prion proteins with an unconventional nucleic acid-based immunization strategy. *J Biotechnol.,* 73: 119-129.

Kurt, T.D., Aguilar-Calvo, P., Jiang, L., Rodriguez, J.A., Alderson, N., Eisenberg, D.S., Sigurdson, C.J. (2017) Asparagine and glutamine ladders promote cross-species prion conversion. *J Biol Chem,* 292: 19076-19086.

Lawson, V.A., Priola, S.A., Wehrly, K., Chesebro, B. (2001) N-terminal truncation of prion

protein affects both formation and conformation of abnormal protease-resistant prion protein generated *in vitro*. *J Biol Chem,* 276: 35265-35271.

Lee, J., Chang, I., Yu, W. (2019) Atomic insights into the effects of pathological mutants through the disruption of hydrophobic core in the prion protein. *Sci Rep,* 9: 19144.

Lee, P.S., Yoshida, R., Ekiert, D.C., Sakai, N., Suzuki, Y., Takada, A., Wilson, I.A. (2012) Heterosubtypic antibody recognition of the influenza virus hemagglutinin receptor binding site enhanced by avidity. *Proc Natl Acad Sci U S A,* 109: 17040-17045.

Liemann, S., Glockshuber, R. (1999) Influence of amino acid substitutions related to inherited human prion diseases on the thermodynamic stability of the cellular prion protein. *Biochemistry,* 38: 3258-3267.

Marijanovic, Z., Caputo, A., Campana, V., Zurzolo, C. (2009) Identification of an intracellular site of prion conversion. *PLoS Pathog,* 5: e1000426.

Masujin, K., Kaku-Ushiki, Y., Miwa, R., Okada, H., Shimizu, Y., Kasai, K., Matsuura, Y., Yokoyama, T. (2013) The N-terminal sequence of prion protein consists an epitope specific to the abnormal isoform of prion protein (PrP^{Sc}). *PLoS One,* 8: e58013.

Masujin, K., Shimada, K., Kimura, M.K., Imamura, M., Yoshida, A., Iwamaru, Y., Mohri, S., Yokoyama, T. (2007) Applicability of current bovine spongiform encephalopathy (BSE) diagnostic procedures for chronic wasting disease (CWD). *Microbiol Immunol,* 51: 1039-1043.

Mathiason, C.K., Power, J.G., Dahmes, S.J., Osborn, D.A., Miller, K.V., Warren, R.J., Mason, G.L., Hays, S.A., Hayes-Klug, J., Seelig, D.M., Wild, M.A., Wolfe, L.L., Spraker, T.R., Miller, M.W., Sigurdarson, C.J., Telling, G.C., Hoover, E.A. (2006) Infectious prions in the saliva and blood of deer with chronic wasting disease. *Science,* 314: 133-136.

McNulty, E., Nalls, A.V., Mellentine, S., Hughes, E., Pulscher, L., Hoover, E.A., Mathiason, C.K. (2019) Comparison of conventional, amplification and bio-assay detection methods for a chronic wasting disease inoculum pool. *PLoS One,* 14: e0216621.

Meng, L.P., Zhao, D.M., Liu, H.X., Yang, J.M., Ning, Z.Y., Wu, C.D., Han, C.X. (2005) Polymorphisms of the prion protein gene (*PRNP*) in Chinese domestic sika deer (*Cervus nippon hortulorum*). *Anim Genet,* 36: 266-267.

Mestre-Frances, N., Nicot, S., Rouland, S., Biacabe, A.G., Quadrio, I., Perret-Liaudet, A., Baron, T., Verdier, J.M. (2012) Oral transmission of L-type bovine spongiform encephalopathy in primate model. *Emerg Infect Dis,* 18: 142-145.

Meyer, R.K., McKinley, M.P., Bowman, K.A., Braunfeld, M.B., Barry, R.A., Prusiner, S.B. (1986) Separation and properties of cellular and scrapie prion proteins. *Proc Natl Acad Sci U S A,* 83: 2310-2314.

Miller, M.B., Wang, D.W., Wang, F., Noble, G.P., Ma, J., Woods, V.L., Jr., Li, S., Supattapone, S. (2013) Cofactor molecules induce structural transformation during infectious prion formation. *Structure,* 21: 2061-2068.

Miller, M.W., Williams, E.S., Hobbs, N.T., Wolfe, L.L. (2004) Environmental sources of prion transmission in mule deer. *Emerg Infect Dis,* 10: 1003-1006.

Ministry of Agriculture Forestry and Fisheries (MAFF), 2020. Statistical Data, Survey on Wildlife Resource Utilization. https://www.maff.go.jp/j/tokei/kouhyou/jibie/index.html [accessed on Jun 14].

Moreno, J.A., Telling, G.C. (2018) Molecular Mechanisms of Chronic Wasting Disease Prion Propagation. *Cold Spring Harb Perspect Med,* 8, a024448.

Moroncini, G., Kanu, N., Solforosi, L., Abalos, G., Telling, G.C., Head, M., Ironside, J., Brockes, J.P., Burton, D.R., Williamson, R.A. (2004) Motif-grafted antibodies containing the replicative interface of cellular PrP are specific for PrP^{Sc}. *Proc Natl Acad Sci U S A,* 101: 10404-10409.

Müller, K.M., Arndt, K.M., Plückthum, A. (1998) Model and Simulation of Multivalent Binding to Fixed Ligands. *Analytical Biochemistry,* 261: 149-158.

Okada, H., Iwamaru, Y., Imamura, M., Masujin, K., Matsuura, Y., Shimizu, Y., Kasai, K., Mohri, S., Yokoyama, T., Czub, S. (2011) Experimental H-type bovine spongiform encephalopathy characterized by plaques and glial- and stellate-type prion protein deposits. *Vet Res,* 42: 79.

Olson, W.C., Spitznagel, T.M., Yarmush, M.L. (1989) Dissociation kinetics of antigen-antibody interactions: studies on a panel of anti-albumin monoclonal antibodies. *Molecular Immunology,* 20: 129-136.

Orru, C.D., Groveman, B.R., Raymond, L.D., Hughson, A.G., Nonno, R., Zou, W., Ghetti, B., Gambetti, P., Caughey, B. (2015) Bank Vole Prion Protein As an Apparently Universal Substrate for RT-QuIC-Based Detection and Discrimination of Prion Strains. *PLoS Pathog,* 11: e1004983.

Orru, C.D., Hughson, A.G., Groveman, B.R., Campbell, K.J., Anson, K.J., Manca, M., Kraus, A., Caughey, B. (2016) Factors That Improve RT-QuIC Detection of Prion Seeding Activity. *Viruses,* 8.

Orru, C.D., Wilham, J.M., Hughson, A.G., Raymond, L.D., McNally, K.L., Bossers, A., Ligios, C., Caughey, B. (2009) Human variant Creutzfeldt-Jakob disease and sheep scrapie PrP^{res} detection using seeded conversion of recombinant prion protein. *Protein Eng Des Sel,* 22: 515-521.

Orru, C.D., Wilham, J.M., Raymond, L.D., Kuhn, F., Schroeder, B., Raeber, A.J., Caughey, B.

(2011) Prion disease blood test using immunoprecipitation and improved quaking-induced conversion. *mBio,* 2: e00078-00011.

Orru, C.D., Wilham, J.M., Vascellari, S., Hughson, A.G., Caughey, B. (2012) New generation QuIC assays for prion seeding activity. *Prion,* 6: 147-152.

Osterholm, M.T., Anderson, C.J., Zabel, M.D., Scheftel, J.M., Moore, K.A., Appleby, B.S. (2019) Chronic Wasting Disease in Cervids: Implications for Prion Transmission to Humans and Other Animal Species. *mBio,* 10.

Paramithiotis, E., Pinard, M., Lawton, T., LaBoissiere, S., Leathers, V.L., Zou, W.Q., Estey, L.A., Lamontagne, J., Lehto, M.T., Kondejewski, L.H., Francoeur, G.P., Papadopoulos, M., Haghighat, A., Spatz, S.J., Head, M., Will, R., Ironside, J., O'Rourke, K., Tonelli, Q., Ledebur, H.C., Chakrabartty, A., Cashman, N.R. (2003) A prion protein epitope selective for the pathologically misfolded conformation. *Nat Med,* 9: 893-899.

Pastrana, M.A., Sajnani, G., Onisko, B., Castilla, J., Morales, R., Soto, C., Requena, J.R. (2006) Isolation and characterization of a proteinase K-sensitive PrP^{Sc} fraction. *Biochemistry,* 45: 15710-15717.

Pattison, I.H., Hoare, M.N., Jebbett, J.N., Watson, W.A. (1972) Spread of scrapie to sheep and goats by oral dosing with foetal membranes from scrapie-affected sheep. *Vet Rec,* 90: 465-468.

Peden, A.H., McGuire, L.I., Appleford, N.E.J., Mallinson, G., Wilham, J.M., Orru, C.D., Caughey, B., Ironside, J.W., Knight, R.S., Will, R.G., Green, A.J.E., Head, M.W. (2012) Sensitive and specific detection of sporadic Creutzfeldt-Jakob disease brain prion protein using real-time quaking-induced conversion. *J Gen Virol,* 93: 438-449.

Peretz, D., Williamson, R., Matsunaga, Y., Serban, H., Pinilla, C., Bastidas, R., Rozenshteyn, R., James, T., Houghten, R., Cohen, F., Prusiner, S., Burton., D. (1997) A conformational transition at the N terminus of the prion protein features in formation of the scrapie isoform. *J Mol Biol,* 273: 614-622.

Piccardo, P., Langeveld, J.P.M., Hill, A.F., Dlouhy, S.R., Young, K., Giaccone, G., Rossi, G., Bugiani, M., Bugiani, O., Meloen, R.H., Collinge, J., Tagliavini, F., Ghetti, B. (1998) An antibody raised against a conserved sequence of the prion protein recognizes pathological isoforms in human and animal prion diseases, including Creutzfeldt-Jakob disease and bovine spongiform encephalopathy. *Am J Pathol,* 152: 1415-1420.

Pimpinelli, F., Lehmann, S., Maridonneau-Parini, I. (2005) The scrapie prion protein is present in flotillin-1-positive vesicles in central- but not peripheral-derived neuronal cell lines. *Eur J Neurosci,* 21: 2063-2072.

Polymenidou, M., Moos, R., Scott, M., Sigurdson, C., Shi, Y.Z., Yajima, B., Hafner-Bratkovic,

I., Jerala, R., Hornemann, S., Wuthrich, K., Bellon, A., Vey, M., Garen, G., James, M.N., Kav, N., Aguzzi, A. (2008) The POM monoclonals: a comprehensive set of antibodies to non-overlapping prion protein epitopes. *PLoS One,* 3: e3872.

Pritzkow, S., Morales, R., Moda, F., Khan, U., Telling, G.C., Hoover, E., Soto, C. (2015) Grass plants bind, retain, uptake, and transport infectious prions. *Cell Rep,* 11: 1168-1175.

Prusiner, S.B. (1998) Prions. *Proc Natl Acad Sci U S A,* 95: 13363-13383.

Race, B., Meade-White, K.D., Miller, M.W., Barbian, K.D., Rubenstein, R., LaFauci, G., Cervenakova, L., Favara, C., Gardner, D., Long, D., Parnell, M., Striebel, J., Priola, S.A., Ward, A., Williams, E.S., Race, R., Chesebro, B. (2009) Susceptibilities of nonhuman primates to chronic wasting disease. *Emerg Infect Dis,* 15: 1366-1376.

Ridgway, J.B., Presta, L.G., Carter, P. (1996) 'Knobs-into-holes' engineering of antibody CH3 domains for heavy chain heterodimerization. *Protein Eng,* 9: 617-621.

Saborio, G.P., Permanne, B., Soto, C. (2001) Sensitive detection of pathological prion protein by cyclic amplification of protein misfolding. *Nature,* 411: 810-813.

Saijo, E., Hughson, A.G., Raymond, G.J., Suzuki, A., Horiuchi, M., Caughey, B. (2016) PrP^{Sc}-Specific Antibody Reveals C-Terminal Conformational Differences between Prion Strains. *J Virol,* 90: 4905-4913.

Sakai, K., Hasebe, R., Takahashi, Y., Song, C.H., Suzuki, A., Yamasaki, T., Horiuchi, M. (2013) Absence of CD14 delays progression of prion diseases accompanied by increased microglial activation. *J Virol,* 87: 13433-13445.

Sawada, K., Suzuki, A., Yamasaki, T., Iwamaru, Y., Matsuura, Y., Miyazawa, K., Masujin, K., Atarashi, R., Horiuchi, M. (2019) Estimation of prion infectivity in tissues of cattle infected with atypical BSE by real time-quaking induced conversion assay. *J Vet Med Sci,* 81: 846-850.

Scott, M., Foster, D., Mirenda, C., Serban, D., Coufal, F., Walchli, M., Torchia, M., Groth, D., Carlson, G., DeArmond, S., Westerway, D., Prusiner, S. (1989) Transgenic mice expressing hamster prion protein produce species-specific scrapie infectivity and amyloid plaques. *Cell,* 59: 847-857.

Serban, D., Taraboulos, A., DeArmond, S.J., Prusiner, S.B. (1990) Rapid detection of Creutzfeldt-Jakob disease and scrapie prion proteins. *Neurology,* 40: 110-117.

Shan, Z., Yamasaki, T., Suzuki, A., Hasebe, R., Horiuchi, M. (2016) Establishment of a simple cell-based ELISA for the direct detection of abnormal isoform of prion protein from prion-infected cells without cell lysis and proteinase K treatment. *Prion,* 10: 305-318.

Shinagawa, M., Munekawa, E., Doi, S., Takahashi, K., Goto, H., Sato, G. (1986) Immunoreactivity of a synthetic pentadecapeptide corresponding to the N-terminal region

of the scrapie prion protein. *J Gen Virol,* 67: 1745-1750.

Shindoh, R., Kim, C.L., Song, C.H., Hasebe, R., Horiuchi, M. (2009) The region approximately between amino acids 81 and 137 of proteinase K-resistant PrP^{Sc} is critical for the infectivity of the Chandler prion strain. *J Virol,* 83: 3852-3860.

Sigurdson, C.J., Manco, G., Schwarz, P., Liberski, P., Hoover, E.A., Hornemann, S., Polymenidou, M., Miller, M.W., Glatzel, M., Aguzzi, A. (2006) Strain fidelity of chronic wasting disease upon murine adaptation. *J Virol,* 80: 12303-12311.

Sigurdson, C.J., Nilsson, K.P., Hornemann, S., Manco, G., Fernandez-Borges, N., Schwarz, P., Castilla, J., Wuthrich, K., Aguzzi, A. (2010) A molecular switch controls interspecies prion disease transmission in mice. *J Clin Invest,* 120: 2590-2599.

Silveira, J.R., Raymond, G.J., Hughson, A.G., Race, R.E., Sim, V.L., Hayes, S.F., Caughey, B. (2005) The most infectious prion protein particles. *Nature,* 437: 257-261.

Simmons, M.M., Chaplin, M.J., Konold, T., Casalone, C., Beck, K.E., Thorne, L., Everitt, S., Floyd, T., Clifford, D., Spiropoulos, J. (2016) L-BSE experimentally transmitted to sheep presents as a unique disease phenotype. *Vet Res,* 47: 112.

Somerville, R.A., Birkett, C.R., Farquhar, C.F., Hunter, N., Goldmann, W., Dornan, J., Grover, D., Hennion, R.M., Percy, C., Foster, J., Jeffrey, M. (1997) Immunodetection of PrP^{Sc} in spleens of some scrapie-infected sheep but not BSE-infected cows. *J Gen Virol,* 78: 2389-2396.

Stemmer, W., Crameri, A., Ha, K., Brennan, T., Heyneker, H. (1995) Single-step assembly of a gene and entire plasmid from large numbers of oligodeoxyribonucleotides.

Suardi, S., Vimercati, C., Casalone, C., Gelmetti, D., Corona, C., Iulini, B., Mazza, M., Lombardi, G., Moda, F., Ruggerone, M., Campanani, L., Piccoli, E., Catania, M., Groschup, M.H., Balkema-Buschmann, A., Caramelli, M., Monaco, S., Zanusso, G., Tagliavini, F. (2012) Infectivity in skeletal muscle of cattle with atypical bovine spongiform encephalopathy. *PLoS One,* 7: e31449.

Suzuki, A., Sawada, K., Yamasaki, T., Denkers, N.D., Mathiason, C.K., Hoover, E.A., Horiuchi, M. (2020) Involvement of N- and C-terminal region of recombinant cervid prion protein in its reactivity to CWD and atypical BSE prions in real-time quaking-induced conversion reaction in the presence of high concentrations of tissue homogenates. *Prion,* 14: 283-295.

Suzuki, A., Yamasaki, T., Hasebe, R., Horiuchi, M. (2019) Enhancement of binding avidity by bivalent binding enables PrP^{Sc}-specific detection by anti-PrP monoclonal antibody 132. *PLoS One,* 14: e0217944.

Tamguney, G., Giles, K., Bouzamondo-Bernstein, E., Bosque, P.J., Miller, M.W., Safar, J.,

DeArmond, S.J., Prusiner, S.B. (2006) Transmission of elk and deer prions to transgenic mice. *J Virol,* 80: 9104-9114.

Tamguney, G., Miller, M.W., Wolfe, L.L., Sirochman, T.M., Glidden, D.V., Palmer, C., Lemus, A., DeArmond, S.J., Prusiner, S.B. (2009) Asymptomatic deer excrete infectious prions in faeces. *Nature,* 461: 529-532.

Tanaka, M., Fujiwara, A., Suzuki, A., Yamasaki, T., Hasebe, R., Masujin, K., Horiuchi, M. (2016) Comparison of abnormal isoform of prion protein in prion-infected cell lines and primary-cultured neurons by PrP^{Sc}-specific immunostaining. *J Gen Virol,* 97: 2030-2042.

Taraboulos, A., Serban, D., Prusiner, S.B. (1990) Scrapie prion proteins accumulate in the cytoplasm of persistently infected cultured cells. *J Cell Biol,* 110: 2117-2132.

Tzaban, S., Friedlander, G., Schonberger, O., Horonchik, L., Yedidia, Y., Shaked, G., Gabizon, R., Taraboulos, A. (2002) Protease-sensitive scrapie prion protein in aggregates of heterogeneous sizes. *Biochemistry,* 41: 12868-12875.

Ushiki-Kaku, Y., Endo, R., Iwamaru, Y., Shimizu, Y., Imamura, M., Masujin, K., Yamamoto, T., Hattori, S., Itohara, S., Irie, S., Yokoyama, T. (2010) Tracing conformational transition of abnormal prion proteins during interspecies transmission by using novel antibodies. *J Biol Chem,* 285: 11931-11936.

van Rheede, T., Smolenaars, M.M., Madsen, O., de Jong, W.W. (2003) Molecular evolution of the mammalian prion protein. *Mol Biol Evol,* 20: 111-121.

Veith, N.M., Plattner, H., Stuermer, C.A., Schulz-Schaeffer, W.J., Burkle, A. (2009) Immunolocalisation of PrP^{Sc} in scrapie-infected N2a mouse neuroblastoma cells by light and electron microscopy. *Eur J Cell Biol,* 88: 45-63.

Vikoren, T., Vage, J., Madslien, K.I., Roed, K.H., Rolandsen, C.M., Tran, L., Hopp, P., Veiberg, V., Heum, M., Moldal, T., Neves, C.G.D., Handeland, K., Ytrehus, B., Kolbjornsen, O., Wisloff, H., Terland, R., Saure, B., Dessen, K.M., Svendsen, S.G., Nordvik, B.S., Benestad, S.L. (2019) First Detection of Chronic Wasting Disease in a Wild Red Deer (*Cervus elaphus*) in Europe. *J Wildl Dis,* 55: 970-972.

Wang, F., Wang, X., Yuan, C.G., Ma, J. (2010) Generating a prion with bacterially expressed recombinant prion protein. *Science,* 327: 1132-1135.

Watts, J.C., Giles, K., Serban, A., Patel, S., Oehler, A., Bhardwaj, S., Guan, S., Greicius, M.D., Miller, B.L., DeArmond, S.J., Geschwind, M.D., Prusiner, S.B. (2015) Modulation of Creutzfeldt-Jakob disease prion propagation by the A224V mutation. *Ann Neurol,* 78: 540-553.

Weiss, E., Orfanoudakis, G. (1994) Application of an alkaline phosphatase fusion protein system suitable for efficient screening and production of Fab-enzyme conjugates in

Escherichia coli. *J Biotechnol,* 33: 43-53.

Wells, G.A., Scott, A.C., Johnson, C.T., Gunning, R.F., Hancock, R.D., Jeffrey, M., Dawson, M., Bradley, R. (1987) A novel progressive spongiform encephalopathy in cattle. *Vet Rec,* 121: 419-420.

Wilesmith, J.W., Wells, G.A., Cranwell, M.P., Ryan, J.B. (1988) Bovine spongiform encephalopathy: epidemiological studies. *Vet Rec,* 123: 638-644.

Wilham, J.M., Orru, C.D., Bessen, R.A., Atarashi, R., Sano, K., Race, B., Meade-White, K.D., Taubner, L.M., Timmes, A., Caughey, B. (2010) Rapid end-point quantitation of prion seeding activity with sensitivity comparable to bioassays. *PLoS Pathog,* 6: e1001217.

Will, R.G. (2003) Acquired prion disease: iatrogenic CJD, variant CJD, kuru. *Br Med Bull.,* 66: 255-265.

Will, R.G., Ironside, J.W., Zeidler, M., Cousens, S.N., Estibeiro, K., Alperovitch, A., Poser, S., Pocchiari, M., Hofman, A., Smith, P.G. (1996) A new variant of Creutzfeldt-Jakob disease in the UK. *Lancet,* 347: 921-925.

Williams, E.S., Miller, M.W. (2002) Chronic wasting disease in deer and elk in North America. *Rev Sci Off Int Epiz,* 21: 305-316.

Williams, E.S., Young, S. (1980) Chronic Wasting Disease of Captive Mule Deer: A Spongiform Encephalopathy. *J Wildl Dis,* 16: 89-98.

Williamson, R.A., Peretz, D., Pinilla, C., Ball, H., Prusiner, S.B., Burton, D.R. (1998) Mapping the prion protein using recombinant antibodies. *J Virol,* 72: 9413-9418.

Williamson, R.A., Peretz, D., Smorodinsky, N., Bastidas, R., Serban, H., Mehlhorn, I., DeArmond, S.J., Prusiner, S.B., Burton, D.R. (1996) Circumventing tolerance to generate autologous monoclonal antibodies to the prion protein. *Proc Natl Acad Sci U S A,* 93: 7279-7282.

Wopfner, F., Weidenhofer, G., Schneider, R., von Brunn, A., Gilch, S., Schwarz, T.F., Werner, T., Schatzl, H.M. (1999) Analysis of 27 mammalian and 9 avian PrPs reveals high conservation of flexible regions of the prion protein. *J Mol Biol,* 289: 1163-1178.

Yamasaki, T., Baron, G.S., Suzuki, A., Hasebe, R., Horiuchi, M. (2014a) Characterization of intracellular dynamics of inoculated PrP-res and newly generated PrP^{Sc} during early stage prion infection in Neuro2a cells. *Virology,* 450-451: 324-335.

Yamasaki, T., Suzuki, A., Hasebe, R., Horiuchi, M. (2014b) Comparison of the anti-prion mechanism of four different anti-prion compounds, anti-PrP monoclonal antibody 44B1, pentosan polysulfate, chlorpromazine, and U18666A, in prion-infected mouse neuroblastoma cells. *PLoS One,* 9: e106516.

Yamasaki, T., Suzuki, A., Hasebe, R., Horiuchi, M. (2018) Flow Cytometric Detection of PrP^{Sc}

in Neurons and Glial Cells from Prion-Infected Mouse Brains. *J Virol,* 92.

Yamasaki, T., Suzuki, A., Shimizu, T., Watarai, M., Hasebe, R., Horiuchi, M. (2012) Characterization of intracellular localization of PrP^{Sc} in prion-infected cells using a mAb that recognizes the region consisting of aa 119−127 of mouse PrP. *J Gen Virol,* 93: 668-680.

Zahn, R., Liu, A., Luhrs, T., Reik, R., von Schetter, C., Garcia, F.L., Billeter, M., Calzolai, L., Wider, G., Wuthrich, K. (2000) NMR solution structure of the human prion protein. *Proc Natl Acad Sci U S A,* 97: 145-150.

和文抄録

プリオン病の病原体であるプリオンは，異常型プリオンタンパク質 (PrP^{Sc}) から構成される。PrP^{Sc} は，宿主由来正常型プリオンタンパク質 (PrP^{C}) から構造転換を含む翻訳後修飾により産生される。PrP^{C} と PrP^{Sc} の結合，および，その後の α-ヘリックスに富む PrP^{C} から β 構造に富む PrP^{Sc} への構造転換は，プリオン増殖において鍵となる事象であると考えられている。プリオン感染後，PrP^{Sc} の産生が始まり，長い潜伏期間の間に中枢神経系に徐々に蓄積する。最終的に，PrP^{Sc} の産生自体，または PrP^{Sc} の形成や蓄積に対する応答による神経組織環境の変化により神経細胞死が引き起こされる。PrP^{Sc} はプリオンの主要構成要素であり，PrP^{Sc} の産生過程はプリオンの増殖とみなされているため，PrP^{Sc} の特異的な検出は，プリオン増殖やプリオン病の神経病態機序の解析に重要である。さらに，PrP^{Sc} 特異的検出は，プリオン病の診断やサーベイランスにも重要である。そこで本学位論文では，PrP^{Sc} 特異的染色に非常に有用であるモノクローナル抗体 (mAb) 132 による PrP^{Sc} 特異的検出のメカニズムと，組換えシカ PrP (rCerPrP) を基質として用いた Real-Time Quaking-Induced Conversion (RT-QuIC) による PrP^{Sc} 検出の有用性について研究した。

第一章では，mAb 132 による PrP^{Sc} 特異的検出のメカニズムを解明するため，一価および二価の mAb 132 の組換えマウス PrP (rMoPrP) に対する反応性を ELISA，表面プラズモン共鳴法 (SPR) により解析した。ELISA 法では，mAb 132 の一価での結合は二価型での結合に比べ有意に弱いことから，二価での結合が mAb 132 に高い結合安定性を与えていることが示唆された。また，他の抗 PrP 抗体に比べ mAb 132 の二価結合は，抗原濃度の減少により容易に影響を受けることが明らかとなった。SPR 法では，mAb 132 の反応速度論は ELISA による結果と一致しており，一価結合の解離速度定数は二価結合より 260 倍大きかった。これは一価結合は二価結合より安定性が低い事を示唆している。さらに，抗原密度が低く抗体が二価結合できない場合，rMoPrP に結合した mAb 132 の量は減少した。一方，2 つの PrP^{C} が二価結合が可能な距離内に存在する場合，mAb 132 は PrP^{C} に結合した。これらの結果は，単量体 PrP^{C} への弱い一価結合が PrP^{C} のシグナルをバックグラウンド

レベルに減少させるのに対し，mAb 132 は PrP^{Sc} のエピトープ露出後に二価結合により PrP^{Sc} に安定して結合する事を示している。

第二章では，rCerPrP を含む様々な組換え PrP (rPrP) を用いて，脳乳剤濃度が高い場合でも低レベルの慢性消耗病 (CWD)，牛海綿状脳症 (BSE) プリオンを検出可能な RT-QuIC の反応条件について検討した。試した rPrP のうち，rCerPrP のみが，CWD，非定型 BSE プリオンに対する反応性が高濃度の非感染脳乳剤による影響を受けにくいという特徴的な反応性を示した。この rCerPrP 特有の反応性は，N 末端領域アミノ酸 25−93 を除去することにより消失した。また，MoPrP のアミノ酸 23−149 を CerPrP の対応する領域と置換することで，RT-QuIC 反応での CerPrP 特有の反応性が部分的に回復した。さらに，MoPrP の C 末端領域アミノ酸 219−231 を CerPrP の対応する領域と置換すると rCerPrP 特有の反応性が rMoPrP に付与されたことから，N 末端，C 末端領域の両方が rCerPrP 特有の反応性に関与することが示唆された。加えて，CerPrP のアミノ酸 25−153，MoPrP のアミノ酸 150−218，および CerPrP のアミノ酸 223−233 から構成される $rCer^{N}$−Mo−Cer^{C}PrP は，この N 末端，C 末端領域の相加効果を示した。これらの結果は，CWD および非定型 BSE を検出する際の rCerPrP の作用機序を示すとともに，RT-QuIC の更なる改善に役立つと思われる。

第三章では，日本における CWD の状態を明らかにするために，全長 rCerPrP を使用した RT-QuIC による CWD モニタリングを行った。北海道，本州で捕獲または狩猟された合計 690 個のニホンシカ，ジャワマメジカの延髄閂部サンプルを RT-QuIC により検査した。CWD 陽性例は認められなかったことから，CWD は日本で発生していない可能性が高いと考えられる。さらに，ニホンシカの PrP 遺伝子の塩基配列の解析により，日本の広い地域に生息するニホンシカが CWD 感受性の個体群により構成されていることが示唆された。従って，より広い地域のシカについての継続的なモニタリングは，CWD の発生時における早期の検出及び対応やシカ由来製品の安全性を確保するために必要と思われる。

本学位論文では，抗 PrP 抗体 mAb 132 による PrP^{Sc} 特異的染色のメカニズムを解明した。これらの知見は，プリオンの増殖およびプリオン病の神経病態機序を明らかにする

ための mAb 132 の使用に対する論理的根拠を提供しうる。また，RT-QuIC 反応において CWD と BSE を検出する際の rCerPrP の有用性について示した。これらの結果は，RT-QuIC の実用性を示すとともに，RT-QuIC の更なる改善にも役立つと思われる。PrP^{Sc} 特異的検出及びその応用についての知見は，プリオン病の神経病態学の解明や，プリオン病の診断，サーベイランスの更なる改善に貢献するものである。